SOME ASPECTS OF TOOL WEAR AND MACHINABILITY

OF

FREE-MACHINING STEELS

SOME ASPECTS OF TOOL WEAR AND MACHINABILITY
OF
FREE-MACHINING STEELS

BY

K.L. VERMA, B. Eng. (Hons.)

A Thesis
Submitted to the School of Graduate Studies
in Partial Fulfillment of the Requirements
for the Degree
Master of Engineering

McMaster University
May 1976

MASTER OF ENGINEERING (1976) McMASTER UNIVERSITY
(Mechanical) Hamilton, Ontario

TITLE: Some Aspects of Tool Wear and Machinability of Free-Machining Steels

AUTHOR: K.L. Verma, B.Eng. (Hons.)

SUPERVISOR: Professor, Dr. J. Tlusty

NUMBER OF PAGES: xii, 114

ABSTRACT

Machinability is a key factor for the profitability and is an elusive variable specially for automatic machining operations. Metallurgists faced with this subjective requirement have nevertheless succeeded in developing a number of modifications to the base alloys that do possess superior machinability. These modified alloys are commonly known as Free-Machining Steels or Free-Cutting Steels.

The report commences with a general description of the mechanism by which three different types of manganese sulphide inclusions are formed in resulphurized steel. Both the selected free-machining steels have globular type of inclusions and probably are of Type I. Lead phase in leaded resulphurized steel exists in association with sulphide inclusions or free lead particles. Tests have shown that the free-machining additives have a negligible effect on the mechanical properties of steel.

The results on the comparative machinability of plain carbon steel and free-machining steels, under a wide range of cutting conditions, have revealed a clear difference in machinability. Free-machining steels are much superior to unmodified steels. This conclusion is based on the following criteria: tool wear, cutting forces, built up edge, shear angle, contact length, and surface finish produced.

It is evident from the microscopic analysis of the chips produced during the cutting process that the free-machining

steels have decreased chip thickness, decreased roughness at the back of the chip, and decreased wipe-down, than the plain carbon steel. All these factors are in favour of better machinability.

Finally, it is concluded that the leaded resulphurized steel (12L15) is superior than straight resulphurized steel (1215) below a certain critical speed. It is proposed that this critical speed is directly related to the cutting temperature, which is a function of cutting variables.

ACKNOWLEDGMENTS

The author wishes to express his sincere appreciation to Dr. J. Tlusty for the invaluable guidance and advice supplied throughout the course of this work.

The author also acknowledges the expertise and encouragement offered by Professor S. Ramalingam of the State University of New York at Buffalo, Buffalo, New York.

The author is also indebted to many other faculty and staff members who have made his study at McMaster enjoyable.

Mrs. Annette Neumayer is thanked for her skillful and diligent typing of the manuscript.

Finally, to his wife Manju, the author wishes to express his special gratitude for all her help, patience and encouragement during the study.

TABLE OF CONTENTS

<u>LIST OF FIGURES</u>

LIST OF SYMBOLS

S.E.M.	Scanning Electron Microscopy	
A.E.S.	Auger Electron Spectroscopy	
B.U.E.	Built Up Edge	in.
Q	Shear Angle	°(degrees)
F_v	Cutting Force	lbf.
F_f	Feed Force	lbf.
α	Rake Angle of Cutting Tool	°(degrees)
t_1	Undeformed Chip Thickness	in.
t_2	Deformed Chip Thickness	in.
r	Chip Thickness Ratio (t_1/t_2)	
Q_T	Tool Temperature	°C
m	Constant	
V	Cutting Speed	ft/min
a	Depth of Cut	in.
s	Feed	in/rev
U	Cutting energy	in-lb/in^3
k	Thermal Conductivity	cal/sec.cm°C
ρ	Density	gram/cm^3
c	Specific Heat	cal/gram°C
K	Constant	

CHAPTER I

FREE MACHINING STEELS

1.1 Introduction

While the term "machinability" has gained currency over past many years as a property describing the relative ease of metal removal in the course of machining, it remains an enigmatic concept. Neither a precise definition of this material "property" nor its absolute measurement is still possible, since the concept encompasses too broad a range of performance criteria. The performance criteria are in reality quite subjective and in fact represent a metal user's desire to produce a large number of components that meet the quality criteria (dimensional and surface finish) with minimal tool problem (tool wear) in the least amount of time (high metal removal rates).

Metallurgists, faced with these subjective requirements and in the absence of a detailed understanding of the mechanism of chip formation, of tool wear, and of the resulting surface quality, have nevertheless succeeded in empirically developing a number of modifications to the base alloys that are superior and can be objectively shown to be so by the actual measurement of specific energy for metal removal, of tool life and of surface finish produced.

These modified steels are commonly known as free-machining steels or free-cutting steels. The principal free-machining additives that render non-ferrous alloys free-machining are sulphur, lead and tellurium. In ferrous alloys, the free-machining variety consists of resulphurized, rephosphorized steels with or without lead and rare earth additions. The use of tellurium, selenium and nitrogen is also common.

1.2 Intra-Ingot and Inter-Ingot Variations

In commercial production these modified alloys exhibit a large scatter in machinability. Intra-ingot variations in machinability are common and these are frequently larger than the corresponding inter-ingot variations. This problem has its origin in the mechanism by which the free-machining additives are incorporated in the modified alloys, and the role played by the additives in rendering the modified alloys more easily machinable.

One is then faced with the problem, how these variations come about. Probably, the answer to this question is

(i) variations in the chemistry from ingot to ingot

(ii) segregation problems during solidification which alter local chemical composition, and

(iii) the shape/form in which these additives exist in the base metal.

Most of the commercial steels contain less than 1% carbon. The carbon content of steel is controlled by oxidation process during steel making. Various elements may be added singly or in combination, during or after the carbon removal to produce an alloy steel. On attainment of desired chemical composition the molten steel is poured into moulds, where it solidifies to form ingots.

After the steel has been refined to the desired chemistry, it contains appreciable amounts (usually 0.05 to 1.0%)[1] of oxygen, which interferes with the subsequent processing, and the performance properties of steel. In order to achieve the desired properties, the oxygen content must be brought to the desired level before tapping. The concentration of oxygen in the steel during tapping is dependent on the carbon content of the bath, and on the addition of deoxidizers which form stable oxides in the melt. The amount of oxygen that remains in the melt in equilibrium with carbon is shown in the Fig. 1.1.

As seen in the Fig. 1.1, carbon in excess of 0.4 wt% does not help in reducing the oxygen content of steel below 0.006 wt%, because the carbon oxygen plot becomes a straight line after 0.4 wt% carbon. Depending upon the type of steel to be produced (killed, semi-killed and rimming steel), higher oxygen content may not be desired. For producing low carbon steel, the excess oxygen is removed or is fixed in an inactive form by forming stable oxides by addition of deoxidants. The common elements added as deoxidants are manganese, silicon, aluminium and less commonly added are titanium, zirconium and calcium. The effectiveness of these elements depends on the conditions of the metal at the instant of deoxidizer addition.

Oxygen is the principle gas dissolved in the steel, and that makes it possible to produce different ingot structures. Oxygen exists in the form of FeO. It reacts with carbon during cooling and solidification, i.e.

$$FeO + C = Fe + CO(gas)$$

At the tapping temperature, the iron oxide and carbon contents of the liquid steel are essentially in the equilibrium state. However, the solubility of oxygen in the molten iron is affected by the alloying elements. The activity co-efficient of oxygen is raised or lowered, depending on the interaction between the oxygen and elements dissolved in steel. Upon cooling of the molten iron, gases are produced by associated chemical reaction. The last gases to be evolved are not able to escape from the ingot and collect as bubbles to form blow holes.

The solidified ingots exhibit a marked degree of segregation. Segregation represents a departure from average chemical composition. The tendency of individual elements to segregate can be expressed as the ratio between the concentration of the elements in the first metal to solidify and the concentration of the elements in the last metal to solidify. The amount of segregation found in an ingot depends upon several factors, such as chemical composition of steel, type of ingot (killed, semi-killed or rimming) and ingot size.

In general, the metal that solidifies very rapidly, close to the mould wall (the chill zone), has about the same composition as the liquid metal entering the mould. However, as the rate of solidification decreases, the mechanism of solidification is such that crystals of purer metal solidify first. The last amount of liquid to solidify, thus contains the largest amount of rejected elements from purer metal solidifed earlier. When the content of an element is greater than the average amount in bulk metal, the segregation is termed as positive segregation and when the content is less than the average, it is termed as negative segregation. The tendency for elements to segregate in a solidifying ingot increases with an increased time for solidification. Thus large ingots exhibit more severe segregation than small ingots.

1.3 Types of Ingot Structures

Bascially there are three types of ingot structures:

(i) semi-killed structure

(ii) killed structure

(iii) rimming structure.

The difference between these ingot structures is the result of a difference in the amount of gas evolved during solidification. Fig. 1.2 shows the three different kinds of structures. For rimmed steel very little or no deoxidant (aluminium or silicon) is added in the ladle before pouring. The gases evolved during solidification are trapped, which results in porosity in the interior surface. In semi-killed steel, some amount of deoxidant is added. Due to partial deoxidation, it results in lower oxygen content, when compared with rimmed steel. Sufficient amount of deoxidant is added for producing killed steel, which reduces the oxygen level in the steel. The oxygen level in steel is a very important factor for the formation of free-machining inclusions in steel and it is discussed in depth in the following paragraphs.

1.4 Types of MnS Inclusions

In view of the problems during solidification (segregation/non-uniformity of chemistry), it is of interest to examine the mechanism by which the free-machining additive inclusions are formed during solidification.

In examining ferrous alloys, one finds that widely used low carbon screw machining stocks, consist of three principle types of free-machining steels[2] such as:

(i) resulphurized, rephosphorized steels

(ii) leaded steels (usually also resulphurized)

(iii) leaded steel further modified by the addition of R.E.M. (rare earth metals) or bismuth.

In fact these are manganese deoxidized, semi-killed steels. Some silicon and aluminium (in small quantities) may also be added to assist deoxidation, since manganese is not the most effective deoxidizer. R.E.M. additions are usually very small quantities of selenium and tellurium. Cerium and lathalum are also occasionally used. More often, they are used with higher carbon and alloy steels, prone to form Type II and Type III MnS inclusions. Bismuth is sometimes used, but generally in conjunction with lead. Three different types of sulphide inclusions can result during solidification. They have been classified as:

(i) Type I MnS inclusions

(ii) Type II MnS inclusions

(iii) Type III MnS inclusions.

Studies carried out by Ramalingam[2,3], Baker and Charles[4] and Moore[5] have given detailed analysis by which three different kinds of MnS inclusions are formed in steel during the process of solidification, and it is summarized as follows.

1.4.1 Type I MnS Inclusions

Typical Type I MnS inclusions are shown in the Fig. 1.3. They are globular in shape. They are predominantly single phase MnS inclusions, but are also associated with duplex constituents. The size of these inclusions ranges from 3 to 100 μm, but mostly are in the range of 10 to 30 μm[4]. The larger size inclusions are invariably two phase inclusions, and as a general rule the greater the proportion of the duplex phase, the larger is their size. A typical two phase inclusion is shown in Fig. 1.4.

Micro-probe X-ray analysis of many of the single phase sulphide inclusions have indicated the mean composition of 59.8% Mn, 35.4% S and 3% Fe[4].

The major factor leading to the formation of Type I MnS inclusion is the presence of oxygen in the steel[4,5]. That is why rimming and semi-killed steel containing higher oxygen content, when compared with completely oxidized killed steel, have a tendency to form Type I MnS inclusions. Fig. 1.5 shows the carbon oxygen relationship for the formation of Type I, Type II and Type III MnS inclusions. As shown, high oxygen content favours the formation of Type I MnS inclusions and low oxygen content forms Type III MnS inclusions.

Since the sulphur solubility is very low even at temperatures when steel is molten, precipitation of MnS takes place in the liquid state(4). The interfacial surface tension between one liquid suspended in another is responsible for the globular shape of these inclusions. The spherical form of Type I sulphides indicates that they were precipitated as liquids in a liquid metal. The freezing point of MnS is 2910°F(1600°C), and the liquidus of steel is about 2730°F(1500°C)(6). Sulphide precipitation may be suppressed to a lower temperature if the oxygen concentration of the liquid steel is low. The addition of oxidizing agents such as silicon and aluminium reduces the oxygen percentage in steel. Thus, in medium carbon and alloy steel where oxygen concentration is quite low, the precipitation of MnS may be suppressed to a lower temperature. However, the addition of rare earth elements in the form of cerium and lathalum alters the situation considerably in this class of steel.

The rare earth sulphides and oxides have a much higher melting point (3500°F) than both MnS and steel(4). They are then expected to precipitate as rare earth oxide crystals, sulphides or oxysulphides, depending on the rare earth to sulphide ratio. These precipitates distributed discretely throughout the matrix may act as nucleation sites, around which the Type I MnS inclusion can form. In the absence of quantitative data, it is not presently possible to be specific about the exact mechanism by which rare earth metal addition promotes the formation of Type I MnS inclusions. Both optical metallographic analysis using polarized light and electron microscopic analysis, as reported by Wells and Wilson[7], strongly suggest that Type I manganese sulphide precipitates and grows around the rare earth oxides and sulphides nuclei.

At high ratios of rare earth to sulphur (greater than 1.5), the sulphides are predominantly rare earth sulphides. Luyckx[8] reports that higher ratio cause little or no manganese sulphide formation, but predominance of rare earth sulphides (verified by micro-probe analysis). These rare earth sulphides formed in such instances are found to be globular- and massive-like; however, they are less plastic than the manganese sulphide inclusions.

1.4.2 Type II MnS Inclusions

These are non-spherical inclusions. They occur at intermediate levels of oxygen, as shown before in Fig. 1.5. Addition of deoxidizers in the form of aluminium and silicon, reduces the oxygen content by forming stable oxides; this results in the formation of Type II or Type III MnS inclusions. The sulphur activity in the liquid metal is decreased to the extent that liquid freezing at a later stage during solidification is sulphur rich, and freezes in the eutectic pattern. The temperature encountered in forming Type II is consequently lower than required to form Type I MnS inclusions. Hence, the particles do not have much time to grow. In contrast to Type I, Type II exhibits a significantly small size distribution. Steels with Type II MnS inclusions have lower machinability index compared to steels with Type I MnS inclusions.

1.4.3 Type III MnS Inclusions

These are large angular inclusions occurring at a low level of oxygen, as shown before in Fig. 1.5. When the residual aluminium content of steel exceeds about 0.01%, Type III sulphides form[6]. These inclusions appear as crystalline particles. The addition of 0.038 wt% aluminium in the ladle is enough to change sulphide solubility and morphology from Type I to Type III. The effect of increasing amount of deoxidizers is to reduce the melting point of Fe and to significantly alter the sulphur activity. Sim[6] found that aluminium in excess of 0.005% and silicon in excess of 0.1% alters the sulphide oxygen activity in such a way that sulphide precipitates as a last product of solidification. The nucleation and growth occurs at a lower temperature than Type I and Type II.

The association of Type III, with excess deoxidizers and high carbon implies that Type III forms in steel of lower oxygen content than required for Type I and Type II.

Thus, the ingots exhibiting regions of high positive segregation of carbon are prone to Type III MnS precipitations in those regions. Type III is usually associated with oxides of aluminium and silicon which are hard and abrasive. These are detrimental to machinability.

Segregation induced during solidification of large ingots can therefore be responsible for different sulphide morphologies existing in the same ingot. More solidification time in large ingots favours high degree of segregation. When the molten steel is poured in the mould, if it is too gassy, aluminium and/or silicon is sometimes added to prevent ingot bleeding. However, these additions facilitate segregation tendency by changing the rate of solidification. Thus, variation in sulphide morphology within the same ingot is inevitable. Subsequent machining operations on samples of the same ingot then exhibit significant non-uniformity in machinability.

The different morphologies of sulphide encountered do not differ markedly in their mechanical properties[9], whereas Type II and Type III MnS inclusions significantly degrade machinability.

Research conducted by Baker and Charles[10] has shown that Type I MnS inclusions in a free-cutting steel deform less than the matrix during hot rolling. In contrast, they found that Type II and Type III MnS deform extensively. The deformation causes the MnS inclusions to preferentially elongate in the direction of rolling. This anisotropic effect results in non-uniform machining behavior in the rolling and transverse directions. Further, the measured relative plasticity for both Type I and Type II MnS inclusions, have been plotted against temperature and is shown in Fig. 1.6. Significant differences in relative plasticity is apparent and it is considered that this arises from variations in the matrix and/or inclusion composition and properties. The analysis of results shows that the principle difference in composition between steel containing Type I MnS and that containing Type III MnS, is carbon, silicon and aluminium.

Paliwoda(11) studies showed that improved machinability usually accompanies higher oxygen contents. As stated earlier, the oxygen content of steels containing Type I MnS is higher than the steels containing Type II and Type III. Thus, Paliwoda's observations imply that Type I MnS improves machinability compared to Type III.

Studies by Van Vlack(12) on free-machining steels, are in agreement with the above discussion. In brief, the work done by Van Vlack is summarized as follows.

Steels of higher silicon contents posses lower machinability index rating and have more plastic type inclusions. Conversely, steels with higher machinability indices have globular type inclusions. However, this idea is based on the quantitative measure of shape, i.e. the length over width ratio. Not only the shape of inclusion is considered but also the number of inclusions per unit area. The number of inclusions per unit volume can be determined more easily than the shape of inclusions and the results are subject to fewer statistical errors.

A method to measure the length over width ratio is shown in the Fig. 1.7. The maximum length and width is considered. The number of inclusions per unit area can be determined by counting the inclusions observed microscopically in the full width of the microsection. The total number counted can later on be converted into inclusions per square millimeter. Since those sulphide inclusions which are greater than 0.005 millimeter in length are believed to be important for machinability(12), the inclusions which are 0.006 millimeter or greater in length should be counted as shown in Fig. 1.8. Inclusion length over width ratio increases with the increase of silicon percentage, i.e. the inclusion will be more of elongated type (Type III). Similarly, the number of inclusions per unit area increases as the percentage of silicon increases. This suggests that silicon affects the distribution of inclusions, which in turn controls the machinability.

The effect of percentage of sulphur on inclusion size, their number and variation of machinability is shown in the Fig. 1.9. Increased sulphur content improves machinability. Increased inclusion size decreases the number of inclusions per unit area but improves machinability. From the above discussions it may be concluded that the machinability index is affected by inclusion in three different ways, such as:

(i) larger inclusions in size favour machinability

(ii) higher sulphur content improves machinability

(iii) glassy oxide inclusions reduce machinability.

1.5 Leaded Steel

A good deal has been said by many authors about the improvement of machinability, as a result of adding a small percentage of lead. Leaded steels which are also resulphurized(2) have been given different opinions about their performance by different research workers. The approach of a few of them in this field is summarized here, and in subsequent chapters the author has given his comments based on his experiments on leaded steel.

Experiments by Norman Zlatin(13) have shown that the lead additives in medium carbon alloy steels result in appreciable increase in tool life for those steels having hardness of RC 30 or less. The advantage of lead addition in steel decreases as the hardness of steel goes beyond RC 30. At some point in the hardness range of RC 35 to 45 or higher, the presence of lead additive may be detrimental to tool life. However, appreciable improvement in surface finish is obtainable on medium carbon steel, regardless of the hardness of the steel.

Data collected by Chepto(14) have shown that the addition of sulphur and lead improves machinability characteristics in two ways. Firstly, by decreasing the amount of work done or energy required to form chip, and secondly by increasing the tendency for chip to curl and to form discontinuous chips, which helps in chip clearance and disposal. Presence of free-machining additives reduces the area of contact between chip and tool rake face, besides enhancing the tool performance. These additives also improve surface finish considerably.

Research work done by Lewis(15), has shown that the free-machining additives impart anti-seizure properties to steel, which in fact reduces the tendency for the formation of built up edge on the rake face of the cutting tool. This leads to better surface finish. Better machinability index of free-machining steels is due to the fact that MnS and lead inclusions reduce the friction between the chip and tool. The low coefficient of friction is due to low melting point of inclusions when compared with steel. They are considered as softening and tending to smear over the tool face at the normal cutting temperatures. This acts as a lubricant between two surfaces, and thus assists in preventing metal to metal contact.

Shaw's(16,17) experiments on leaded and non-leaded steels (0.14 C) have shown that lead addition reduces the formation of B.U.E. at all cutting speeds, irrespective of hardness and composition of steel. However, it has greatest beneficial effect upon surface finish at the values of cutting speeds below 100 ft/min.

Shaw(18,19) has also shown that leaded steel produces thinner and greater curled chips than the corresponding non-leaded steel chips. This results in a smaller area of contact between chip and cutting tool and lower frictional force. It may be concluded from his experimental results that lead is most suitable at high cutting speeds and sulphur is most suitable at speeds below 200 ft/min.

Unlike cutting fluids which cease to be effective in decreasing frictional force at a cutting speed of about 150 ft/min, lead continues to lower frictional force at all the speeds. However, cutting fluids continue to play an important role in cooling the tool to speeds beyond where they cease to lubricate the tool cutting edge. Cutting fluid can have a detrimental effect in the case of free-machining steels containing lead or sulphur by interfering with the action of these additives. Thus when cutting fluid is used in conjunction with an internal lubricant such as lead or sulphur, it is extremely important that the two be compatible. The external lubricant must not interfere with the action of internal lubricants by making it more difficult for these lubricants (internal) to spread over the surface of the chip.

Thompson[20] and his colleagues recently have done intensive experimental work on free-machining steels by using Scanning Electron Microscopy (S.E.M.) and Auger Electron Spectroscopy (A.E.S.). They have provided some insight into the effect of lead addition on machinability.

They found that lead exists in association with sulphide inclusions or as free lead particles. About 25 - 50% of the sulphide inclusions have lead tails. Leaded steel chips consist of alternate rough and torn areas and smooth areas. It was seen that lead is greater on the smooth areas than on rough areas. Rough areas which predominate on a non-lead chip surface, indicate localized welding and subsequent fracture by tearing, while smoother areas found on leaded steel chips correspond to simple sliding friction.

A.E.S. analysis of the leaded steel chips shows an existence of discontinuous lead film of approximately 20 - 40 Å in thickness. Such a layer also exists on the cutting edge used for cutting leaded steel. However, no such layer was found on the surface of non-leaded steel chips.

The summarized investigation shows that steels modified with free-machining additives, do render them free-machining, to exhibit superior machinability. It is of interest to examine what factors influence the effectiveness of additives in rendering modified alloys free-machinable. It is also noted from the above discussion that the chemistry of steel production cannot be separated from the mechanical metallurgy of the free-machining steel.

The available data for free-machining steels from the previous investigation has been controversial, and these studies have been unable to confirm the role of free-machining inclusions.

Thus, the purpose of this study was to ascertain the behavior of lead and MnS inclusions in leaded resulphurized low carbon steel (12L15). Non-leaded resulphurized low carbon steel (1215) was selected as a base for comparing the effects of lead on the machinability of 12L15, and plain low carbon steel 1018 was selected as a base for comparing the effects of both lead and manganese sulphide on the machinability of 1215 and 12L15.

CHAPTER II

CHARACTERIZATION OF EXPERIMENTAL MATERIAL

2.1 Introduction

The effect of free-machining additives on the mechanical properties of steel is a matter of obvious importance and in any event worthy of study. It is a well known fact that free-machining steels have a better machinability index when compared with steels with the same chemical composition but non-free-machining steels without free-machining additives. However, these additives might have some effect on the mechanical properties of the steel. Some research in this field has been conducted by various workers and is summarized as follows:

Lewis(15,21), investigated that these additives have very little or no effect on the mechanical properties of steel. Indeed, some results show a tendency for lead to actually improve the ductility and impact values of low carbon steel. Hardness and tensile values are unaffected.

Shaw(22) has also mentioned that the addition of lead has negligible effect on the mechanical properties of steel. Yield and ultimate stresses are decreased by less than five percent. However this insignificant decrease in strength is accompanied by an increase in ductility. The leaded steels have impact strengths that are of the order of 20 percent greater than those of corresponding non-leaded steels. Weaver's[23] experiments have shown that lead addition has no significant effect on hardness or tensile properties. The addition of lead has shown to give a somewhat smaller grain size to steel, than those of base steel, which may be due to the change in transition temperature.

Swinden[24] has done a comprehensive survey of the effect of lead addition (0.19%) to steel, containing 0.36% carbon, 1.43% manganese and 0.34% molybdenum. The leaded steels have slightly coarser grain size and less depth hardenability than the corresponding non-leaded steels when the specimens were taken in the form of flat or round bars. The notch bar impact toughness of the leaded steel at room temperature measured slightly less than that of non-leaded steel. However, at elevated temperature, both steels were found to have the same impact toughness values.

2.2 Steels Investigated

To determine the effect of free-machining additives, three different types of commercial purpose steels were selected. These are:

(i) AISI 1018 plain carbon steel

(ii) AISI 1215 resulphurized carbon steel

(iii) AISI 12L15 leaded resulphurized carbon steel

The chemical analysis of these were carried out; the calculated chemical composition is shown in the Table 2.1.

Table 2.1 Chemical Composition of Steels (wt%) Investigated

S. No.	AISI No.	C	P	S	Mn	Pb
i	1018	0.17	0.04	0.03	0.08	-
ii	1215	0.09	0.08	0.33	1.03	-
iii	12L15	0.08	0.07	0.33	1.05	0.24

To avoid the size and drawing effects on machining, test specimens of three types of steels were cold-drawn, 1½" in diameter and 3' in length.

2.3 Hardness

The above steels were selected in such a fashion that these have approximately the same hardness level. However, hardness of test specimens was measured at the centre, and near the surface along the direction of rolling. Data obtained by using Rockwell Hardness Tester (B-Scale) is shown below in the Table 2.2.

Table 2.2 Rockwell Hardness (B-Scale) of Three Steels

Measurement No.	AISI 12L15		AISI 1215		AISI 1018	
	Centre	Near the Surface	Centre	Near the Surface	Centre	Near the Surface
1	88.0	92.0	89.0	92.0	86.3	88.0
2	87.0	92.0	89.5	93.0	86.2	87.5
3	87.2	90.0	89.5	93.0	86.8	88.0
4	87.0	92.0	89.5	92.0	86.8	88.0
Average Hardness	87.3	91.5	89.4	92.5	86.5	87.6

2.4 Tensile Test Properties

The most important test to evaluate the mechanical properties of any steel is the tensile test. Tensile tests were performed on the INSTRON tensile testing machine (max. capacity 10,000 lbs.). Tests were carried out to determine yield stress, ultimate stress, percentage elongation and percentage reduction in area for the three kinds of steels. Three test specimens were taken for each steel. The dimensions of a test specimen are shown in Fig. 2.1. The test results obtained are shown in the Table 2.4 and the average values are shown in the Table 2.3 below.

Table 2.3 Results of Tensile Test for Three Different Steels (Average Value)

Steels	Percentage Elongation	Percentage Reduction in Area	Yield Stress psi	Ultimate Tensile Stress psi
12L15	15.9	51.8	66,200	72,400
1215	14.8	54.5	66,500	71,700
1018	18.2	58.7	72,400	75,500

Table 2.4 Results of Tensile Tests for Three Different Steels

Measurement No.	Initial Length L_1	Final Length L_2	Change in Length $L = L_2 - L_1$	Initial Diameter D_1	Final Diameter D_2	Change in Diameter $D = D_1 - D_2$	Percentage Elongation $\frac{L}{L_1} \times 100$	Percentage Reduction in Area	Yield Stress	Ultimate Tensile Stress
12L15										
1	1.9606	2.2768	0.3162	0.3486	0.2441	0.1045	16.3	50.90	67057.8	73658.8
2	1.9574	2.2468	0.2894	0.3472	0.2387	0.1065	14.8	52.73	65724.2	71737.5
3	1.9576	2.3034	0.3458	0.3475	0.2415	0.1060	16.7	51.70	65900.5	71699.7
1215										
1	1.9534	2.2246	0.2712	0.3478	0.2320	0.1158	14.0	55.50	66315.8	71578.9
2	1.9385	2.2261	0.2876	0.3464	0.2400	0.1064	14.8	51.99	66849.2	72154.7
3	1.9472	2.2480	0.3008	0.3472	0.2338	0.1134	15.8	54.65	66194.1	71406.2
1018										
1	1.8687	2.2226	0.3539	0.3498	0.2433	0.1065	18.9	51.62	72840.8	75962.5
2	1.9808	2.3333	0.3525	0.3455	0.2135	0.1320	17.8	67.79	72533.4	75733.4
3	1.9672	2.3178	0.3506	0.3497	0.2134	0.1363	17.9	62.76	71837.6	71752.7

2.5 Microstructure

To study the microstructure of the materials, specimens of the three different steels were taken in the longitudinal and transverse directions. They were mounted separately in bakelite for subsequent polishing. The samples were metallographically polished with diamond paste and etched in 2% Nital (2% nitric acid in alcohol). Photomicrographs at 600 magnification were taken.

Figs. 2.2 and 2.3 represent microstructure for 1018 steel in the longitudinal and transverse directions, respectively. Figs. 2.4 and 2.5 show the longitudinal and transverse section of 1215 steel. The steel has globular type inclusions and are probably of Type I. MnS inclusions have manganese-silicon tails, as it was verified by a Scanning Electron Microscope. Figs. 2.6 and 2.7 represent the microstructure of 12L15 steel in the logitudinal and transverse directions. Probably the MnS inclusions are of Type I. It was very difficult to locate the presence of lead in the steel. The lead phase in the AISI 12L15 steel exists in association with the sulphide inclusions or as free lead particles. It was determined by Thompson[20] that 25 - 50% of the sulphides have associated lead tails. The ratio of free lead particles to sulphide inclusions with lead tails, however, varies substantially with the method of counting, i.e. whether the strings of small lead particles are counted individually or collectively or whether the lead particles immediately adjacent to the sulphide inclusions with lead tails should be counted as free lead or as part of its parent lead tail. Thus, while meaningful percentages cannot be obtained, it can be stated that a significant volume of the total lead is present as free lead.

It is to be supposed that variations in the mechanical properties of three different steels is due to the variation in the basic compositions of these steels and is not necessarily due to the effect of free-machining additives.

CHAPTER III

EXPERIMENTAL PROCEDURE AND RESULTS

3.1 Tool Life and Its Measurement

3.1.1 Tool Life

Life of a cutting tool is defined as the useful cutting time between two regrinds (or indexing in the case of throw-away inserts). Tool change is required when the tool will no longer cut or does not satisfy dimensional, power and surface finish requirements. This happens due to gradual wear or chipping. A tool may fail due to any one of the following reasons:

(i) clearance or flank face wear

(ii) rake face wear or crater wear

(iii) plastic deformation of cutting edge

(iv) thermal cracking or mechanical chipping of the cutting edge

These modes of tool failure depend on the cutting conditions. Flank wear and crater wear are functions of cutting time and they increase with increase in cutting time. However, plastic deformation and thermal cracking can be avoided up to a certain extent with proper selection of tool and work material combination and also by selecting suitable cutting conditions i.e., speed, feed, depth of cut and tool geometry, etc.

3.1.2 Flank Wear

This often takes the form of an even band of wear on the flank face of the tool, the width of which can be measured with reasonable accuracy. Wear band is not always uniform. Often localized wear at one or more positions along the edge is several times greater than the average value. Flank wear occurs under almost all cutting conditions and is a function of speed, feed, depth of cut, and tool geometry.

3.1.3 Crater Wear

On the rake face of the tool, a cavity or crater frequently forms, at a short distance from the cutting edge. Once a crater is established, its depth grows more rapidly than its width. This weakens the tool close to the cutting edge and a major failure may occur by fracture from the crater to the clearance face. This is more likely under discontinuous cutting. Crater wear, however, may reduce cutting forces by increasing the effective rake angle of the cutting tool. Crater ratio was calculated for plotting the graphs.

$$\text{Crater Ratio} = \frac{\text{Maximum Depth of Crater}}{\text{Width of Crater}}$$

Width of crater is measured from the side cutting edge to the centre of the crater on the rake face.

The conventional laboratory method of tool life testing usually consists of machining with a cutting tool either until complete failure occurs, or to a predetermined amount of average or maximum flank wear, as measured with a toolmaker's microscope. In either case, the test requires a great deal of time and test material. This involves considerable cost in order to obtain a relatively small amount of tool wear data. For the present study, both flank wear and crater wear were measured. However, flank wear has been taken as the tool life criterion and crater wear was measured for comparison purposes only.

3.1.4 Tool Material and Tool Geometry

Ultra Capital 395, High Speed Steel (HSS) tools (1.25 C, 4.5 Cr, 5.5 W, 4.0 V, 4.5 Mo), from Balfour Darwin Ltd., were selected for tool life testing. HSS tool material was selected due to the following reasons.

(i) HSS tools are used in practice in a great majority of operations on free-machining steels and almost exclusively on screw type single spindle automatic lathes and on multispindle bar automatic lathes. This is so because a great part of tools used on these machines are form tools, chamfering, parting tools, drills and reamers all of which are not made of sintered carbide because of their complex form. Also, it is practically impossible to run the spindles of these machines at speeds high enough to obtain on the usually small diameters, cutting speeds suitable for carbides. Thus, the tests are carried out at conditions similar to those used mostly in practice.

(ii) Workpiece diameter was only $1\frac{1}{2}$" and due to limitations of spindle speed on the lathe, it was not possible to go beyond the cutting speed of 350 ft/min. This would be too low for carbide tools. Carbide tools have long tool life, especially when used for cutting free-machining steels. Therefore, the tests would take too long and too much test material would be needed. Fig. 3.1 shows the tool geometry for cutting tests. Tools were given proper angles on a universal grinding machine and sharp corners were removed with a fine grinding stone.

3.1.5 Tool Wear Test Procedure

To assess the tool life for three different kinds of steels, tests were performed on a heavy duty, Mazak Lathe, fitted with an infinitely variable speed spindle drive. Some tests were also performed on a SN 40 B/1000 Universal Lathe. During the cutting process, a 2% solution of TRIMOL from Metal Chemicals Canada Ltd. was used as a coolant. Other cutting specifications were as follows:

depth of cut $a = 0.050''$

feed $s = 0.006$ in/rev

tool = HSS 4" x $\frac{1}{2}$" x $\frac{1}{2}$"

rake angle = + 10°

side cutting edge angle = 0°

The cutting tests were performed at three different speeds, i.e.150, 200 and 300 ft/min. Cutting speed was measured with a friction wheel hand tachometer, designed to an accuracy of

2%. To measure the flank wear the cutting process was interrupted at regular intervals, and flank wear was measured with the help of a toolmaker's microscope.

Since the tool face crater frequently plays a major role in tool life studies, an instrument for recording the shape of the crater was devised. The device is shown diagrammatically in the Fig. 3.2. The tracing element is a Linear Variable Displacement Transducer (L.V.D.T.) with a pointed stylus end. The unit was fastened with a stand screwed on the base of a microscope. HSS tool with the rake face on the top was clamped on the surface plate of the microscope, below the L.V.D.T. stylus. By moving the surface plate horizontally, the L.V.D.T. needle deflected vertically. Vertical signals from the transducer were amplified with the help of Accutron Amplifier, Model 51. The amplifier was further connected to a two-dimensional x-y plotter for plotting the vertical displacement. Horizontal displacement (width of crater) was measured by clamping a small (30 k) potentiometer to the graduated drum of the microscope. Output from the potentiometer was fed to the x-y plotter as shown. After selecting the suitable magnification factor, the unit was calibrated for horizontal and vertical scales. Crater wear on the rake face of HSS tool was measured at the same time as the flank wear was measured. A specimen of the results obtained on two-dimensional x-y plotter is shown in Fig. 3.3.

Since the SN 40 B/1000 universal lathe is not fitted with an infinitely variable spindle drive, it results in a lower speed for the second pass, when compared with the first pass, and so on. Since all the test specimens of the three different steels had the same diameter and were cut under the same cutting conditions, the effect of reduced speed due to change in workpiece diameter was therefore of no importance for comparison purposes.

3.1.6 Discussion of Test Results

Figs. 3.4 to 3.6 represent the plots of average flank wear measured with the help of a toolmaker's microscope. Flank wear is plotted against the cutting time in minutes. These plots correspond to tests at cutting speeds of 150, 200 and 300 ft/min respectively. Only the cutting speed was changed from one test to another, whereas other cutting conditions were kept constant. Each test was repeated and the scatter is shown in the plots. Figs. 3.7 to 3.9 represent the plots of depth of crater wear, as measured with the x-y plotter. These plots are for cutting speeds of 100, 200 and 300 ft/min respectively. Figs. 3.10 to 3.12 represent the plots for crater ratio vs. cutting time in minutes at 100, 200 and 300 ft/min cutting speeds.

From the flank wear plots it is evident that free-machining steels have more tool life than the corresponding non-free-machining steels. Up to the cutting speed of 200 ft/min leaded steel (12L15) has less flank wear when compared with 1215 steel. However, at the cutting speed of 300 ft/min there is no significant difference between the flank wear of these two steels. Tests were repeated and almost the same values were obtained. It may be concluded from these tests that the addition of lead in resulphurized low carbon steel is useful in increasing the tool life of HSS tools only below the cutting speed of 300 ft/min, with the above-mentioned cutting conditions.

However, it should be noted that this critical speed of 300 ft/min where lead ceases to be effective in increasing the tool life of HSS tools may not be taken as a standard value. It is proposed that any change in cutting conditions, i.e. tool material, tool geometry, feed, depth of cut, etc. may give different results.

Only tool wear tests were performed with HSS tools. All other tests such as cutting forces measurement, built-up edge measurement, shear angle measurement and contact length measurement were carried out with carbide inserts. Though all these tests should have been carried out with HSS tools, to be in a position to correlate all test results, they were not done so by an oversight.

3.2 Measurement of Cutting Forces

3.2.1 Introduction

A knowledge of the cutting forces is required to assist engineers to design machine tools, jigs and fixtures, as well as to select economical cutting conditions. The measurement of cutting forces in machining corresponds to the analytical problem of determining the components of the general force fector in a chosen orthogonal co-ordinate system. The cutting forces that are exerted by a cutting tool on the workpiece are shown in Fig. 3.13. In 1945, Merchant(27) developed an analysis based on the thin shear plane model, and on the assumption of two-dimensional deformation (no side spread). The two force components F_v, tangential force, and another normal to the direction of cutting, F_f feed force are shown in the Fig. 3.14. Because it is impossible to measure the cutting forces at their actual original, the reactions have to be measured in a defined plane distant from the cutting edge. Therefore, a measuring system is required which measures correctly, and is independent of the point of application of the force and/or moments.

3.2.2 Piezo-Electric Principle

Certain crystals have the property that an electrical charge appears on their surfaces under mechanical stress. This is caused by the "piezo-electric effect" discovered by Curie in 1880[26]. For force transducers, quartz is one of the most suitable piezo-electric materials. The following three piezo-electric effects are observed in quartz[28].

(i) longitudinal effect

(ii) transversal effect

(iii) shear effect

The electrical charges appearing on the quartz surfaces are collected with electrodes and transformed by a charge aplifier into an analogue voltage.

3.2.3 Test Procedure and Results

Suitable cut quartz elements from Kistler mounted in a steel housing were used as force transducers. The steel housing is used to distribute stresses evenly over the quartz element and to hold the assembly dry and clean. A specially designed fixture to hold the transducers and the tool holder, named as force dynamometer was used. The two-component force dynamometer was calibrated by clamping the dynamometer assembly on a surface plate and using a cantilever beam system. The dynamometer was calibrated for both horizontal and vertical loading systems. Under the application of individual loading systems (horizontal and vertical) it was found that there was almost negligible cross-sensitivity (see Fig. 3.15) i.e. full load in any direction produces almost no reading in the other channel.

After calibration the dynamometer assembly was mounted on the Mazak Lathe, at the position of the tool post on the cross-slide. It was clamped properly for rigidity. To measure the magnitude of the cutting forces, following cutting conditions were selected:

depth of cut = 0.050"

feed = 0.0060 in/rev

cutting tool = carbide inserts (TPU-433, K-45)

tool holder = TP-43, with zero degree side cutting edge angle

Cutting tests were performed with and without cutting fluid. During the cutting process, voltage produced by the piezo-electric transducers was magnified by the individual charge amplifiers and was plotted on a multi-channel chart recorder. A specimen of plots obtained during cutting is shown in the Fig. 3.16.

Cutting tests were performed at the surface speeds of 50, 100, 150, 200, 250, 300 and 350 ft/min. To avoid tool wear effect on cutting forces, carbide inserts were changed after every three readings. Plotting was done after about one minute of cutting at all the speeds.

Readings from the plots were multiplied by their respective calibration factors and the resulting cutting forces were plotted. Fig. 3.17 represents the plot of cutting force (F_v) and feed force (F_f) in pounds against cutting speed for 12L15 steel with and without cutting fluid. Similarly, Fig. 3.18 and Fig. 3.19 represent plots for cutting forces vs. cutting speed for 1215 and 1018 steel, respectively.

Magnitude of cutting forces for 12L15 and 1215 steels does not change much with the change of cutting speed, especially after the surface speed of 250 ft/min. The magnitude of feed force is half or even less than half the magnitude of tangential force for all the steels. Fig. 3.20 and Fig. 3.21 is a comparison of cutting forces for three different steels. Forces for 1018 steel have the highest magnitude and lowest for 12L15 steel.

3.3 Built Up Edge and Its Measurement

3.3.1 Built Up Edge

According to Trent[29], in steel cutting, local pressure on the rake face of the tool may be greater than 100,000 lb/in^2. The surface temperature may be several hundred degrees. The clean metal surface is constantly being generated. The freshly cut chip and newly exposed material on the rake face of the tool have an affinity for each other, and a layer of highly compressed material adheres to the tool face. Such a formation is known as Built Up Edge (B.U.E.).

At frequent intervals, pieces of the B.U.E. topple from the pile and adhere to the work surface or pass off with chip.

The fragments of B.U.E. are the main cause of surface roughness of the cut surface. Built up edge, to some extent protects the cutting edge and changes the effective rake angle.

3.3.2 Test Procedure and Results

Built up edge experiment was performed at cutting speeds of 15, 70, 100, 140, 200, 300 and 350 ft/min. During the experiment, feed and depth of cut was kept constant. For each reading, cutting was done for approximately two minutes, and the height of B.U.E. was measured with a toolmaker's microscope. Other machine settings were as follows:

depth of cut = 0.050"

feed = 0.006 in/rev

tool = carbide insert (TPU-433, K-45)

With Coolant

Four readings were taken for each speed, and the average value was considered for plotting. Fig. 3.22 represents the plot of height of B.U.E. vs. cutting speed for three different kinds of steels. AISI 1018 steel has the highest amplitude of B.U.E., and has maximum value at the cutting speed of 100 ft/min. It decreases with the increase of cutting speed, i.e. height of B.U.E. is a function of cutting speed. There is not much difference in the formation of B.U.E. for 12L15 and 1215 steels. However, for 1215 steel, B.U.E. has shown increasing trend with the increase of speed; this probably dictates that manganese sulphide promotes B.U.E. formation at high speeds. Though the surface roughness was not measured it could be qualitatively stated that 12L15 had the best surface and 1018 steel the worst.

3.3.3 Discussion of Test Results

The formation of B.U.E. on the rake face of the cutting tool changes the effective rake angle of the tool. Increase in rake angle reduces the cutting forces. The B.U.E. has the highest magnitude for 1018 steel at the cutting speed of 100 ft/min (Fig. 3.22), and the cutting forces are lowest at this speed (ref. Fig. 3.20 and 3.21). However, the change in the magnitude of cutting forces is not in the same proportion as the change in the formation of B.U.E. There is not much B.U.E. formation for 12L15 and 1215 steels and that is why the variations in the cutting forces for these steels is less.

3.4 Shear Angle and its Measurement

3.4.1 Shear Angle

Many theories of metal cutting have used the concept of shear plane. This is represented by a line inclined at angle (ϕ) to the direction of cutting. Angle (ϕ) as shown in the Fig. 3.14 is known as the shear angle. The significance of shear angle lies in the fact that it indicates to some extent the machinability properties of a work material. According to Enahoro and Welsh[30], high values of shear angle indicate large ranges of continuous chips, good surface finish and low cutting forces. Low shear angle values are associated with small ranges of continuous chips, poor surface finish and large cutting force. But during the normal cutting processes shear tends to occur over a finite zone, and thus it is not an accurate practical test for machinability. In addition to this, shear plane solutions do not generally take account of important factors such as material properties and cutting speed, etc.

There are basically two methods to determine the shear angle of the cutting process. Firstly, shear angle can be measured with a quick stop device to freeze the chip during cutting process, and later on magnify it with a microscope. A second method is a theoretical method and is given by[27]

$$\tan \phi = \frac{\frac{t_1}{t_2} \cos \alpha}{1 - \frac{t_1}{t_2} \sin \alpha} = \frac{r \cos \alpha}{1 - r \sin \alpha}$$

where

ϕ = shear angle

t_1 = undeformed chip thickness

t_2 = deformed chip thickness

α = rake angle of cutting tool

$r = t_1/t_2$ = is known as chip thickness ratio

3.4.2 Test Procedure and Results

A quick stop device as shown in the Fig. 3.23 was used in order to interrupt the cutting process instantaneously. The quick stop device was clamped on the cross-side of heavy duty Mazak Lathe. A Ramset Piston-Set tool (gun) was used to accelerate the tool holder, resting on the shear pin of 1/4" diameter. Green colour cartridges which gave a velocity of 225 ft/sec to the piston, were used. Other cutting conditions were as follows:

depth of cut = 0.050"

feed = 0.006 in/rev

tool = carbide inserts (TPU-322, K-45)

cutting fluid = none

This technique leaves the chip on the workpiece in the same position as it is during the cutting process. A section through the frozen chip was taken and was embedded in epoxy. The sliced samples were metallographically polished and were etched for 45 seconds in 2% Nital. Photo-micrographs at 150 times magnification were taken with the use of a metallurgical optical microscope.

Figs. 3.24 to 3.26 represent the photo-micrographs for 12L15 steel at the cutting speeds of 100, 200 and 300 ft/min respectively. It was found that there was no B.U.E. formation and the shear angle increased with the increase of cutting speed. Similarly, Figs. 3.27 to 3.29 are for 1215 steel and Figs. 3.30 to 3.32 are for 1018 steel. There was a B.U.E. formation for 1018 steel, up to the cutting speed of 200 ft/min.

Shear angle for different steels and at various cutting speeds was measured and is plotted in the Fig. 3.33. It has the highest magnitude for 12L15 steel and the lowest for 1018 steel. It increased with the increase of speed, except for 1018 steel up to the cutting speed of 200 ft/min. This inconsistent result for 1018 steel is probably due to the formation of built up edge. Theoretical values of shear angle have also been calculated and are shown in Fig. 3.33.

3.4.3 Discussion of Test Results

Steel 12L15 has a higher value of shear angle at all the cutting speeds , when compared with 1215 and 1018 steels. 1215 has higher values than 1018 steel. Shear angle for both 1215 and 12L15 increases with the increase of speed. These results are in line with the previous tests, and show that the machinability index of low carbon steel increases with the free-machining inclusions.

However, for 1018 steel, shear angle decreases with the increase of cutting speed, and starts increasing only after the cutting speed of 200 ft/min. This inconsistency for 1018 steel is probably due to the formation of B.U.E. on the rake face of the tool. The decrease in value of shear angle is accompanied by increase in chip thickness (see Fig. 4.1).

Dotted line on Fig. 3.33 shows the plot of calculated values of shear angle against the cutting speed. The only variable factor for calculating the shear angle values was chip thickness. Chip thickness at various cutting speeds was measured. The average measured value of chip thickness is plotted against the cutting speed in Fig. 4.1.

The difference in the calculated and measured values of shear angle may be due to the errors in measurement of chip thickness and measurement of shear angle. It is possible that difference in calculated and measured values of shear angle may also be due to the change in cutting tool, i.e. chips were collected during the tool wear tests performed with HSS tools, whereas quick stop experiments were performed with carbide inserts.

3.5 Contact Length and its Measurement

3.5.1 Introduction

The role which contact length plays in affecting the tool chip friction force and cutting temperature was first pointed out by Trigger(31) in 1951. Later on extensive work done by Shaw(22) indicated that the magnitude of friction force between chip and tool is determined primarily by the size, number and strength of minute welds along the contact length. The quantity and size of these welds depend on the contact length. For a given workpiece and tool geometry, the friction force between chip and tool is a good measure of the tendency for a chip to weld to the tool. When such welding occurs, particles of built up edge are left behind on the finished surface. Invariably, decrease in friction force is accompanied by improvement in surface finish.

3.5.2 Test Procedure and Results

The chip tool contact length for three different kinds of steels was measured at various cutting speeds. Cutting tests were performed at the feed of 0.006 in/rev, depth of cut 0.050 in. Carbide inserts TPU-433, K-45 were used for cutting tests. A thin coating of copper sulphate was applied on inserts by dipping them in dilute solution of copper sulphate for 15 minutes. The cutting was performed for at least one minute for each reading. For each measurement a new cutting edge coated with copper sulphate was used. The wipe-down length of copper sulphate on the tool rake face was measured with the help of a microscope. Three readings were taken for each speed, and average value was considered for plotting. Fig. 3.34 represents the plot of contact length vs. cutting speed for the three steels. AISI 12L15 steel has the lowest amplitude of contact length and the highest is for 1018 steel. The chips produced during this test were tightly curled for 12L15 steel, whereas chips for 1018 steel were straight and long in size as shown in Fig. 3.35.

The free-machining steel chips are seen to have greater curl than the corresponding non-free-machining steel chips, and hence, the smaller area of contact between chip and tool. Tightly curled chips may result in reduced length of contact, and frictional force, which is compatible with the previous discussion.

CHAPTER IV

A DISCUSSION ON TEST RESULTS

To augment the information directly obtainable from the cutting tests, several specialized investigations were performed, seeking the causes of advantages obtained by the free-machining additives.

The first investigation was a microscopic comparison of free-machining and plain steel chips. The chips obtained at various cutting speeds were mounted in plastic and ground until a representative longitudinal cross-section was obtained. The specimens were etched in 2% Nital, and photomicrographs were taken. An examination of these photomicrographs reveals the following differences for free-machining steel chips, when compared with plain steel chips.

(i) decreased chip thickness

(ii) decreased roughness at the back of the chip

(iii) decreased "wipe-down"

4.1 Decreased Chip Thickness

The free-machining additives in steel are seen to have decreased chip thickness during cutting process. Fig. 4.1 represents the measured comparative chip thickness of three different kinds of steel at various cutting speeds. Leaded steel (12L15) chips are thinner than the non-leaded steel chips (1215 and 1018). Similarly for the same cutting speeds, resulphurized steel chips are thinner than plain steel. These results are in confirmation with the results of shear angle. The increased shear angle for free-machining steel reduces the chip thickness. It is also seen from the Fig. 4.1 that chip thickness reduces with the increase of cutting speed. Research work done by Lewis[15,21] has shown that the non-leaded steel chips intersect the uncut surface in a more or less sharp manner, indicating that shear is confined to the narrow zone ABB´ (see Fig. 4.1a). The leaded steel, on the other hand, appears to shear over a broader zone ABB´´, more especially at higher cutting speeds. In view of this difference the mechanism is developed in the following manner. The increase in volume ABB´´, over which the strain occurs should tend to decrease the cutting energy per unit volume, as a consequence of size effect. This state of affairs suggests that part of the benefit which is associated with the addition of free-machining additives may be attributed to an increase in volume, undergoing shear at any one time and not only due to a reduction of friction between chip and tool.

4.2 Decreased Roughness at the Back of The Chip

Microscopic comparison of free-machining and plain steel chips have shown that the chips from free-machining steels have less roughness at the back. Probably this is also a function of shear angle. Further, probably MnS inclusions and finely dispersed lead particles act as stress concentration; the number of active planes could be increased. Shear strain in each plane is reduced, thereby producing softer and more homogeneous chips. The decreased roughness of the free-machining steels could be a direct result of this mechanism.

4.3 Decreased Wipe-Down

Wipe-down pertains to the curvature of the chip grain deformation lines on the tool side of the chip, caused by secondary shear at the tool chip interface. The plain carbon steel chips have nearly constant wipe-down with increased speed, as shown in Figs. 4.2 to 4.4, though at the lower cutting speed (100 ft/min), plain steel has shown slightly more wipe-down. Resulphurized steel (1215) has comparatively smaller wipe-down at the cutting speed of 100 ft/min, and has increased wipe-down with the increase in the cutting speed as shown in the Figs. 4.5 to 4.7. However, leaded steel (12L15) has almost negligible wipe-down at the cutting speed of 100 ft/min as shown in Fig. 4.8 and has increased wipe-down with the increase of cutting speed (see Figs. 4.9 and 4.10). At the critical speed of 300 ft/min, it has almost the same wipe-down as steel 1215 has at 300 ft/min, i.e. there is no difference in wipe-down between 12L15 and 1215 steels at the cutting speed of 300 ft/min.

The decrease in wipe-down by the addition of free-machining additive in steel (especially lead below critical speed) is direct evidence that the shear stress has decreased and the action is less of plastic nature.

In addition to the above microscopic analysis of chips, it is found that free-machining steels frequently give well-broken chips, as shown in Fig. 3.35. The reason why free-machining steels produce small size chips, probably can be found in the fact that lowering the coefficient of friction between the tool and chip by any means causes the chip to curl more tightly. Coefficient of friction is directly related to the frictional force between the chip and the rake face of the cutting tool. The frictional force on the tool face can be calculated with the formula (refer fig 3.14)[27]

$$F = F_v \sin\alpha + F_f \cos\alpha$$

where

F = frictional force in lbf.

F_v = cutting/tangential force in lbf.

F_f = feed force in lbf.

α = rake angle of cutting tool

Since the tangential and feed forces have been measured for + 6° rake angle at various cutting speeds. Using these values, the frictional force was calculated and plotted against cutting speed in Fig. 4.11 shown. Free-machining steels have lower values, as compared to the plain steel (1018) and 12L15 steel has lower friction force, when compared with 1215 steel.

The low frictional force and hence, low coefficient of friction values for free-machining steels may lead to propose that free-machining additives act as lubricants at the tool chip interface. They smear out between the chip and tool to form a lubricating layer. This action would probably provide a low shear strength material[17] between chip and tool, and thus assist in preventing metal to metal contact. This allows a free-sliding of the chip over the tool face, which reduces the tendency to form a built up edge.

The free-machining additives can be compared with cutting fluids. The most important methods of altering the tool chip friction is by introducing a low shear strength material between the high points of the sliding surfaces. This can be accomplished in two ways - by the use of cutting fluids or by the use of free-machining additives in steel.

A cutting fluid reduces friction by reacting on the high points on the chip or tool to form a low shear strength layer that is not easily pushed aside. A good fluid will be perfectly stable towards all metals with which it comes in contact under ordinary conditions of temperature and pressure, but must react quickly under the high pressures and temperatures encountered at high points on the chip. Like cutting fluids, free-machining additives are thought to involve the formation of low shear strength contaminating films at points of contact and in this way may be referred to as "internal lubricants". This designation emphasizes an important difference between a cutting fluid and a free-machining additive. For a fluid to be effective it must penetrate to the tool point, and then react to form a low shear strength film. These are both time-consuming processes and it is not surprising to find that cutting fluids are far more effective in decreasing chip tool friction at cutting speeds below 100 ft/min. Since the free-machining additives are present on the chip surface when it is formed, the important time of penetration is saved and these materials are generally useful in reducing friction at higher speeds than are cutting fluids.

4.4 Investigation on Effect of Lead

Before proceeding to discuss lead as a free-machining additive, it is found that elementary lead has several unusual properties, that are of interest in connection with its role as a free-machining additive. These include(22):

(i) a low melting point (621°F)

(ii) a low shear strength (about 5% that of steel)

(iii) a high coefficient of thermal expansion, second only to zinc (16.3×10^{-6} in per in per degree F for lead as compared to 6.3×10^{-6} for steel).

(iv) a low surface tension in molten state

(v) a low viscosity in the molten state (1.7 centipoises at 700°F compared with 1 c.p. for water at room temperature).

(vi) lead is completely insoluble in iron and steel and oxides of lead are insoluble in lead itself.

As seen from the tool life tests, lead addition in resulphurized low carbon steel improves the tool life of HSS tools up to the cutting speed of 300 ft/min. Further tests carried on 12L15 steel have shown that lead reduces the cutting forces, chip thickness, contact length and increases the shear angle. It appears that lead smears on the tool rake face, and provides lubrication at the tool chip interface.

It cannot be pointed out exactly why lead ceases to improve the tool life at the cutting speed of 300 ft/min. Probably, effectiveness of lead is a function of tool temperature. Tool rake face temperature increases with the increase of speed. Lead has a low melting point and probably it is in the molten state at higher speeds. Due to its low surface tension and low viscosity in the molten state and due to high stresses on the tool rake face lead is probably squeezed out, thus reducing its effectiveness.

However, it is seen that lead is effective in reducing the cutting forces, contact length and chip thickness even at the cutting speed of 300 ft/min. This inconsistency in its performance may be due to the change in cutting tool, since the tool wear tests were performed with HSS tools and cutting forces and other tests were performed with carbide tools. If all the tests would have been carried out with HSS tools, it might have been possible to arrive at a single critical speed, where lead ceases to be effective in improving tool life, reducing cutting forces, chip thickness, contact length and increasing shear angle. A different critical point may exist if tests are performed with carbide inserts or any other change in the cutting conditions.

The critical speed displayed by leaded steel is important when it is to be considered for some specific machining operations and to determine optimum cutting costs. Therefore, it is advantageous to be able to determine the approximate location of the critical point as a function of the machining variables.

The commonly used relation for tool temperature is[32]:

$$Q_T = mF_V\left(\sqrt{\frac{V}{f}}\right) \cdot \left[\frac{0.069}{d\sqrt{k\rho c}}\right] \quad (1)$$

where

Q_T = tool temperature, degrees C

m = constant

V = cutting speed, ft/min

f = feed, in/rev.

k = thermal conductivity of workpiece, cal/cm. degrees C.sec

(1.0 BTU/ft.hr.degrees F = 0.004133 cal/cm. degrees C. sec)

ρ = density of the workpiece, gram/cm^3

(1.0 lb/in^3 = 27.68 grams/cm^3)

c = specific heat of workpiece, cal/gram degrees C

(1.0 BTU/lb. degrees F = 1.0 cal/gram degrees C)

d = depth of cut, inches

F_v is the tangential force and is expressed by relation

$$F_v = Co\ f^a d^b \tag{2}$$

where

Co is function of strength of material

a and b are constants

Combining (1) and (2),

$$Q_T = m\ Co\ f^a d^b \sqrt{\frac{V}{f}} \times \left[\frac{0.069}{d\sqrt{k\rho c}}\right]$$

$$\frac{Q_T}{m} = 0.069\ Co\ f^{a-\frac{1}{2}} d^{b-1} \sqrt{\frac{V}{k\rho c}}$$

$$\left(\frac{Q_T}{m}\right)^2 = \left(0.069\ Co\ f^{a-\frac{1}{2}} d^{b-1}\right)^2 \frac{V}{k\rho c}$$

$$V = \left(\frac{Q_T}{m}\right)^2 \frac{k\rho c}{(0.069\ Co f^{a-\frac{1}{2}} d^{b-1})^2}$$

assuming V attains critical value when lead ceases to be effective at a constant temperature (Q_T).

Replacing $(\frac{Q_T}{m})^2$ by another constant, say K,

$$V_{critical} = K \frac{k\rho c}{(0.069\ Co\ f^{a-\frac{1}{2}} d^{b-1})^2}$$

It can be seen that the critical speed varies indirectly with the square of the strength of the workpiece material. Usually constant, a is double the value of b, showing that the critical speed is affected more by the feed, than by the depth of cut.

An examination of the crater wear obtained on the 1215 and 12L15 steels revealed that the cratering on the face of the tool was greater when the leaded steel was machined.

This condition is not unusual, since the use of lead results in more tightly curled chips which may have more tendency to cause a cratering type of tool wear. Normally, this cratering effect is of no serious consequence; however, it is detrimental when very hard metals are being cut. The net effect of cratering on the face of the tool is to increase the rake angle and thereby reduce the strength of the cutting edge. When the work material is very hard, there is a tendency for the cutting edge to chip off, as the cratering becomes pronounced. Under these circumstances, tool life on the hard leaded steels may be less than on hard plain steels.

The above discussion may be a helpful method of determining when the leaded steel can be applied to increase the tool life. Because the cost of leaded steel is greater, it is not always true that higher life is sufficient to substantiate its use.

CHAPTER V

SUMMARY AND CONCLUSIONS

The objectives of the present study were to examine the effects of free-machining additives in plain low carbon steel. Experimental investigations over a range of cutting conditions were carried out. Three different types of steel were selected, i.e., plain carbon steel (AISI 1018), resulphurized carbon steel (AISI 1215), and leaded resulphurized carbon steel (AISI 12L15). To avoid the size and drawing effects on machinability, the test specimens of these steels were of the same dimensions and were of cold-drawn steels. The experimental procedures and test results have been discussed in the previous chapters. The following summarized observations in explaining the effects of additives in free-machining steels are in order.

The selected steels were found to have almost the same hardness level. The tensile test experiments have shown that these steels are not different from each other in terms of yield stress, ultimate stress,percentage elongation, and percentage reduction in area. The microscopic analyses of these steels have shown that the free-machining steels (12L15 and 1215) have globular type of MnS inclusions, and are probably of Type I MnS inclusions. The lead phase in the leaded steel exists in association with sulphide inclusions or free lead particles.

Tool wear tests performed using HSS tools at various cutting speeds have shown that the free-machining steels have a longer tool life as compared to the plain carbon steel for all cutting speeds. Leaded resulphurized steel has a better tool life than resulphurized steel, but only below the cutting speed of 300 ft/min. At the cutting speed of 300 ft/min there is hardly any difference between the tool life of these two steels. It may be concluded that addition of lead (0.24 wt. %) in resulphurized low carbon steel is a useful additive in improving the tool life of HSS tools only below a certain critical speed. The value of critical speed may change according to the cutting conditions, i.e, feed, depth of cut, tool and workpiece material, and tool geometry.

An examination of crater wear plots indicates that leaded steel has a greater tendency to form crater wear on the rake face of the cutting tool, even below the critical speed. This condition is logical, since leaded steel produces more tightly curled chips, which probably have a greater tendency to cause cratering type of tool wear. Normally, this cratering is of no serious consequence; however, it may be detrimental when very hard materials are being cut.

The measured cutting forces and the calculated frictional force are signficantly lower for free-machining steels. These forces have the highest magnitude for plain carbon steel and lowest for leaded steel, for all the cutting speeds.

The higher friction force is indicative of higher frictional energy dissipation at the tool chip interface. Consequently, a higher tool chip interface temperature is expected in plain carbon steel and hence, this steel is prone to more tool wear (thermally induced) compared to free-machining steels.

Further evidence of improvements in machinability as a result of free-machining additives in steels were revealed by a comparison of height of built up edge and surface finish produced. From the experimental data, it was revealed that there is negligible built up edge formation for both the free-machining steels. Built up edge formation was maximum for 1018 steel, and has maximum height at the cutting speed of 100 ft/min, decreasing with the increase of speed. Since built up edge formation is the main cause of surface roughness, qualitatively, leaded steel had the best surface finish and very poor surface finish was obtained for the 1018 steel under the test conditions. The chips from free-machining steels were shown to have a greater degree of curl than the corresponding non-free-machining chips, and hence, have a smaller apparent area of contact between the chip and the tool.

Microscopic analyses of chips produced at various cutting speeds have shown that free-machining steels have decreased chip thickness, decreased roughness at the back of chips and decreased wipe-down. The chip thickness is lowest for 12L15 steel and highest for 1018 steel, and it decreases with the increase of speed for all the steels. The lower values of chip thickness is due to the increased shear angle for free-machining steels. The plain carbon steel chips have nearly constant wipe-down at all the cutting speeds. Resulphurized steel (1215) has a comparatively smaller wipe-down at the cutting speed of 100 ft/min, and has increased wipe-down with the increase of cutting speed. However, leaded steel has almost negligible wipe-down at the cutting speed of 100 ft/min and there is no difference in wipe-down between 12L15 and 1215 steels at the critical cutting speed of 300 ft/min. The low value of wipe-down for free-machining steel probably reveals that action is less of a plastic nature.

However, it is important to note that tool life tests were performed with HSS tools and all other tests were performed with carbide tools. Thus, a meaningful co-relation between the tool life tests and other tests may not be possible. The critical speed of 300 ft/min, where lead ceases to be effective in improving tool life for resulphurized low carbon steel, should be considered only for HSS tools. It probably will have different critical speed when using carbide tools.

Thus, in conclusion, it can be pointed out that:

(i) Free-machining additives in plain carbon steel may be referred to as "internal lubricants" and unlike cutting fluids, they are effective at all the cutting speeds. They smear out between the chip and tool to form a lubricating layer. This action provides a "sandwich filling" of a low shear strength film between the chip and tool, thus preventing metal to metal contact, and allowing free-sliding of the chip over the cutting tool rake face. The friction coefficient of the tool chip interface is lowered. The frictional energy dissipation is lowered; consequently, lower interface temperature and lower wear will result. Thus, the addition of free-machining additives in steel considerably improves machinability.

(ii) Resulphurized steel further modified with addition of lead (12L15) is a distinctly superior free-machining steel compared to straight resulphurized steel (1215), but only below a certain critical speed. It is proposed that the critical speed is directly related to the tool temperature, which is a function of cutting variables, such as feed, depth of cut, tool material, tool geometry and work material.

LIST OF FIGURES

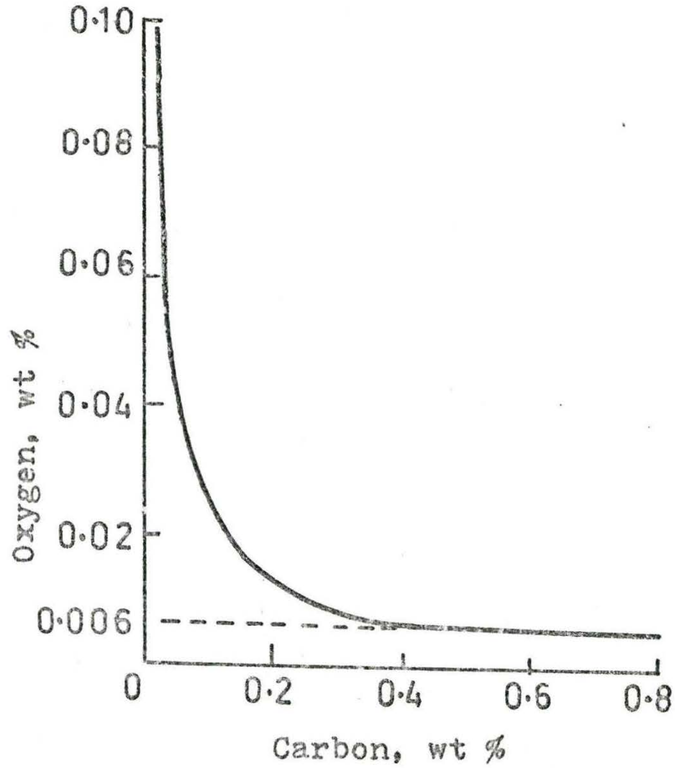

Fig. 1.1 Carbon-Oxygen Relationship

(Ref.I. "The Making Shaping and Treating of Steel.)

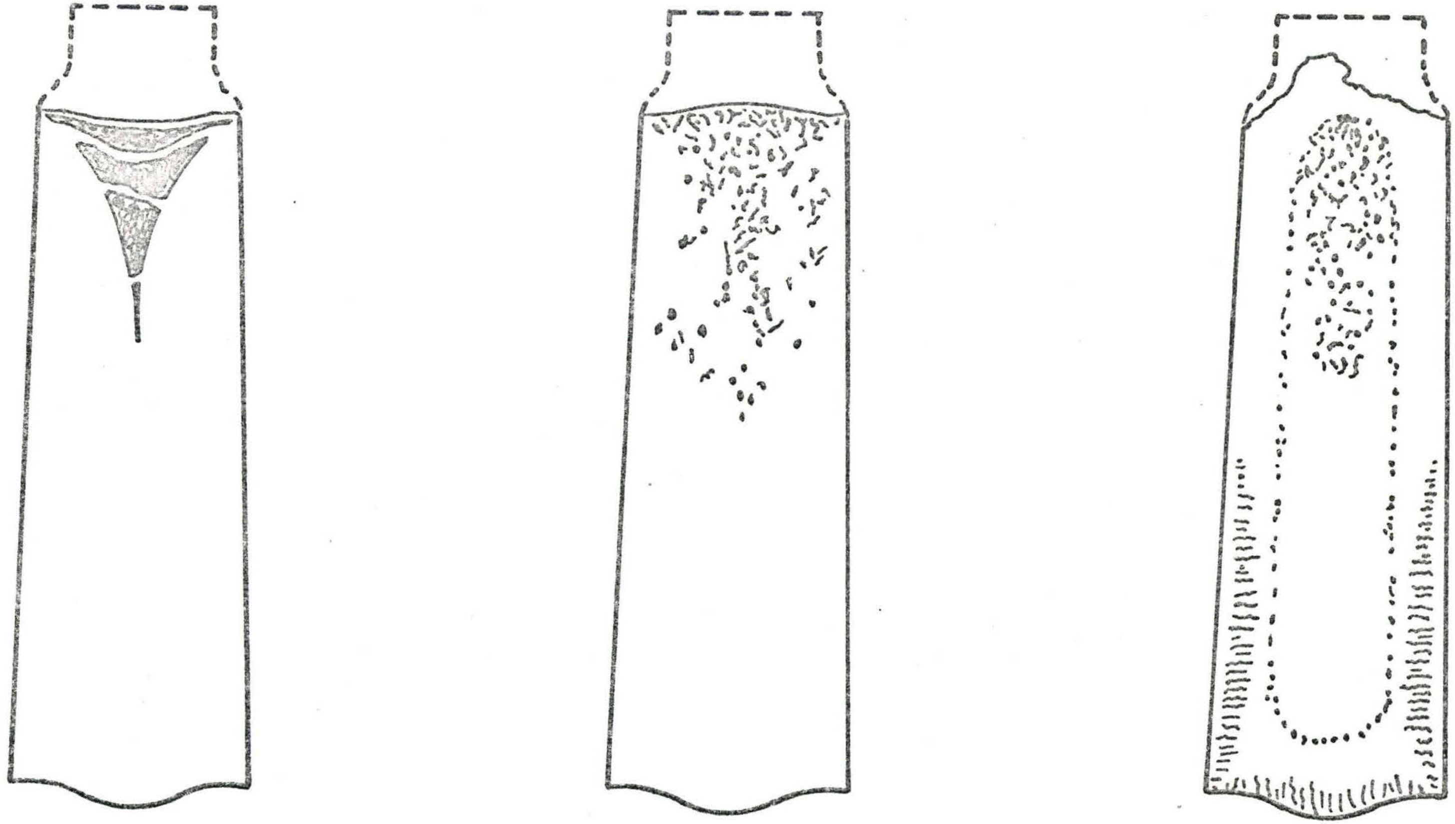

Fig. 1.2. Ingot Structures of Killed, Semi-killed and Rimmed Steel.

(ref. 9.)

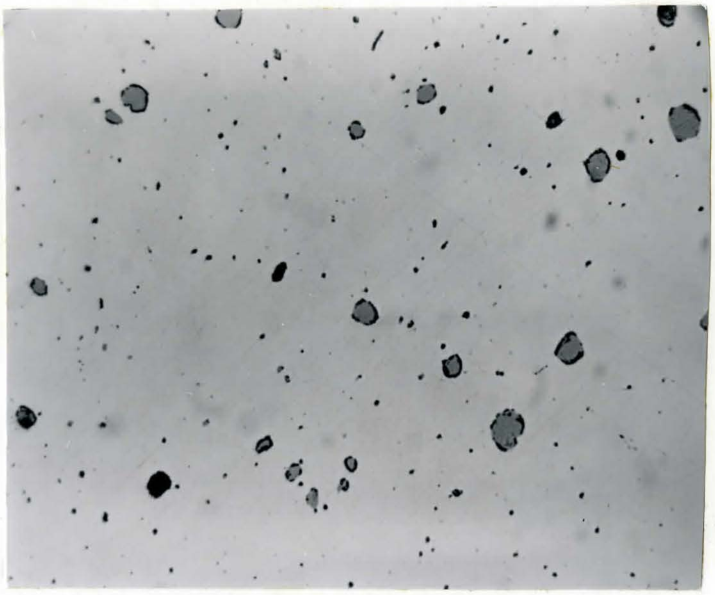

Fig. 1.3. Type I MnS Inclusions in Leaded Resulphurized Carbon Steel.

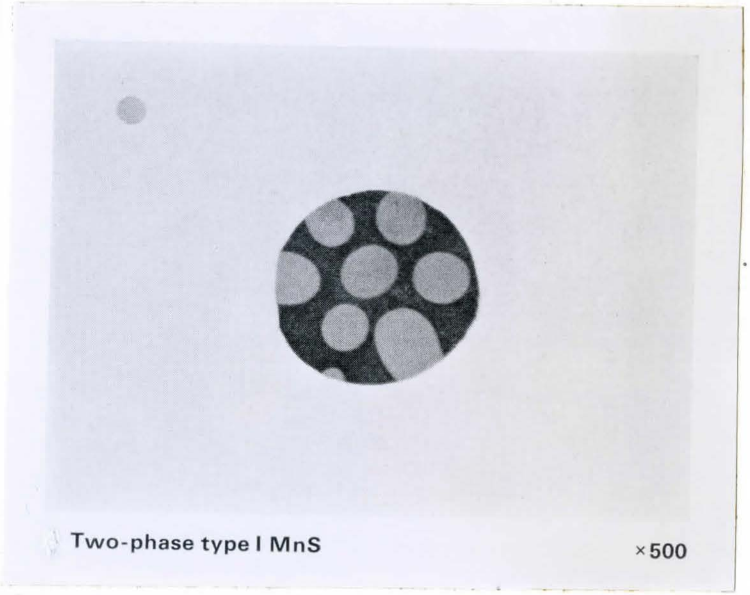

Fig. 1.4. Two-Phase Type I MnS Inclusions. (ref. 4)

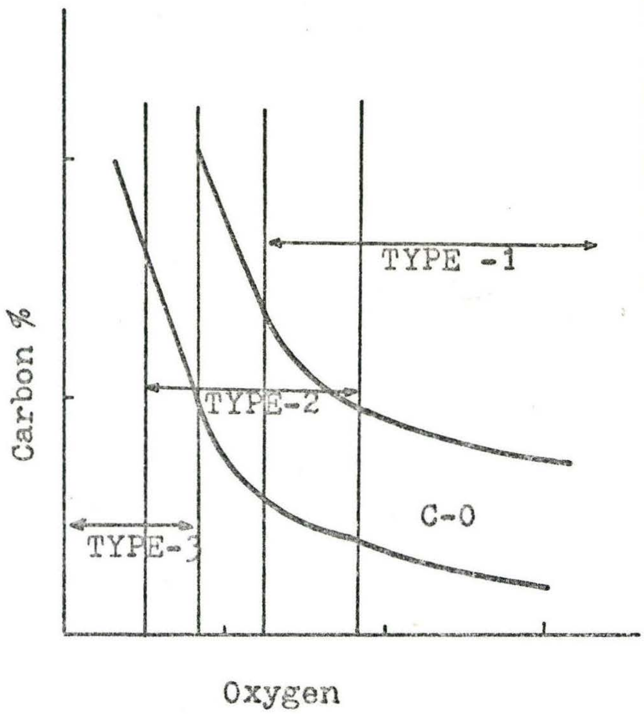

Fig. 1.5 Carbon, Oxygen, and Sulphide type diagram.

(ref. 5.)

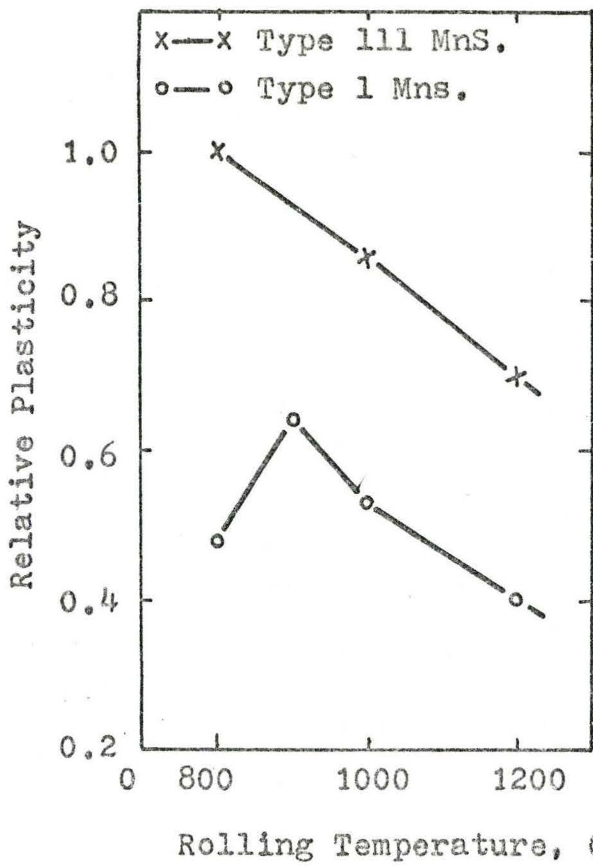

Fig. 1.6 Effect of Rolling Temperature on Relative-Plasticity* of MnS Inclusions.

(ref. 10.)

* Relative Plasticity is defined as the ratio of the inclusion true strain to the steel true strain.

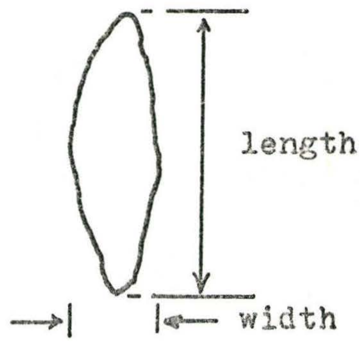

Fig. 1.7 Method to Measure the Shape of Inclusions.

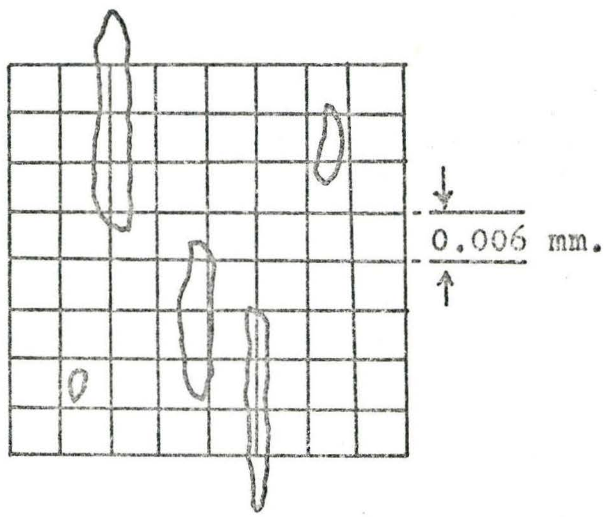

Fig. 1.8 Method to Count the Number of Inclusions.

(ref. 12)

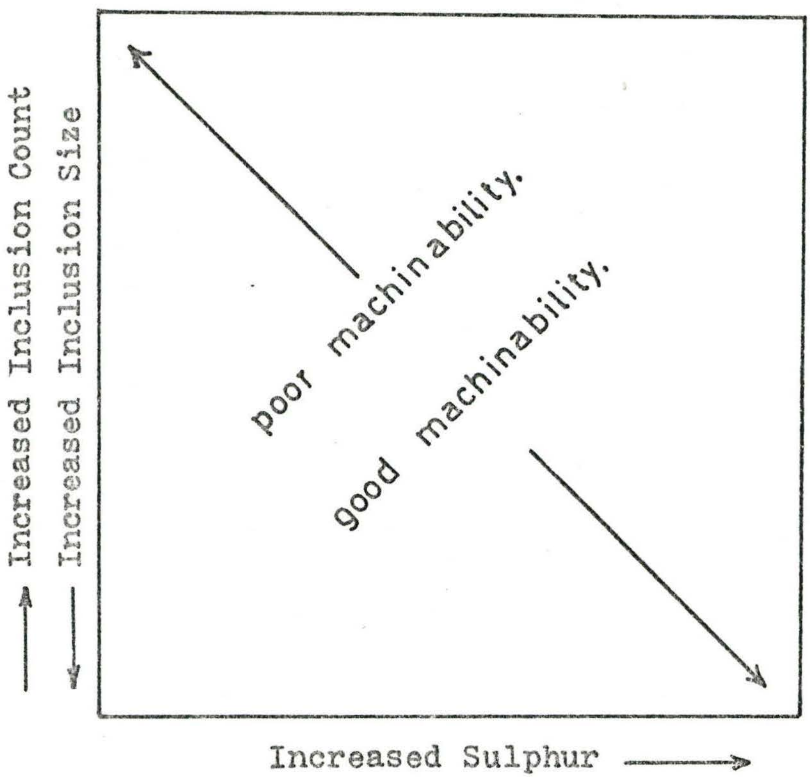

Fig. 1.9. Schematic Representation of the Dependence of Machinability Upon Sulphur Content and Inclusion Count, or Size.

(ref. 12.)

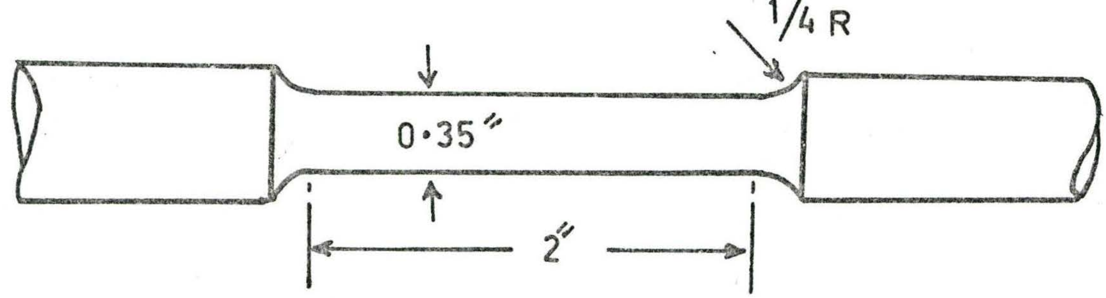

Fig. 2.1. Dimensions of Tensile Test Specimen.

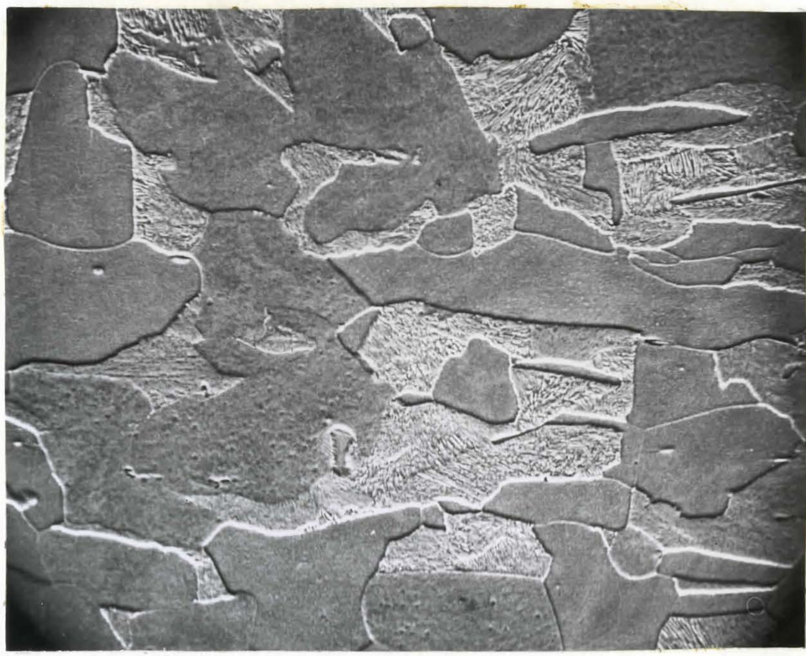

Rolling Direction

X600

Fig. 2.2. Microstructure of AISI 1018 Steel in the Longitudinal Direction.

X600

Fig. 2.3. Microstructure of AISI 1018 Steel in the Transverse Direction

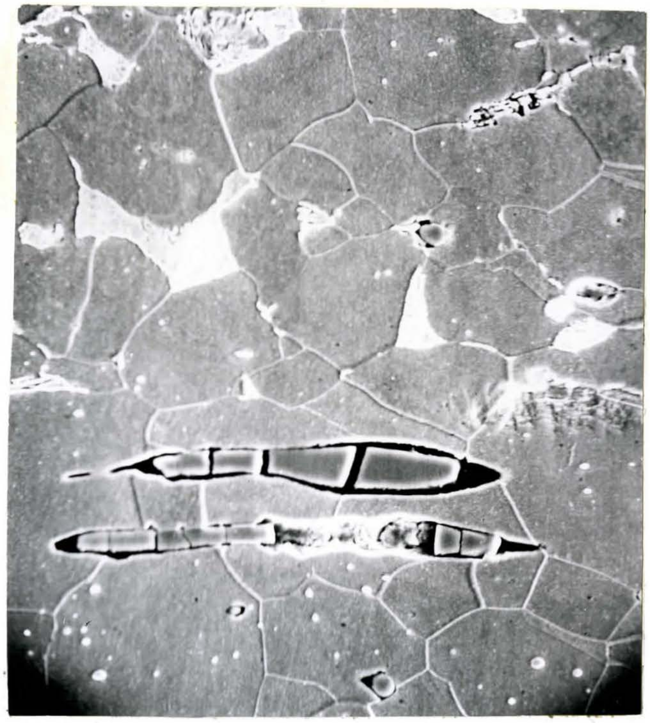

Rolling Direction.

X600

Fig. 2.4. Microstructure of AISI 1215 Steel in the Longitudinal Direction.

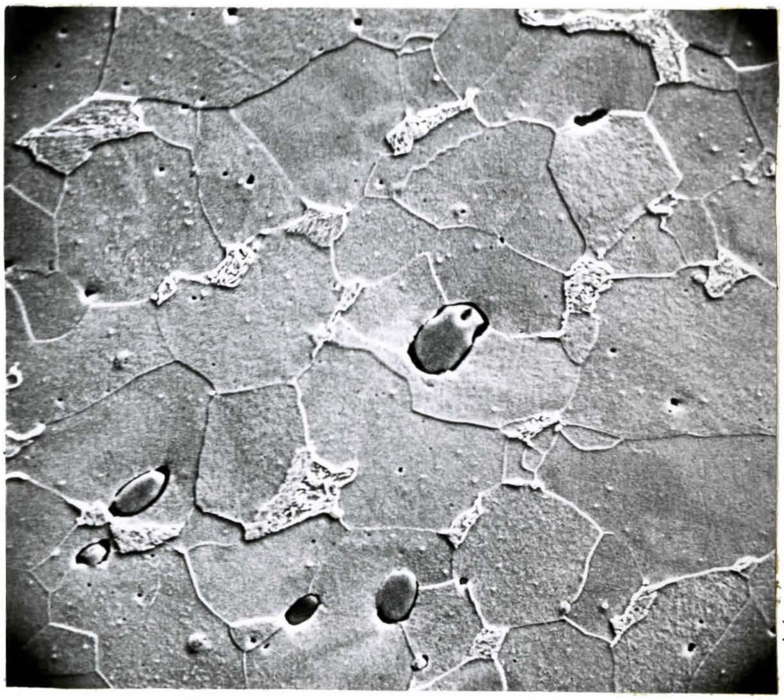

X600

Fig. 2.5. Microstructure of AISI 1215 Steel in the Transverse Direction

Rolling
Direction

X600

Fig. 2.6. Microstructure of AISI 12L15 Steel in Longitudinal Direction.

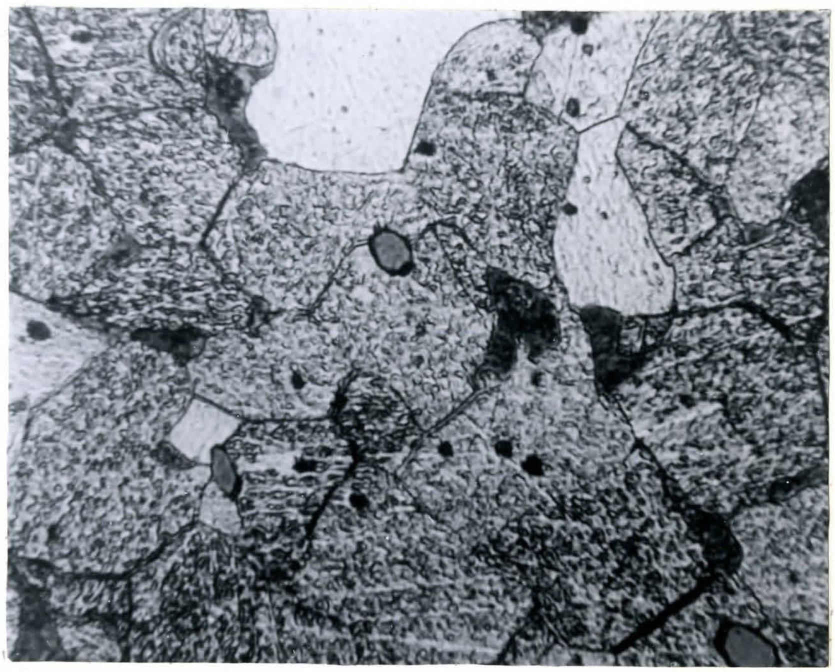

X600

Fig. 2.7. Microstructure of AISI 12L15 Steel in Transverse Direction.

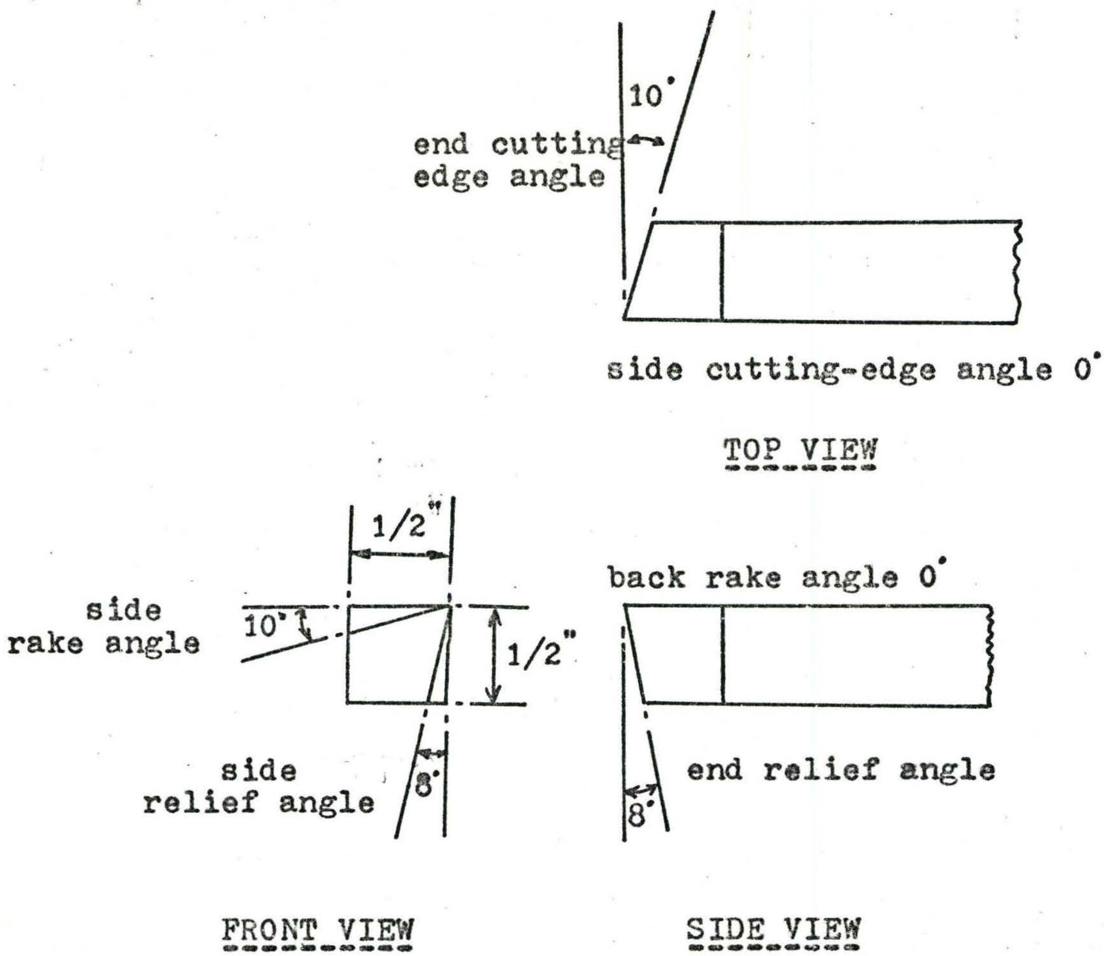

Fig. 3.1 HSS Tool Geometry for Tool Wear Tests.

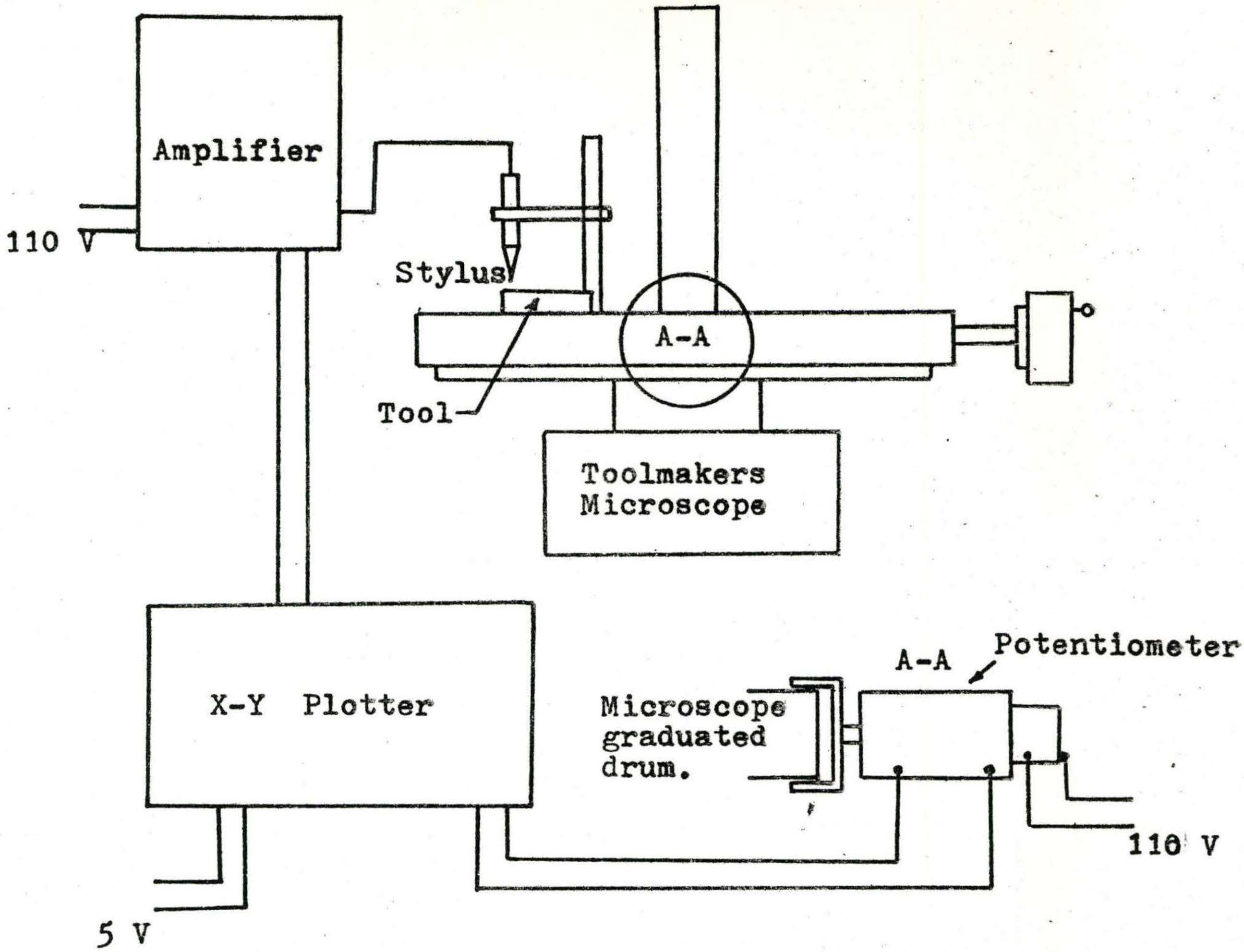

Fig. 3.2 Diagrammatic Sketch of Instrument Used for Recording Tool Face Crater Shape and Depth.

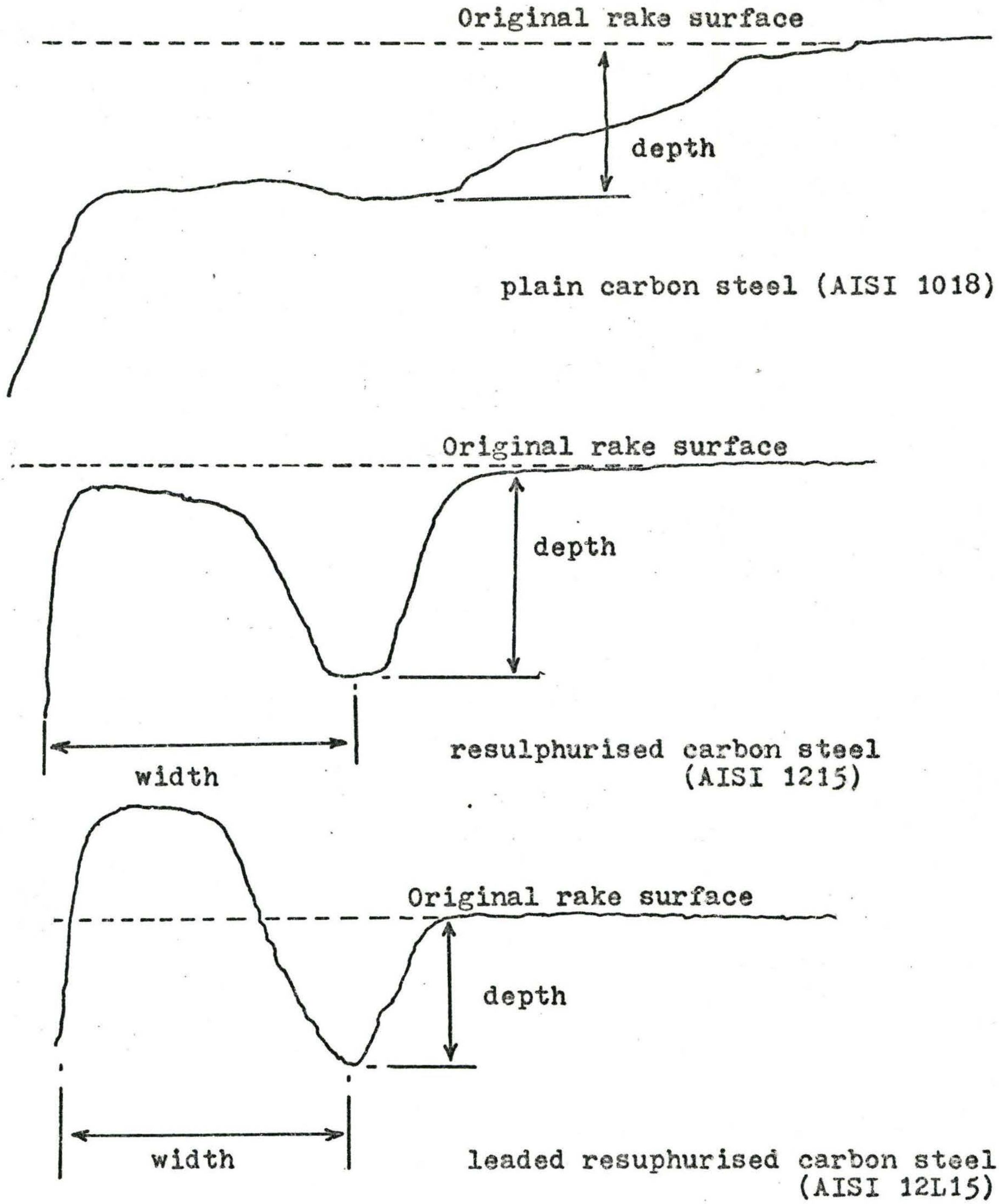

Fig. 3.3 Specimen of Crater Wear Trace on H.S.S. Tool after 8 min of cutting time, at the cutting speed of 200 ft/min., depth of cut 0.050 in., feed 0.006 in/rev.

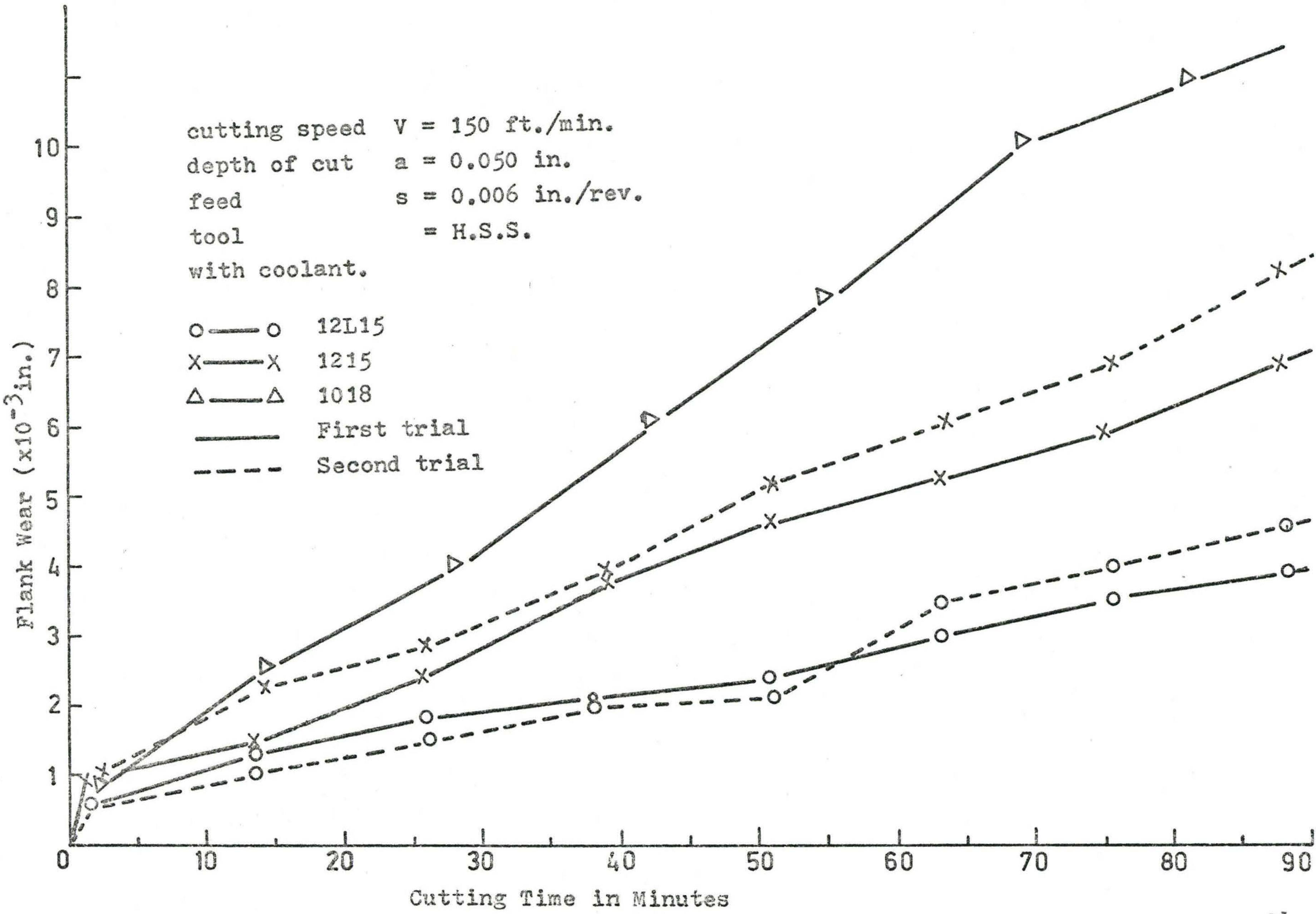

Fig. 3.4 Flank Wear (average value) Versus Cutting Time.

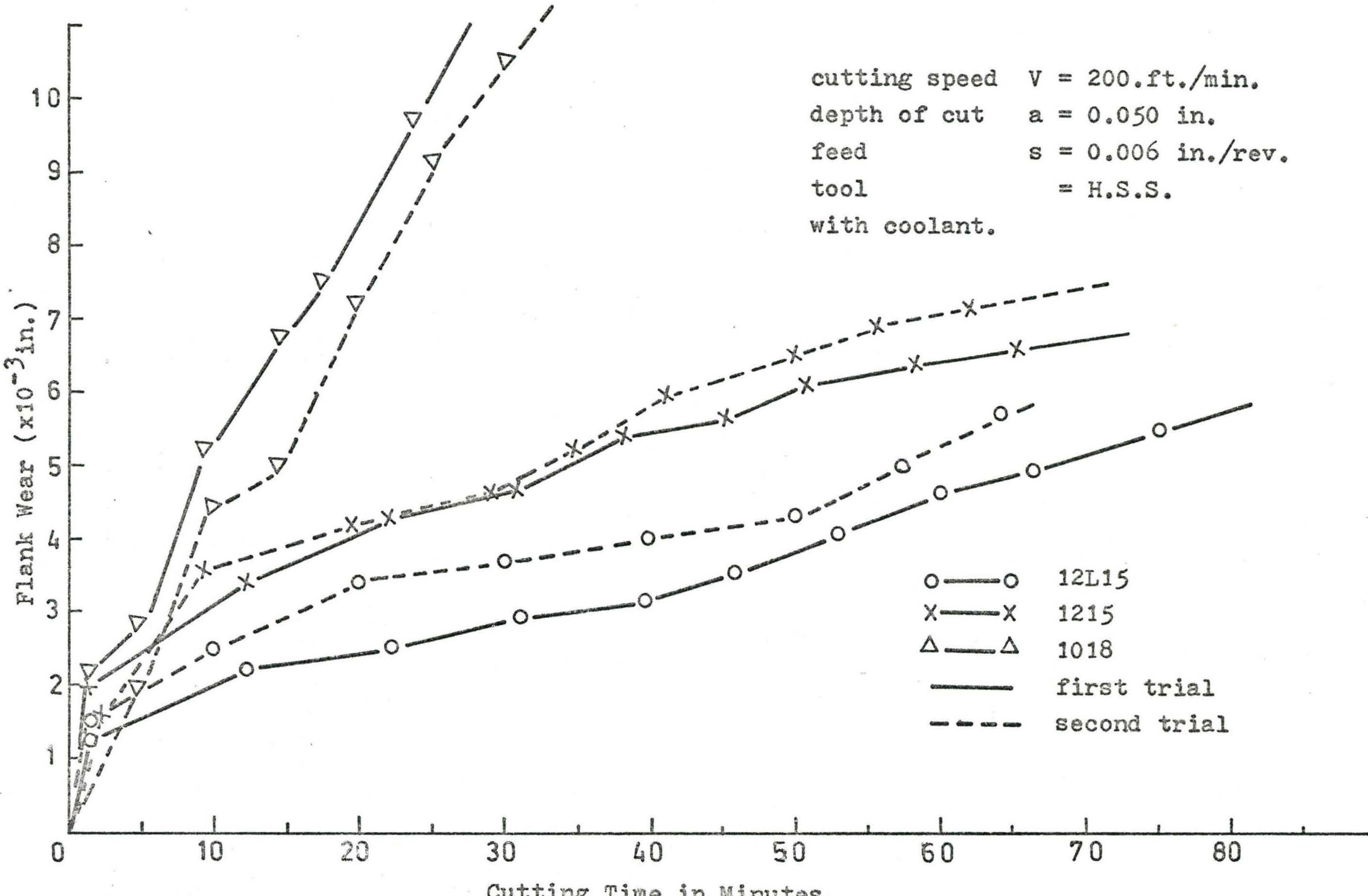

Fig. 3.5. Flank Wear (aveage value) Versus Cutting Time

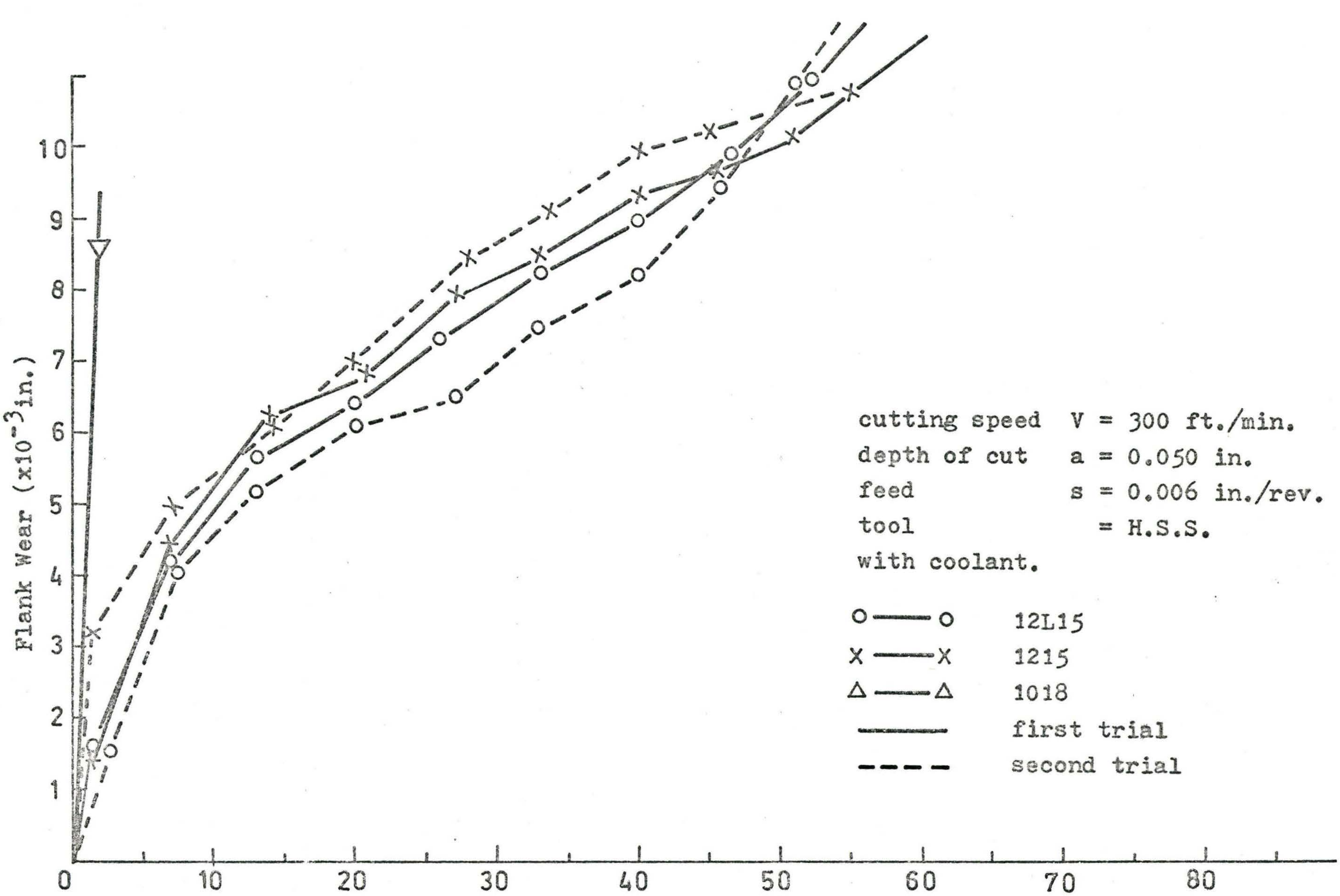

Fig. 3.6. Flank Wear (average value) Versus Cutting Time.

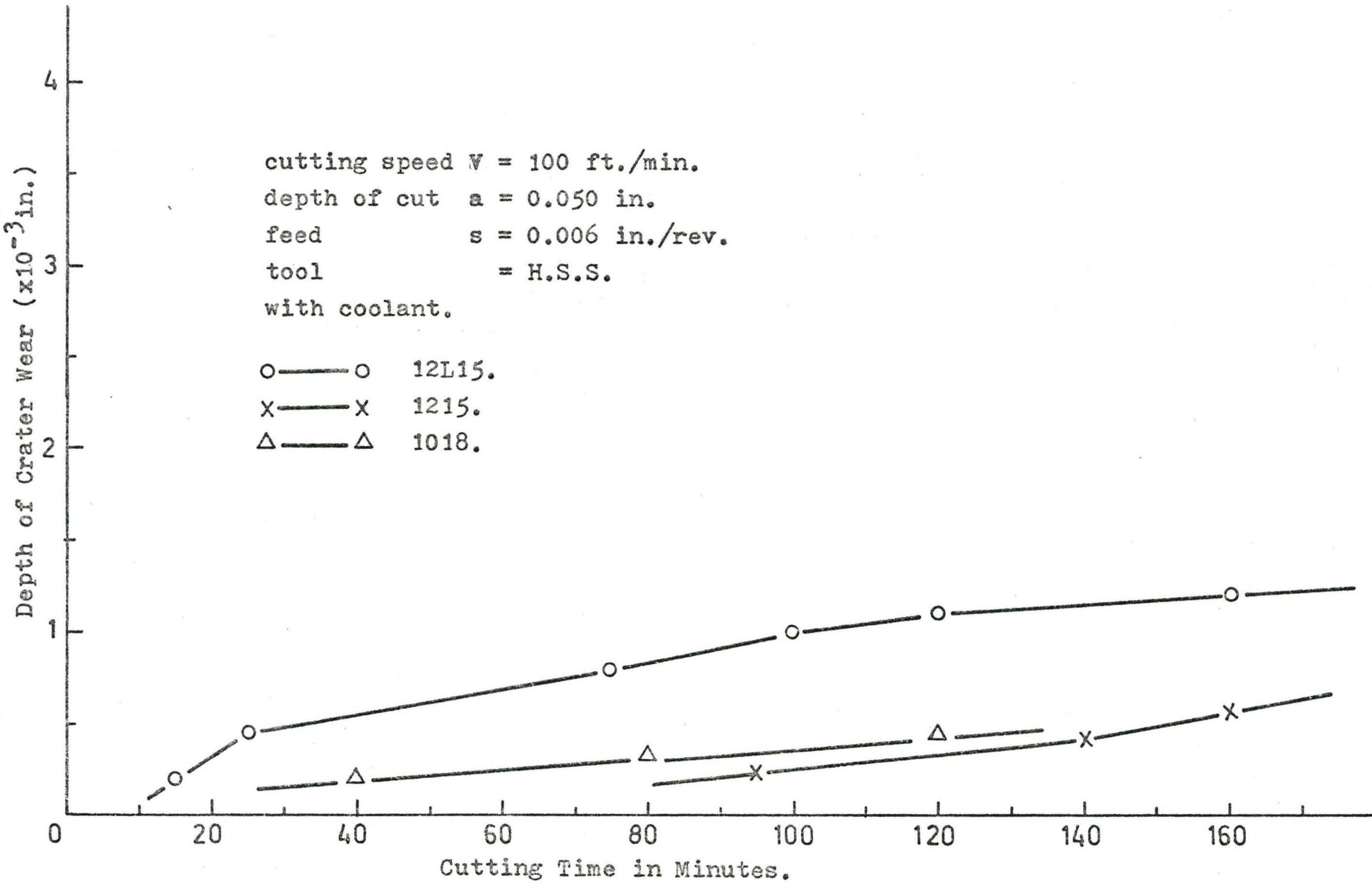

Fig. 3.7. Depth of Crater Wear Versus Cutting Time

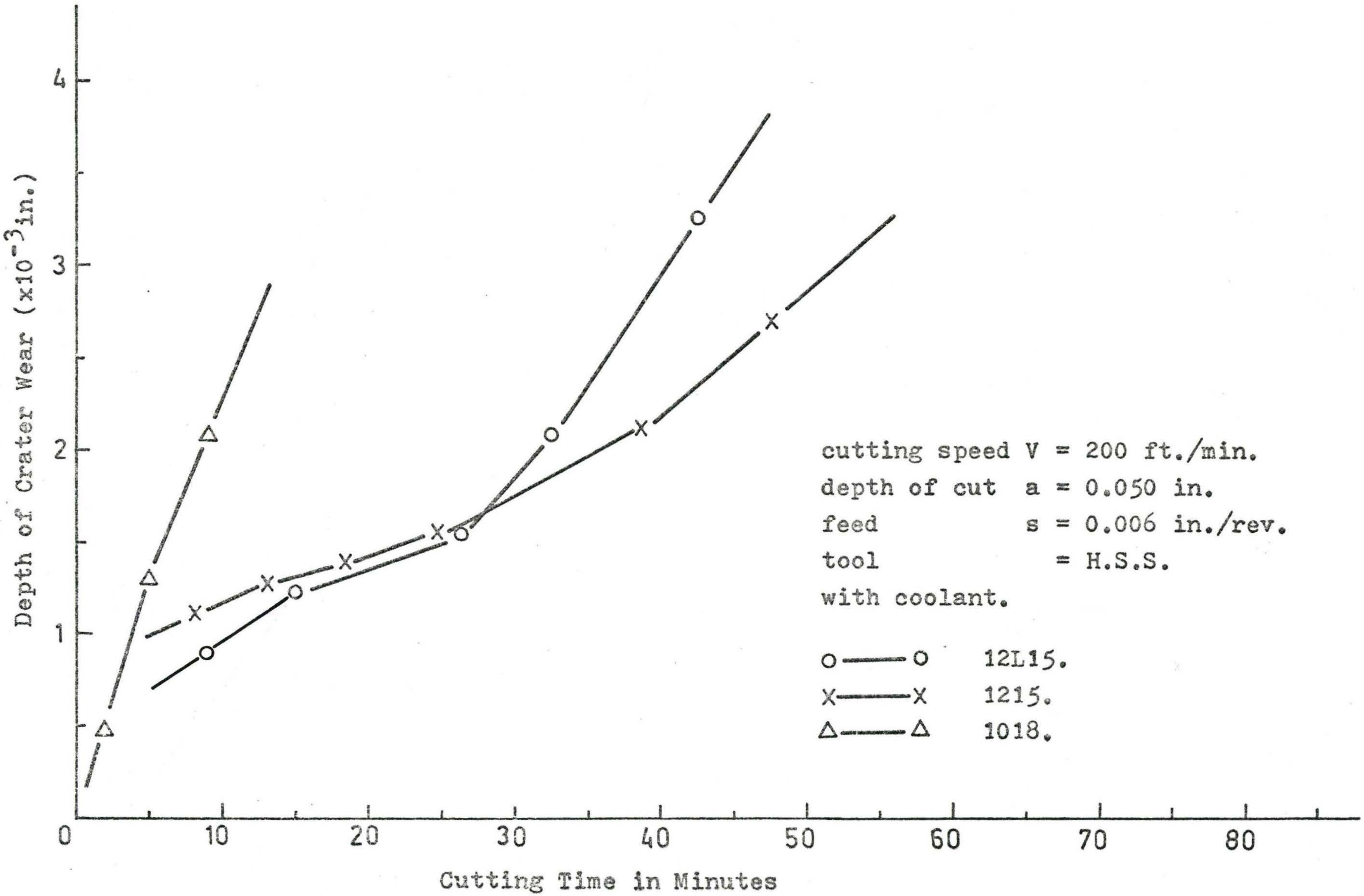

Fig. 3.8 Depth of Crater Wear Versus Cutting Time.

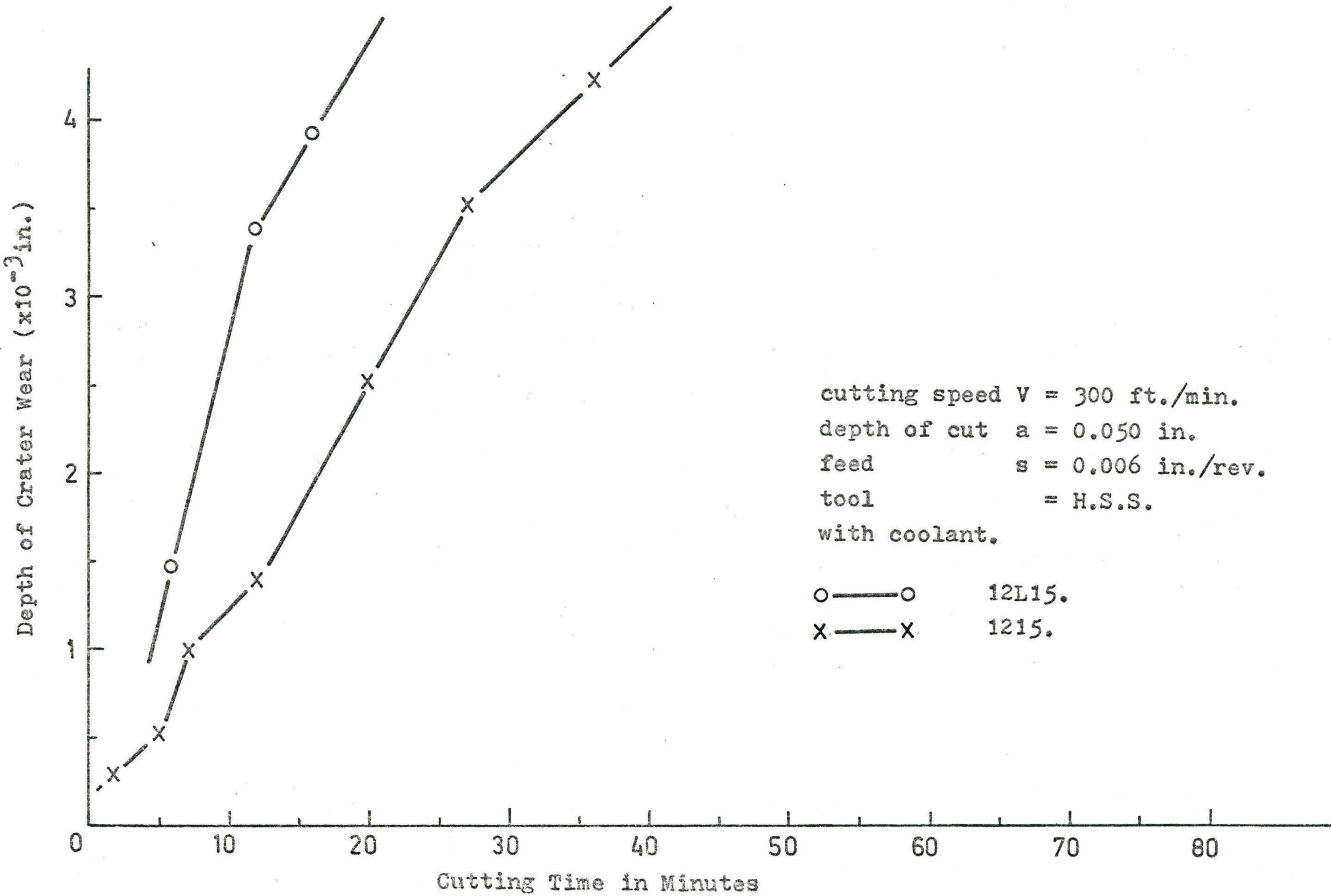

Fig. 3.9 . Depth of Crater Wear Versus Cutting Time.

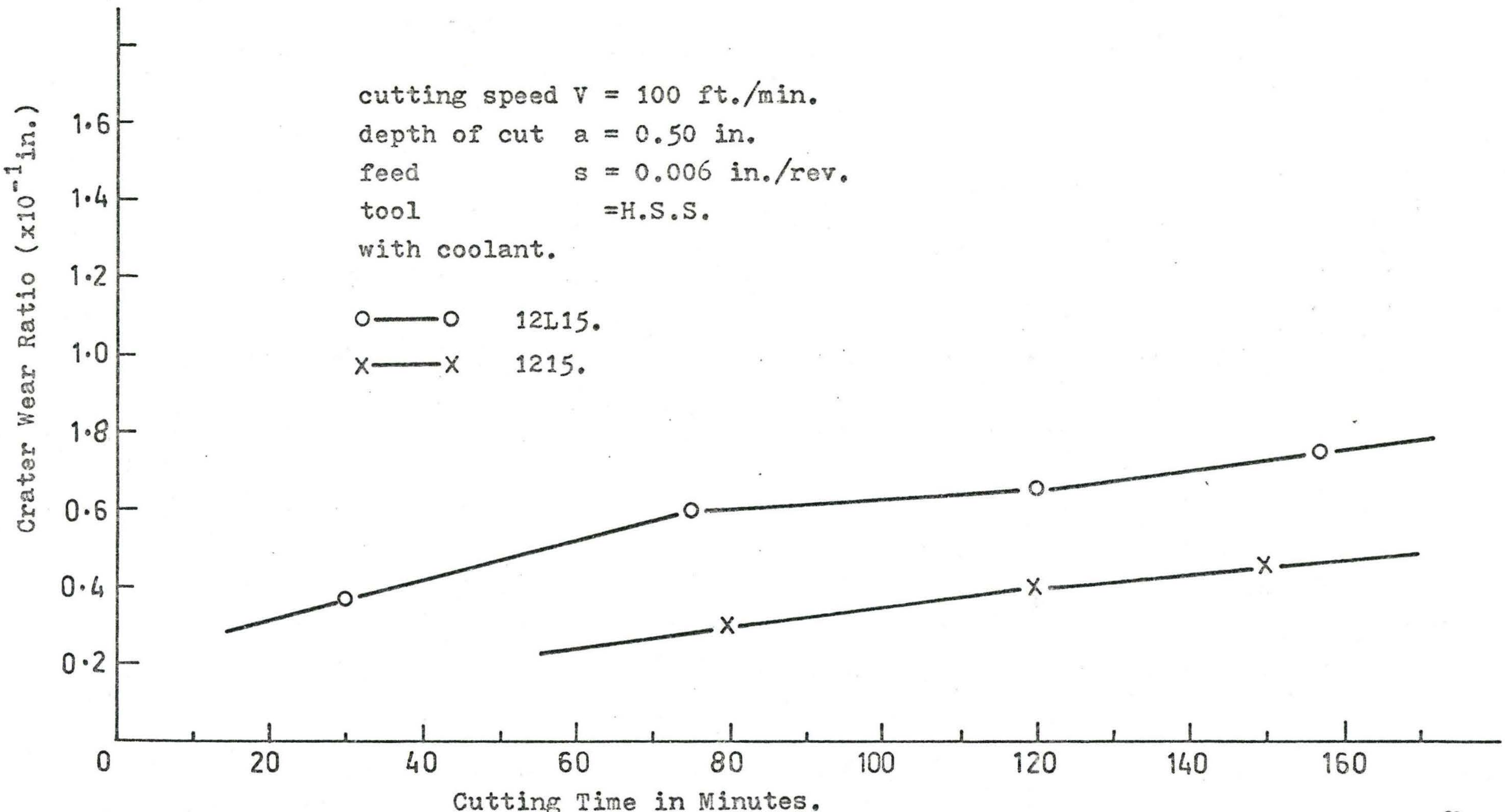

Fig. 3.10 CraterWear Ratio Versus Cutting Time.

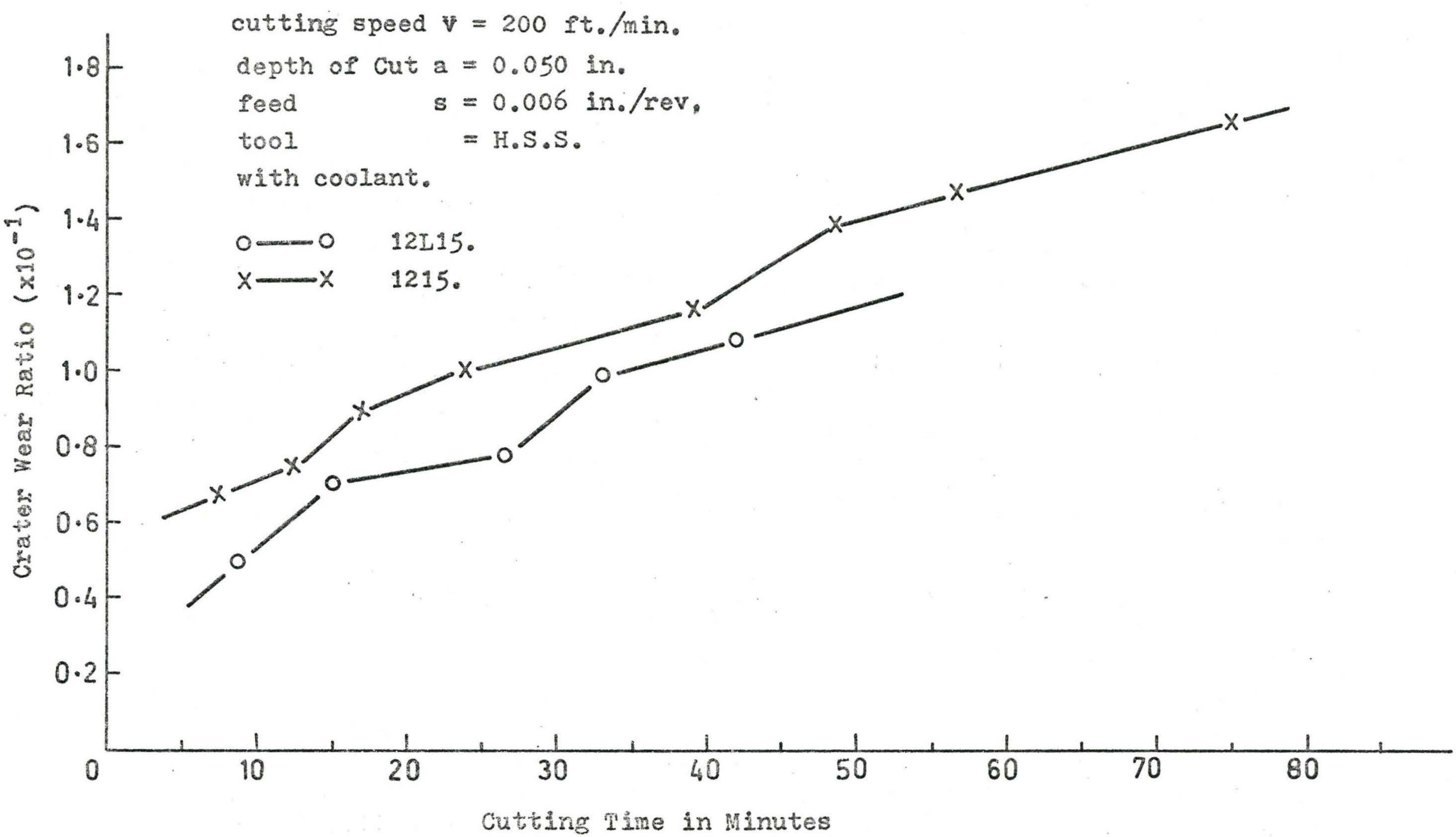

Fig. 3.11 Crater Wear Ratio Versus Cutting Time.

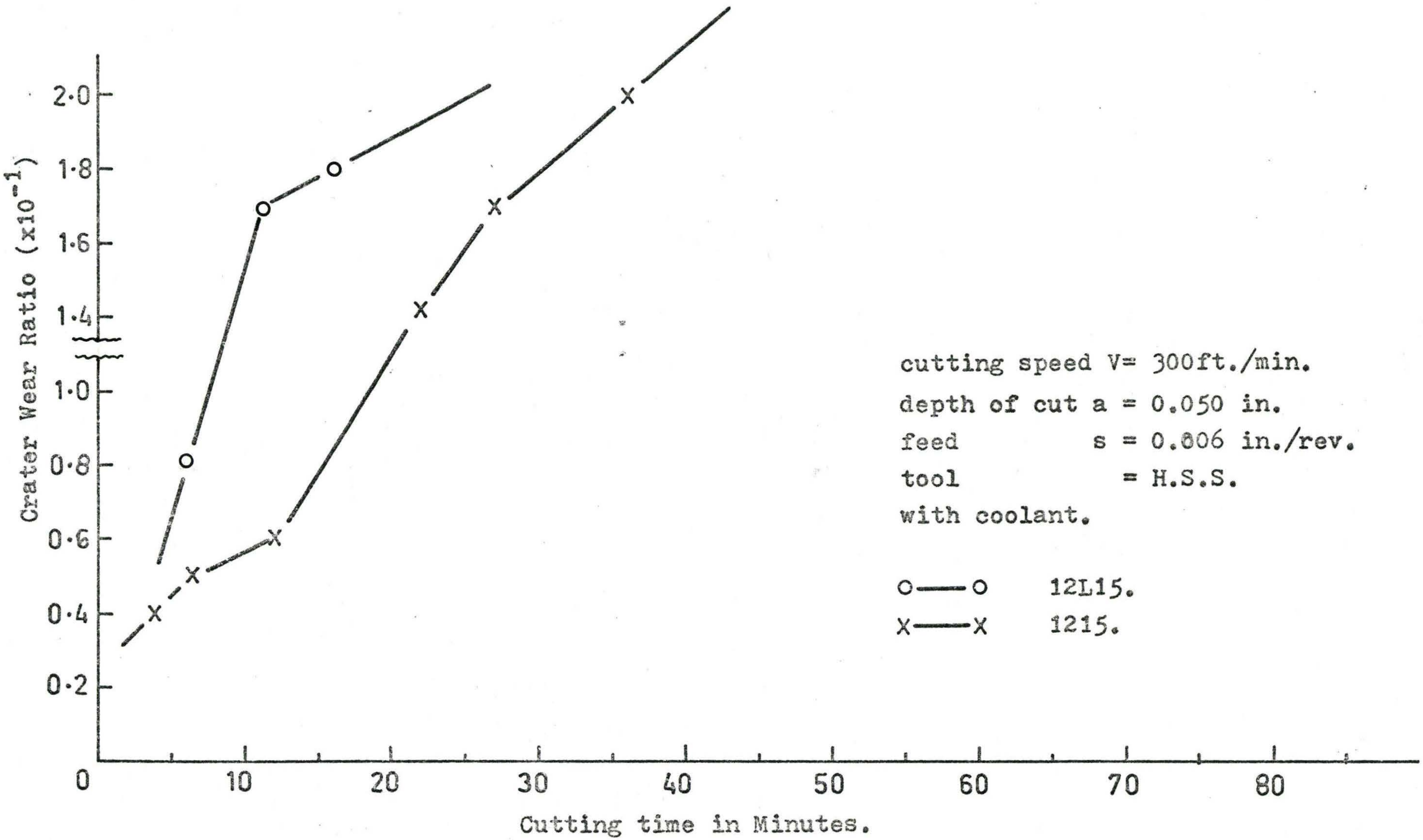

Fig. 3.12 Crater Wear Ratio Versus Cutting Time.

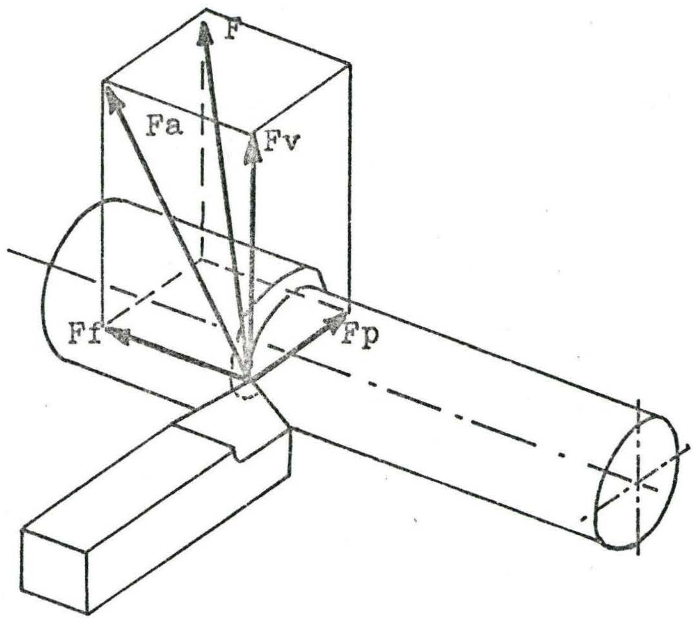

Forces exerted by the cutting tool on the workpiece

Fig. 3.13. Components of Cutting Force.

(ref. 26.)

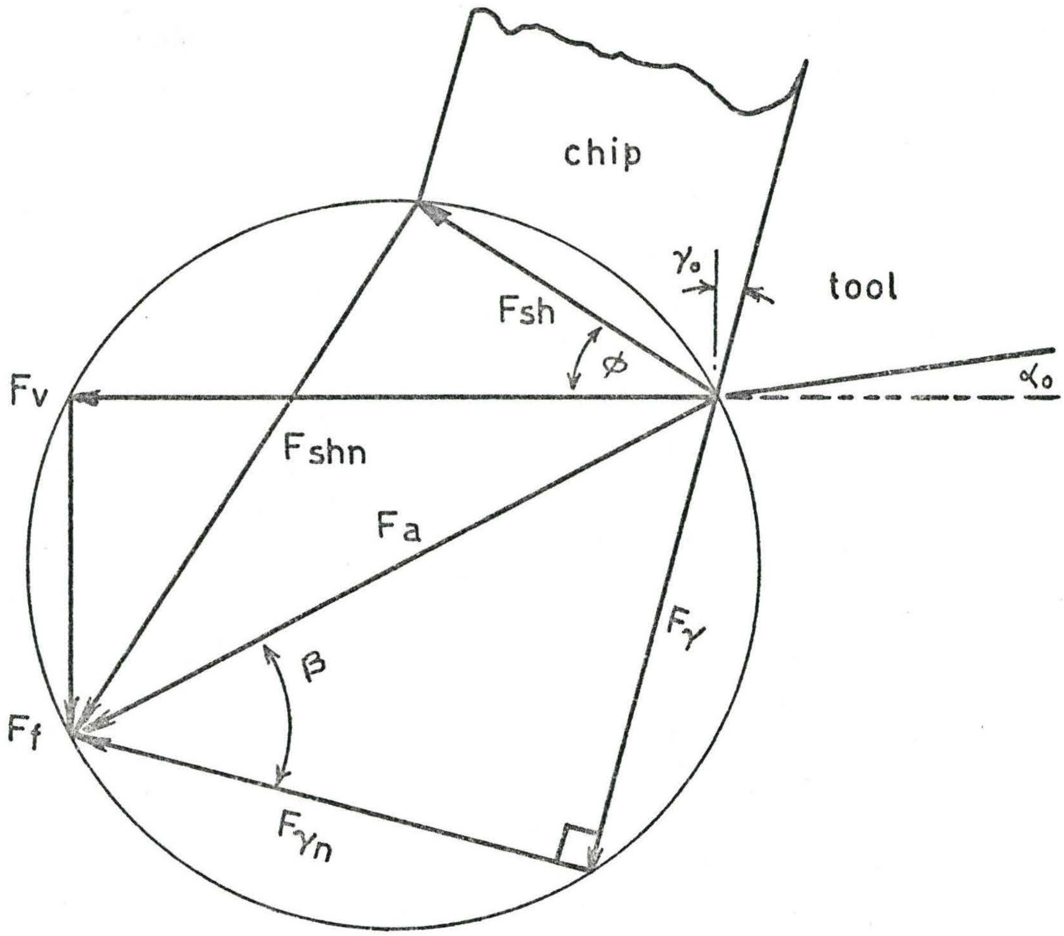

F_v Cutting Force

F_f Feed Force

F_a Active Force

F_γ Shear Force on the Rake Face

$F_{\gamma n}$ Normal Force on the Rake Face

F_{sh} Shear Force on the Shear Plane

F_{shn} Normal Force on the Shear Plane

γ_o Orthogonal Rake Angle

Fig 3.14. Force Configration in Orthogonal Cutting Using a Shear Plane Model.

(ref. 26)

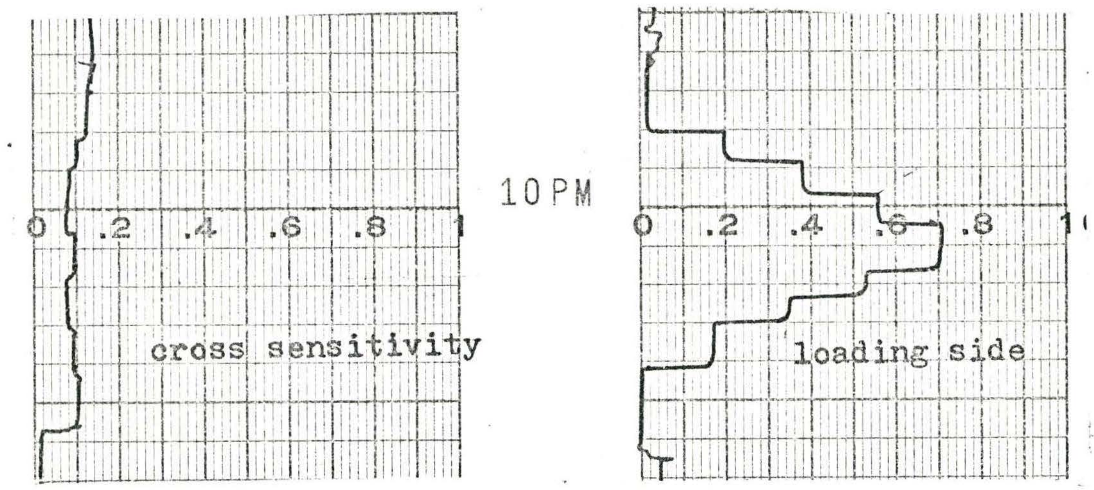

(a) Feed Force Calibration Graph.

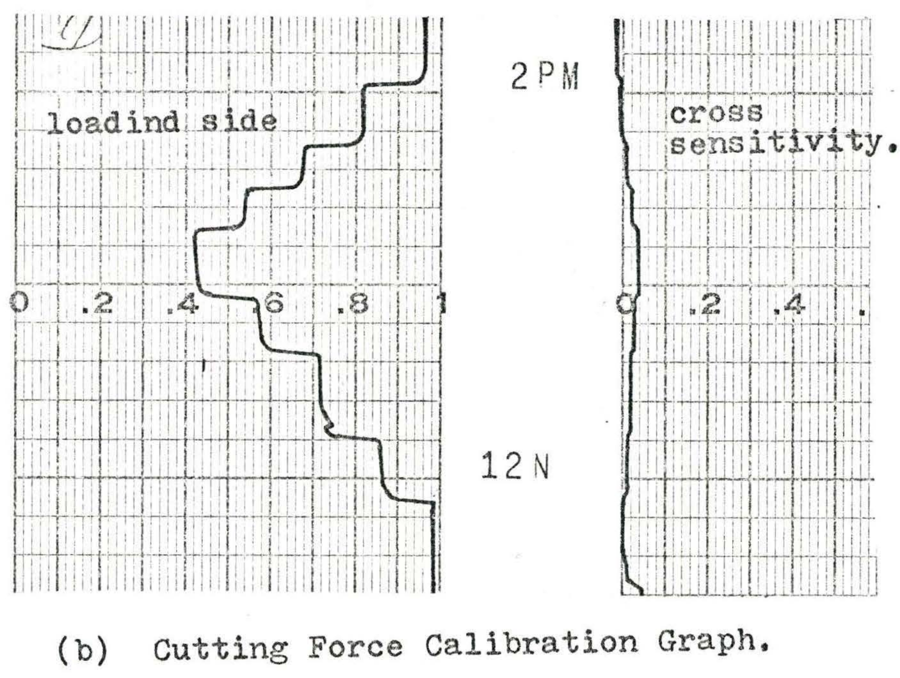

(b) Cutting Force Calibration Graph.

Fig. 3.15. Calibration Graphs of Two Components Force Dynamometer.

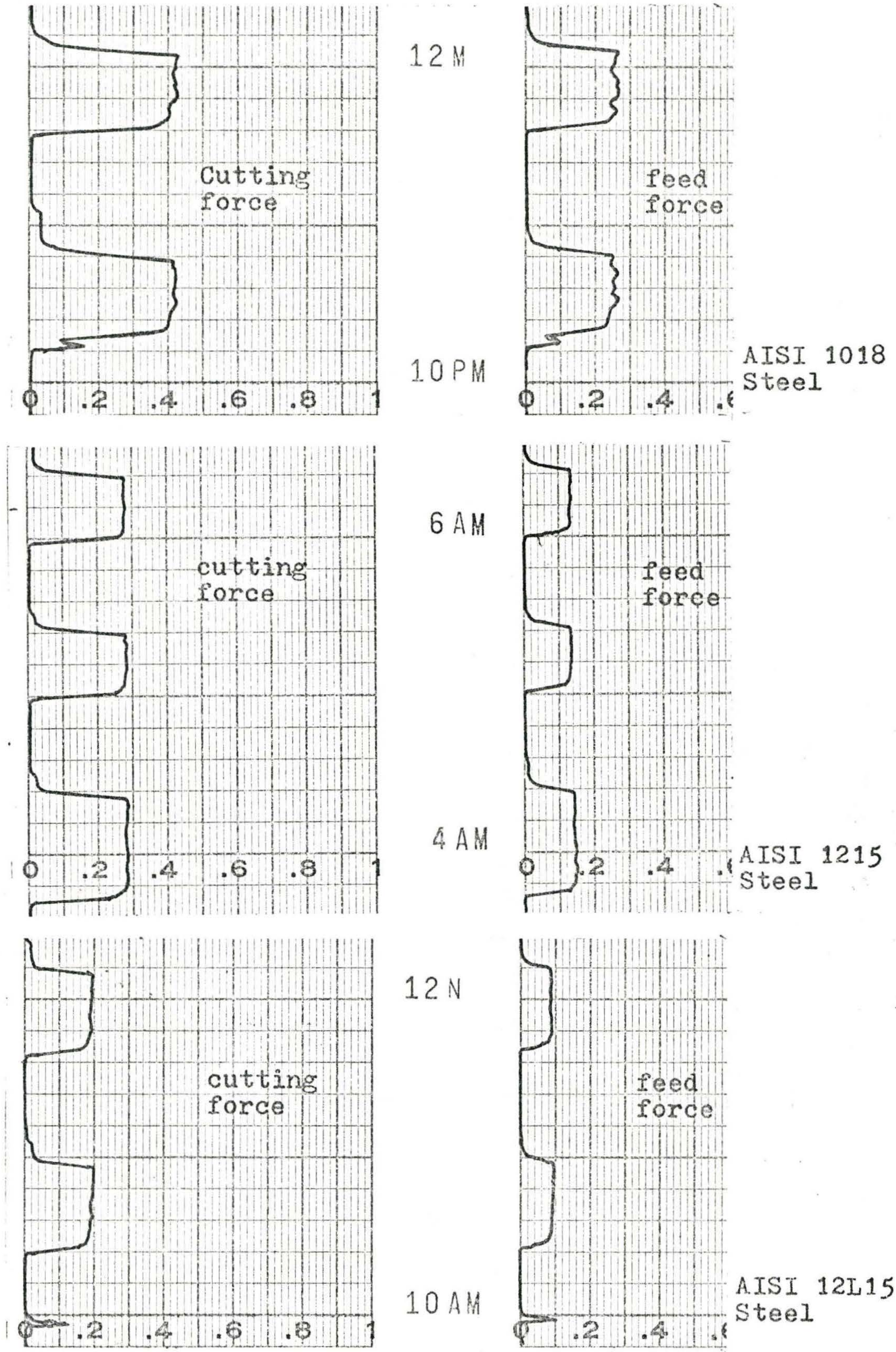

Fig. 3.16. Specimen of Cutting Forces Obtained at the cutting speed of 200 ft/min, depth of cut 0.050 in, feed 0.006 in

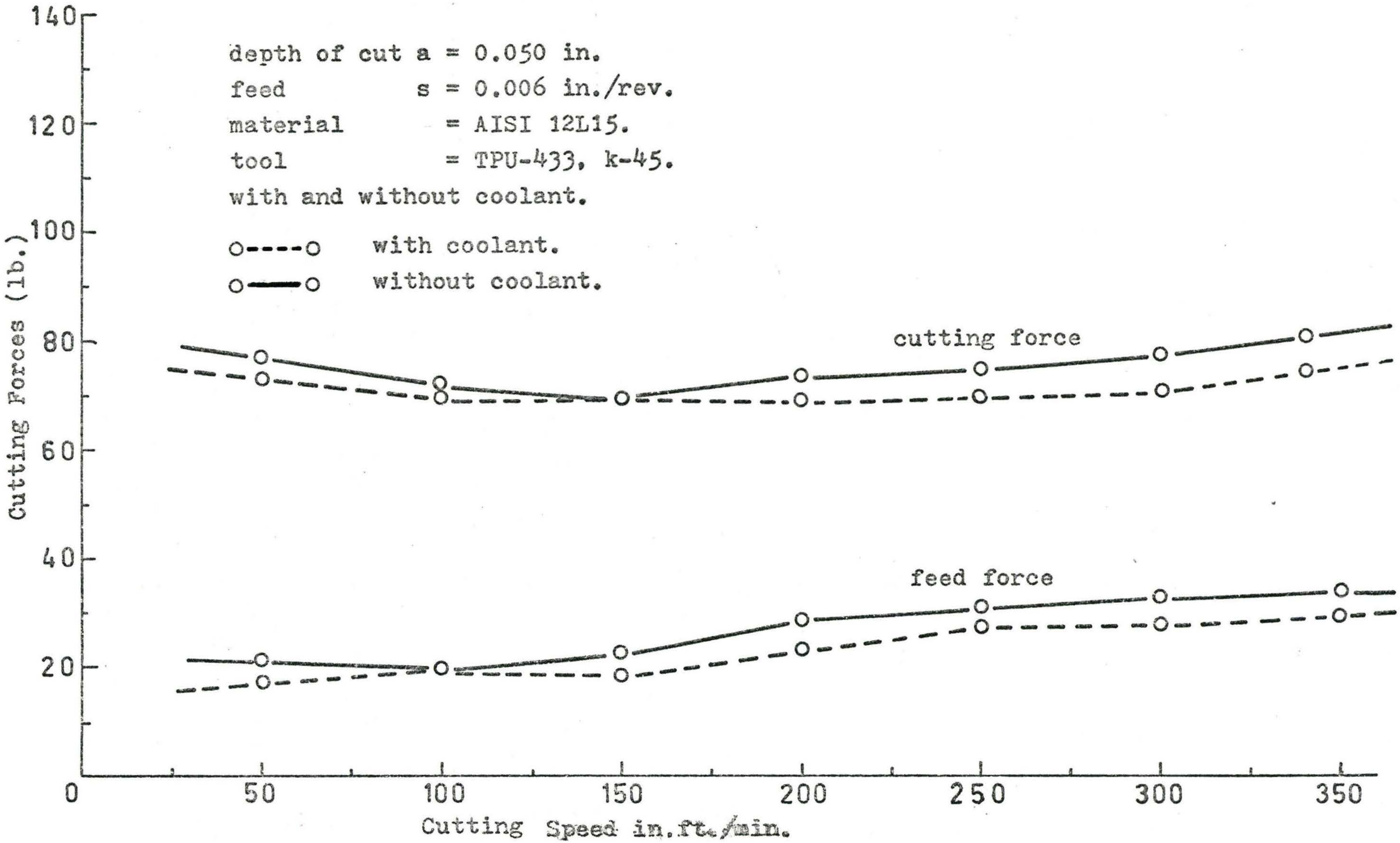

Fig. 3.17. Cutting Forces Versus Cutting Speed.

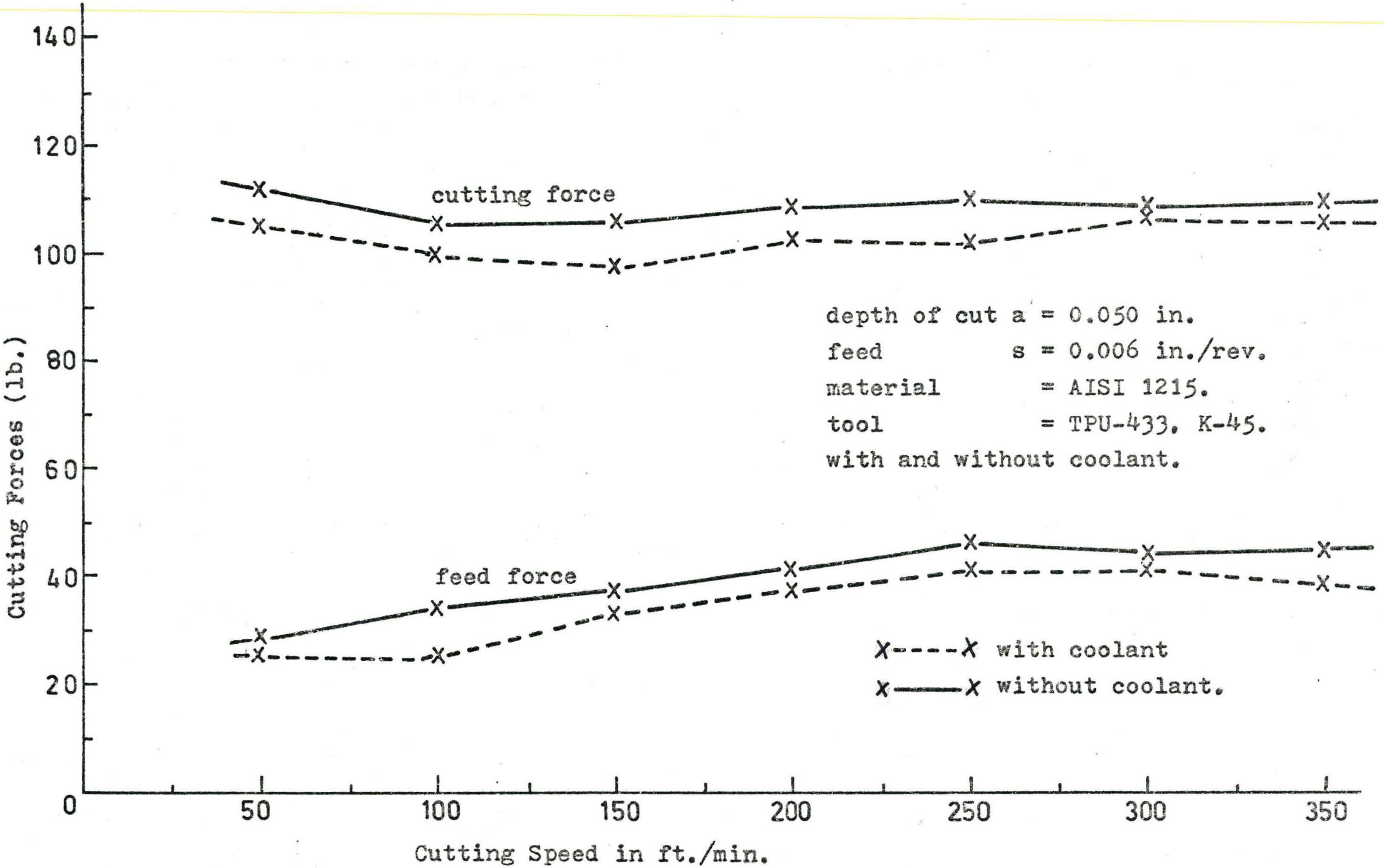

Fig. 3.18. Cutting Forces Versus Cutting Speed.

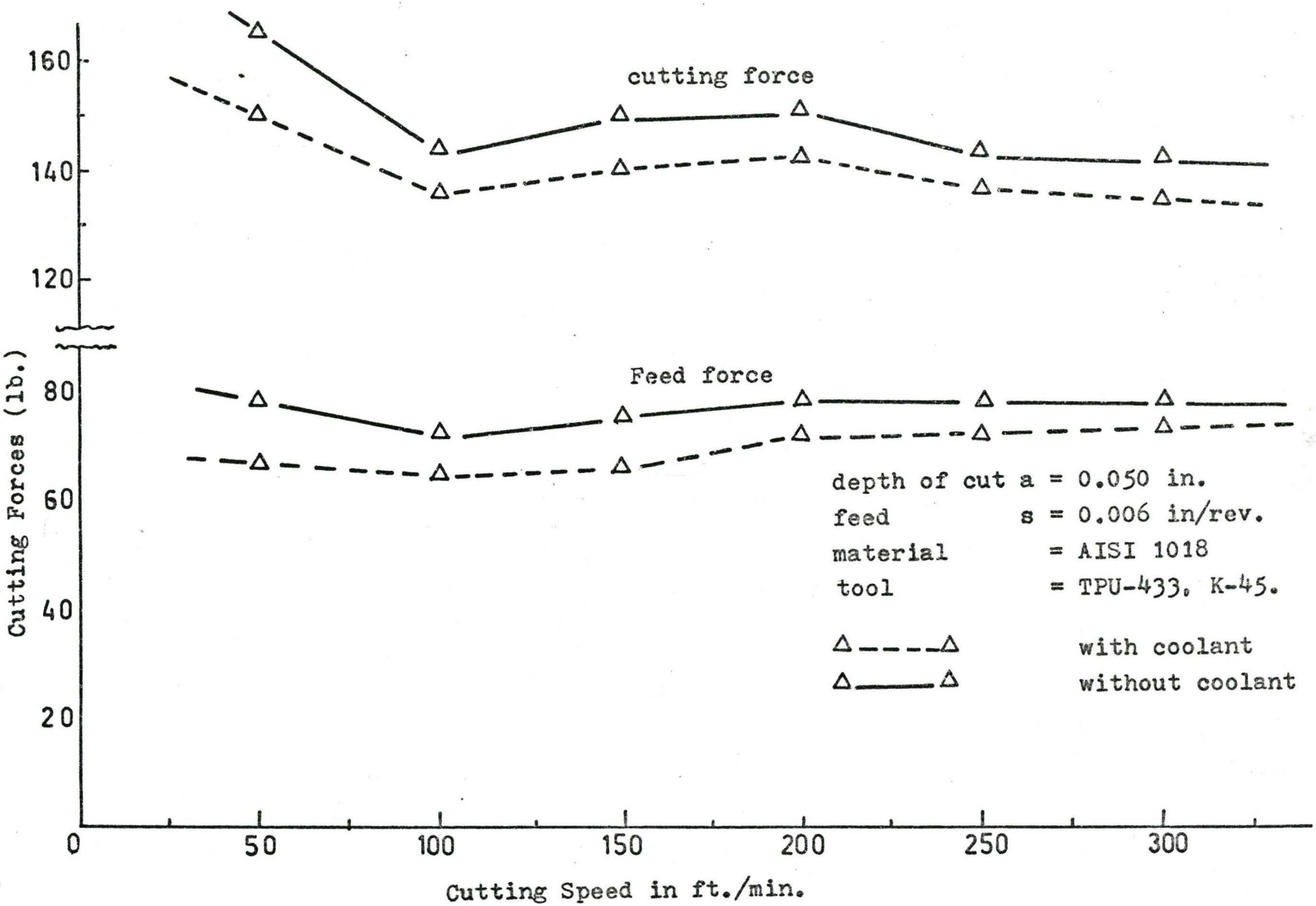

Fig. 3.19. Cutting Forces Versus Cutting Speed.

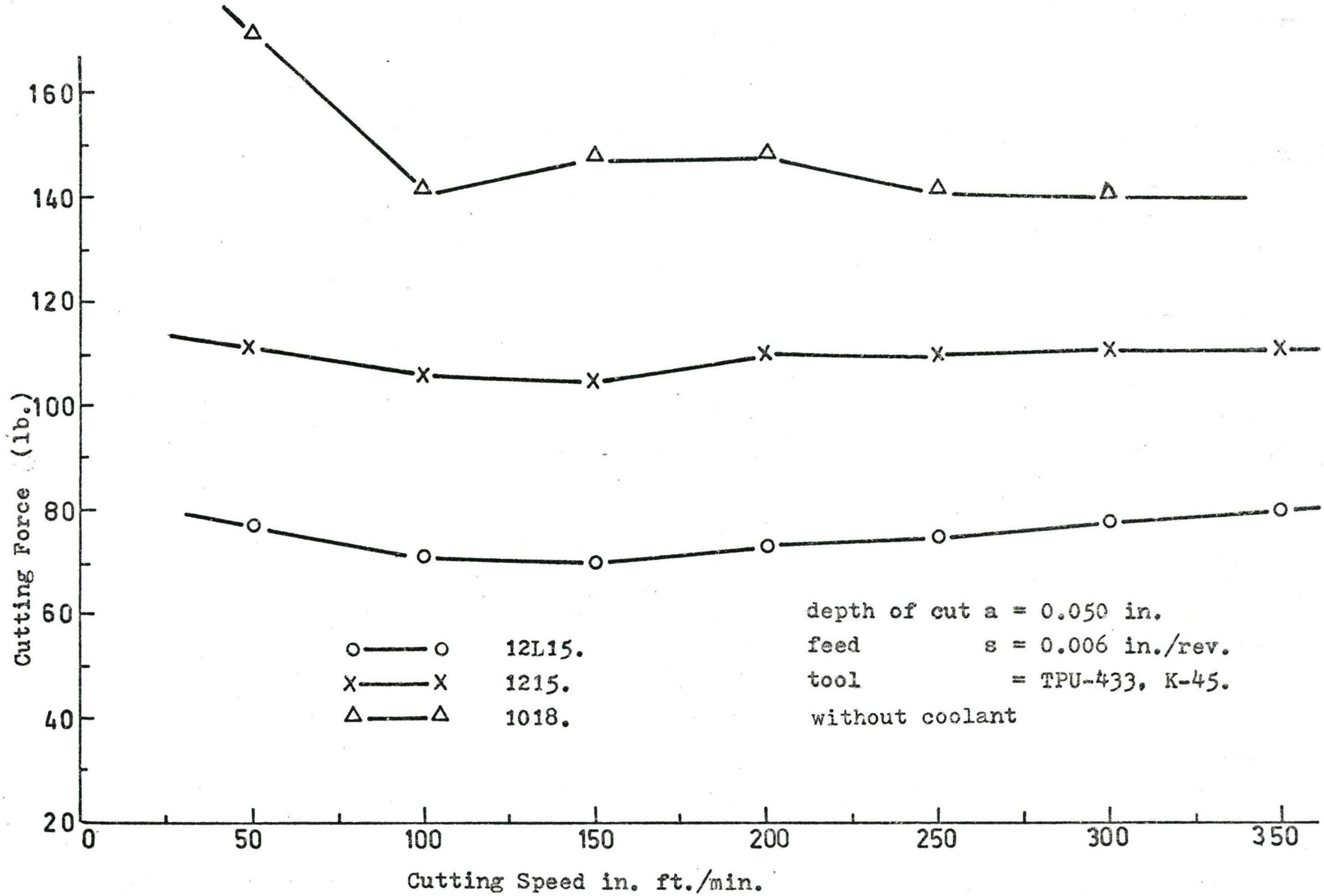

Fig. 3.20. Comparision of Cutting Force for 3 Steels Versus Cutting Speed.

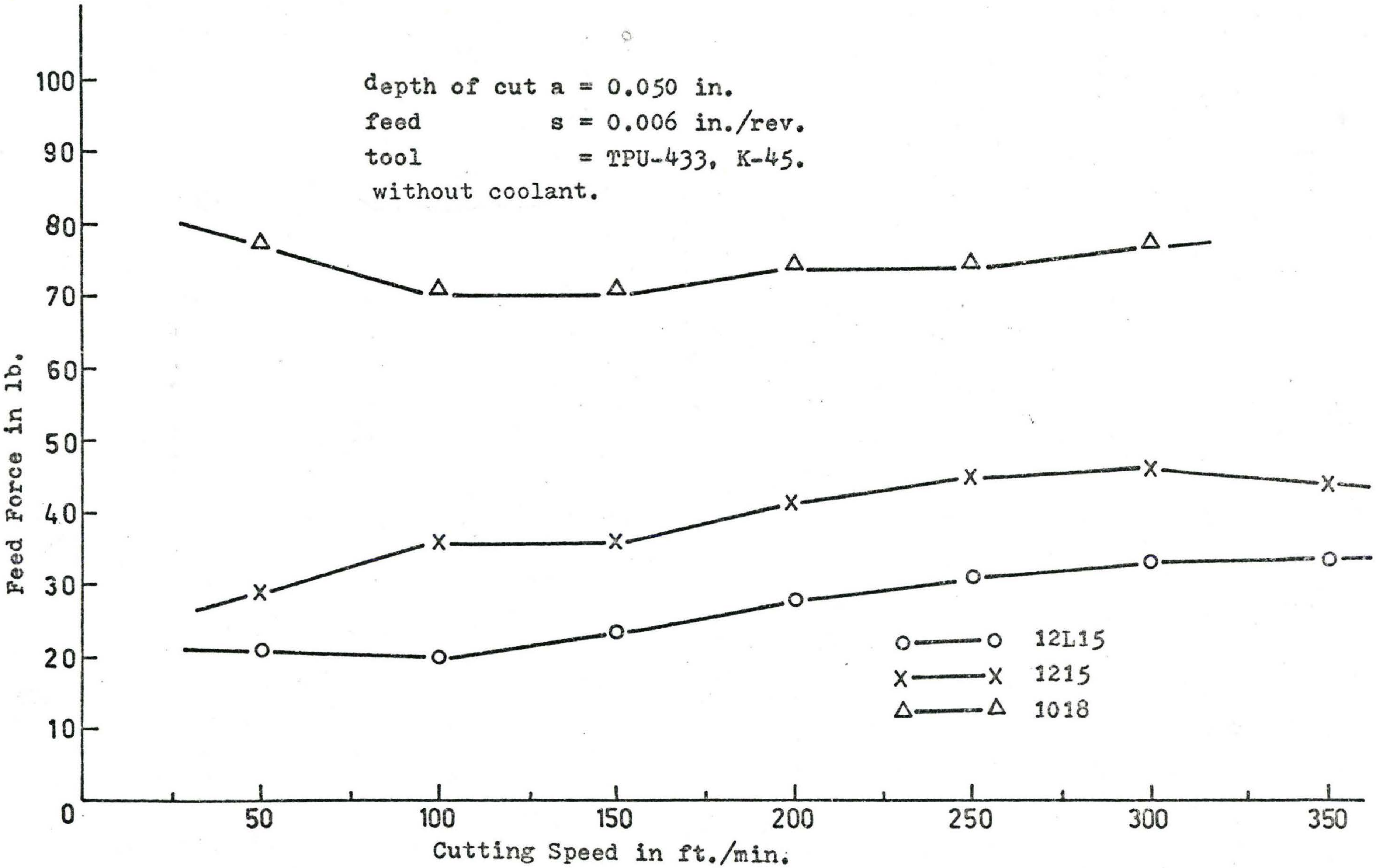

Fig. 3.21. Comparision of Feed Force for 3 Steels Versus Cutting Speed.

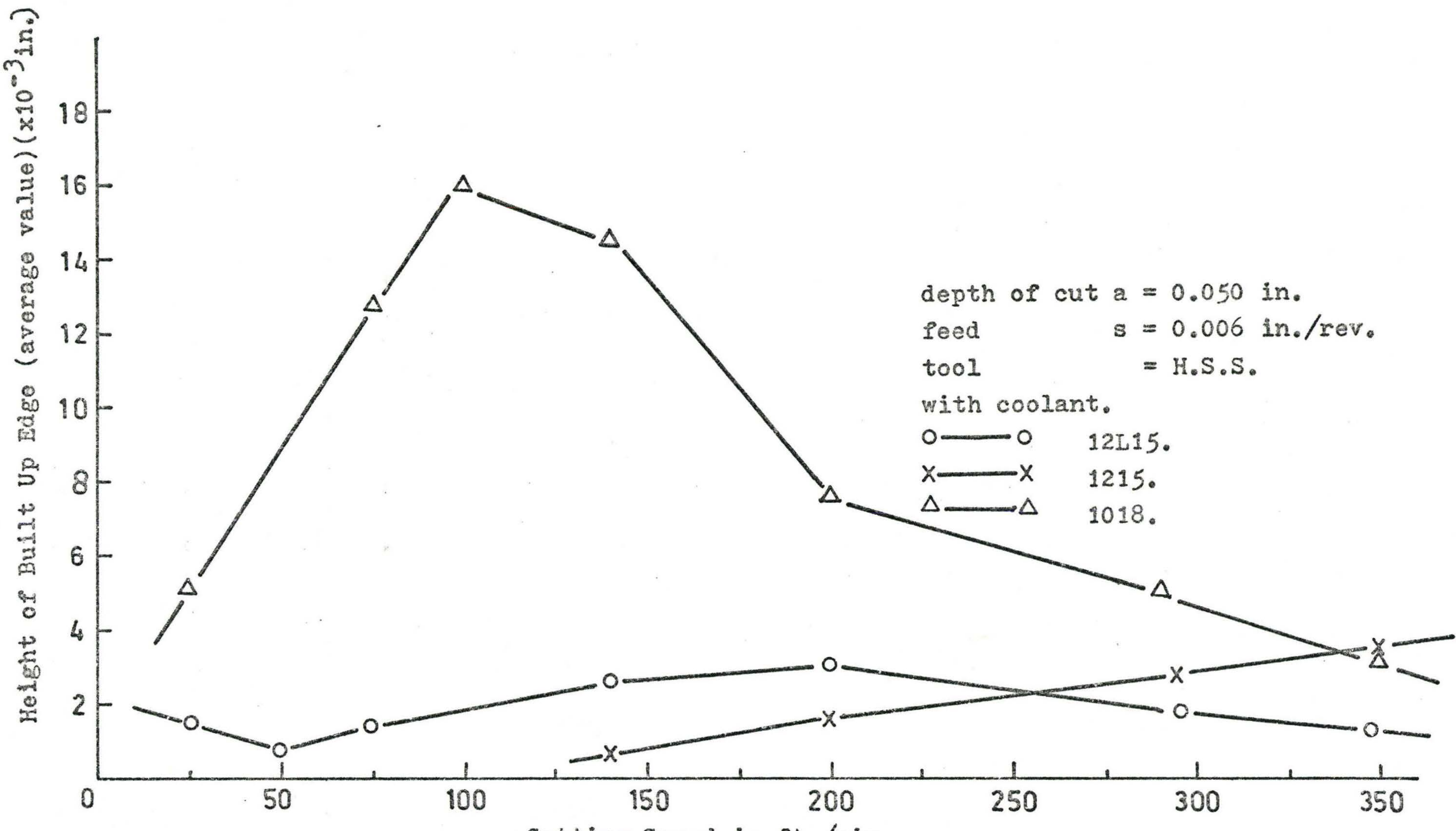

Fig.3.22. Comparision of Built Up Edge for 3 Steels Versus Cutting Speed.

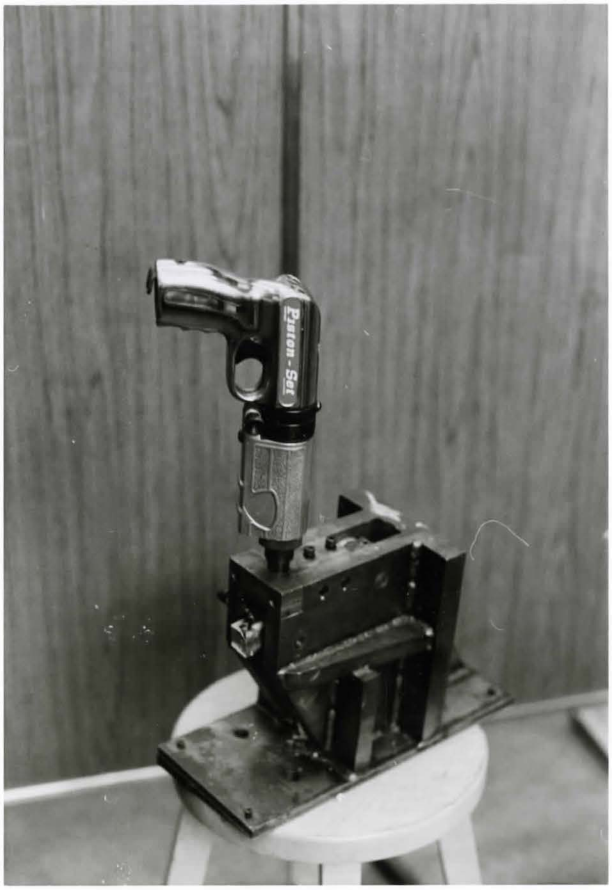

Fig. 3.23. General View of Quick Stop Device.

Rolling Direction

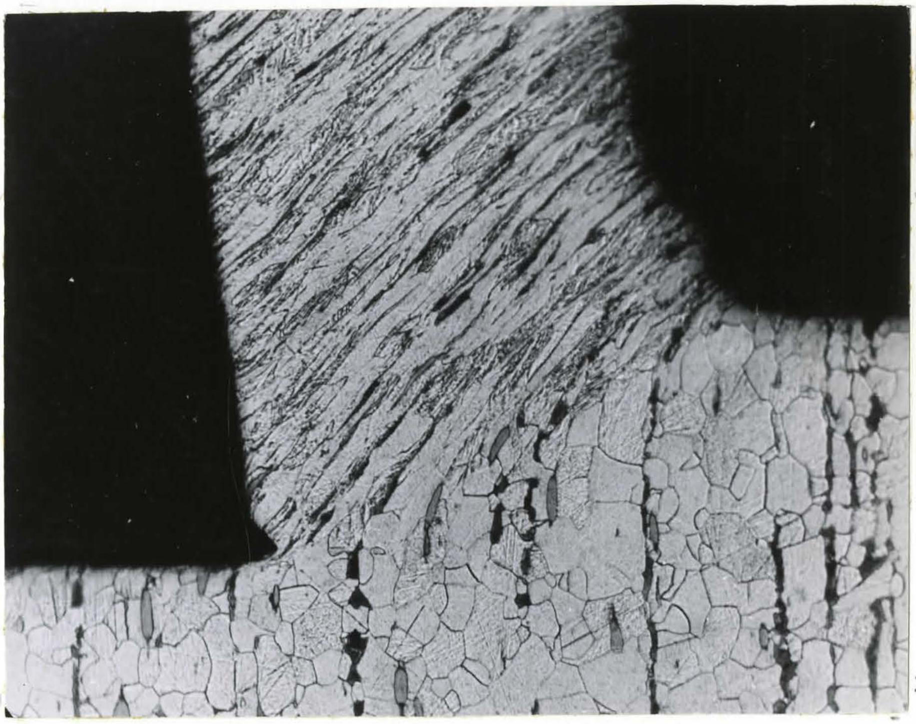

x150

Fig. 3.24 Metallographic Specimen Resulting from Quick Stop Device at the Cutting Speed of 100 ft/min. for AISI 12L15 Steel.

Rolling
Direction

↓

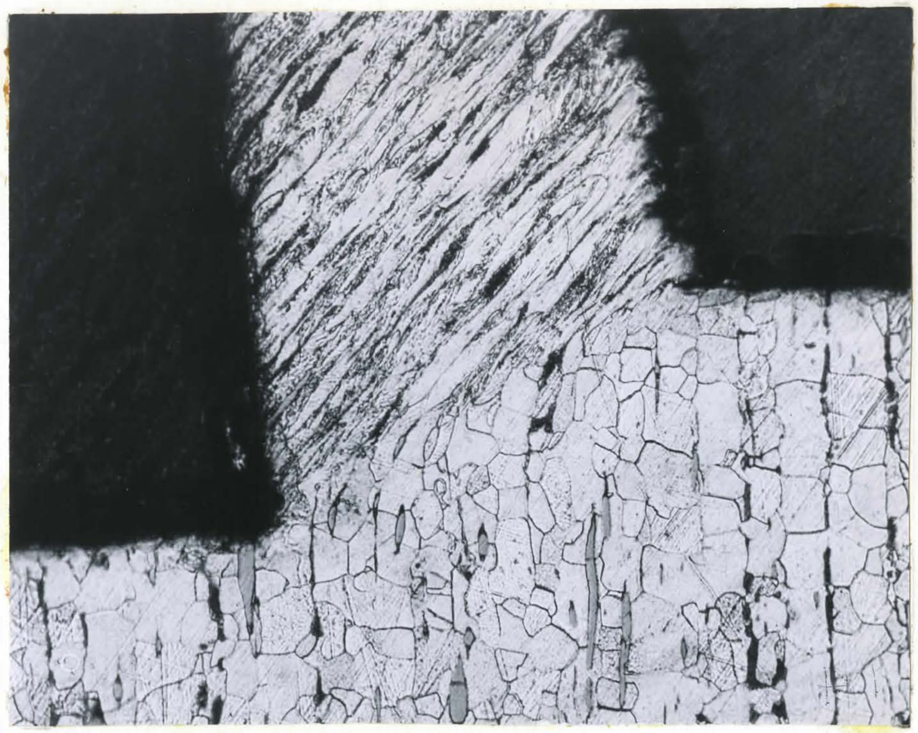

X150

Fig. 3.25 Metallographic Specimen Resulting from the Quick Stop Device at the Cutting Speed of 200 ft/min for AISI 12L15 Steel.

Rolling
Direction

↓

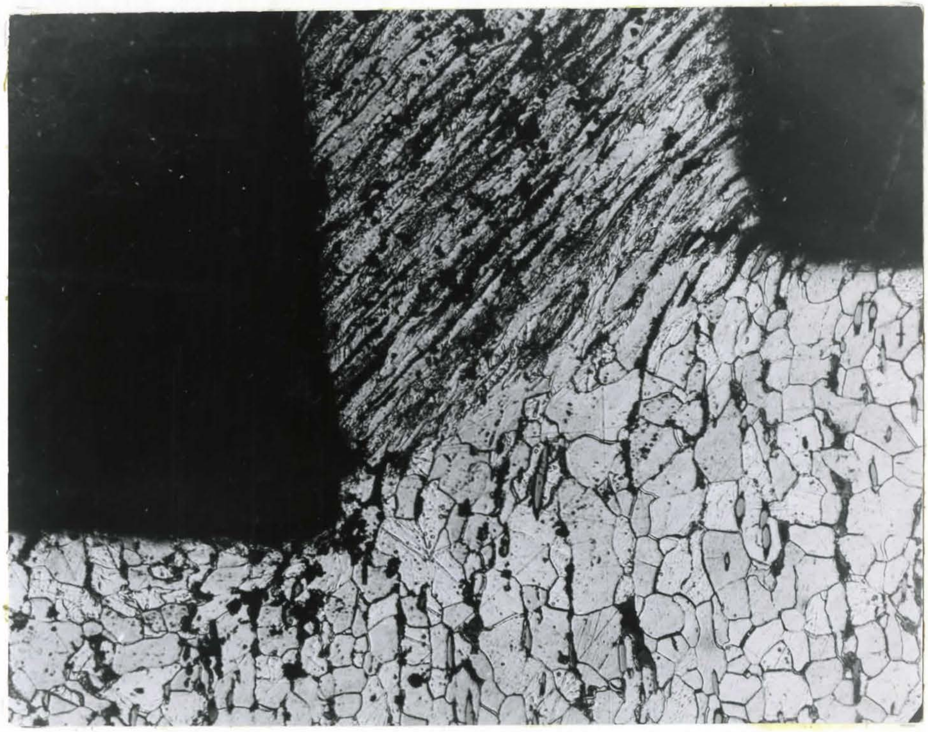

X150

Fig. 3.26. Metallographic Specimen Resulting from the Quick Stop Device at the Cutting Speed of 300 ft/min for AISI 12L15 Steel.

Rolling
Direction

X150

Fig. 3.27. Metallographic Specimen Resulting from Quick Stop Device at the Cutting Speed of 100 ft/min for 1215 Steel.

Rolling
Direction

X150

Fig. 3.28. Metallographic Specimen Resulting from Quick Stop Device at the Cutting Speed of 200 ft/min for 1215 Steel.

Rolling
Direction

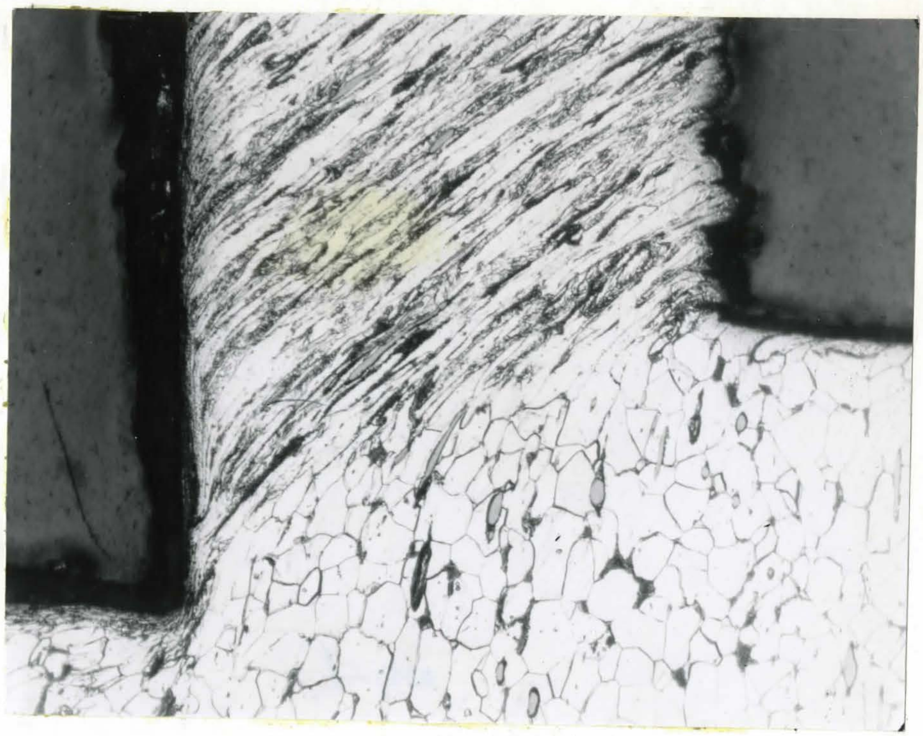

X150

Fig. 3.29. Metallographic Specimen Resulting from Quick Stop Device at the Cutting Speed of 300 ft/min for 1215 Steel.

Rolling
Direction

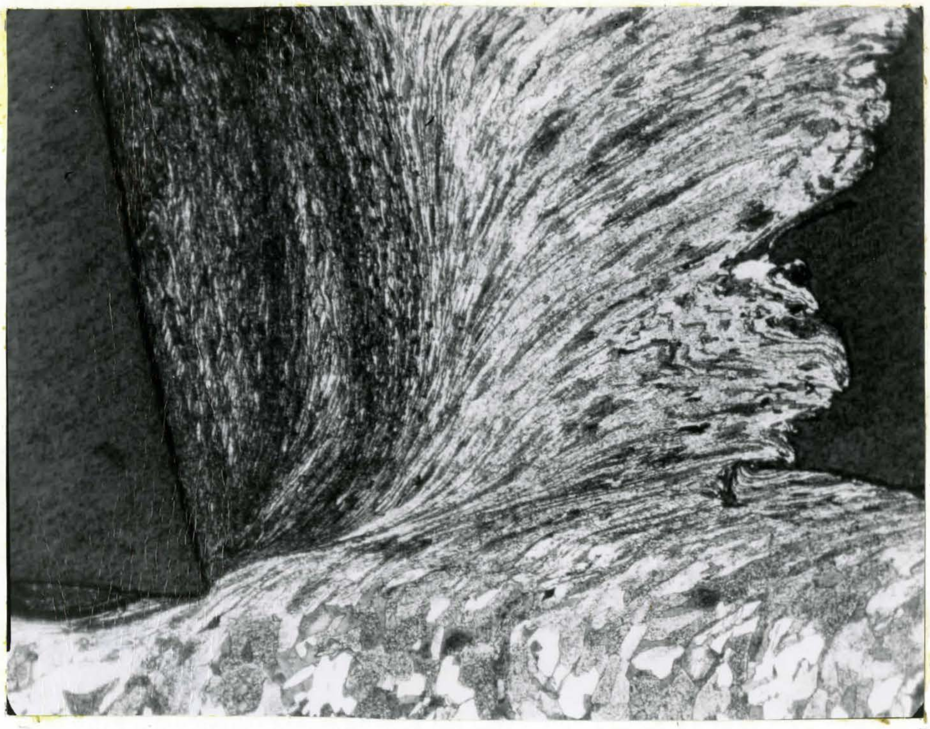

x150

Fig. 3.30 Metallographic Specimen Resulting from Quick Stop Device at the Cutting Speed of 55 ft/min. for AISI 1018 Steel.

Rolling
Direction

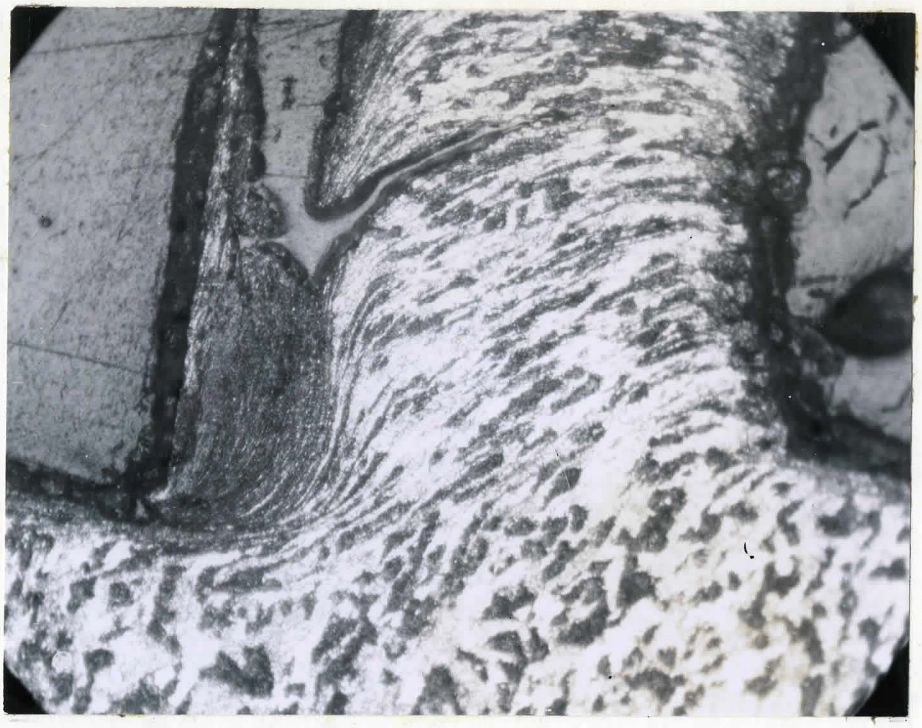

X150

Fig. 3.31. Metallographic Specimen Resulting from Quick Stop Experiment at the Cutting Speed of 200 ft/min for AISI 1018 Steel.

Rolling
Direction

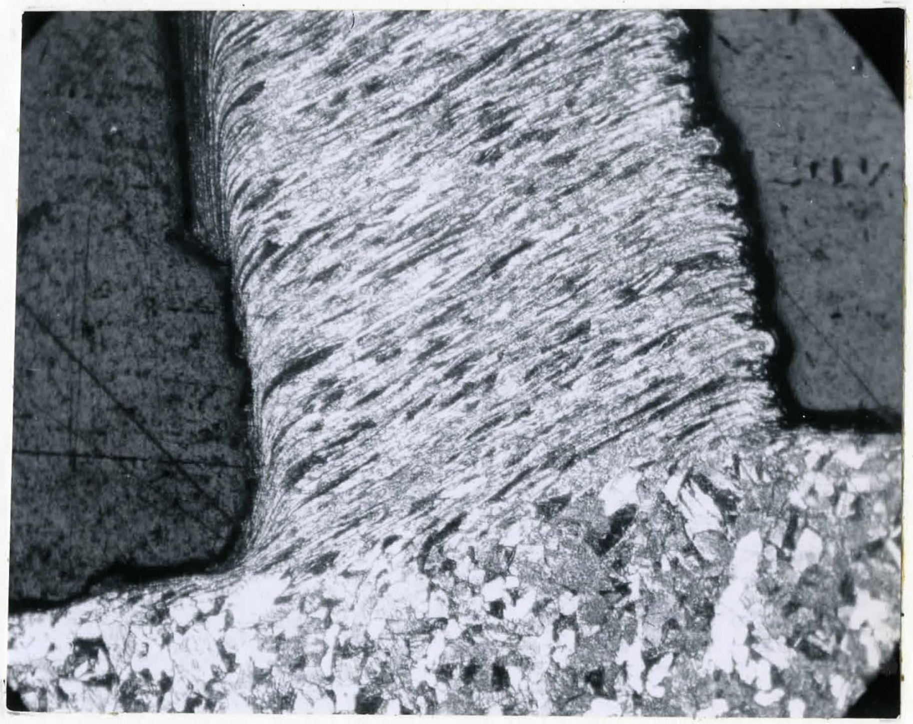

X150

Fig. 3.32. Metallographic Specimen Resulting from Quick Stop Experiment at the Cutting Speed of 300 ft/min for AISI 1018 Steel.

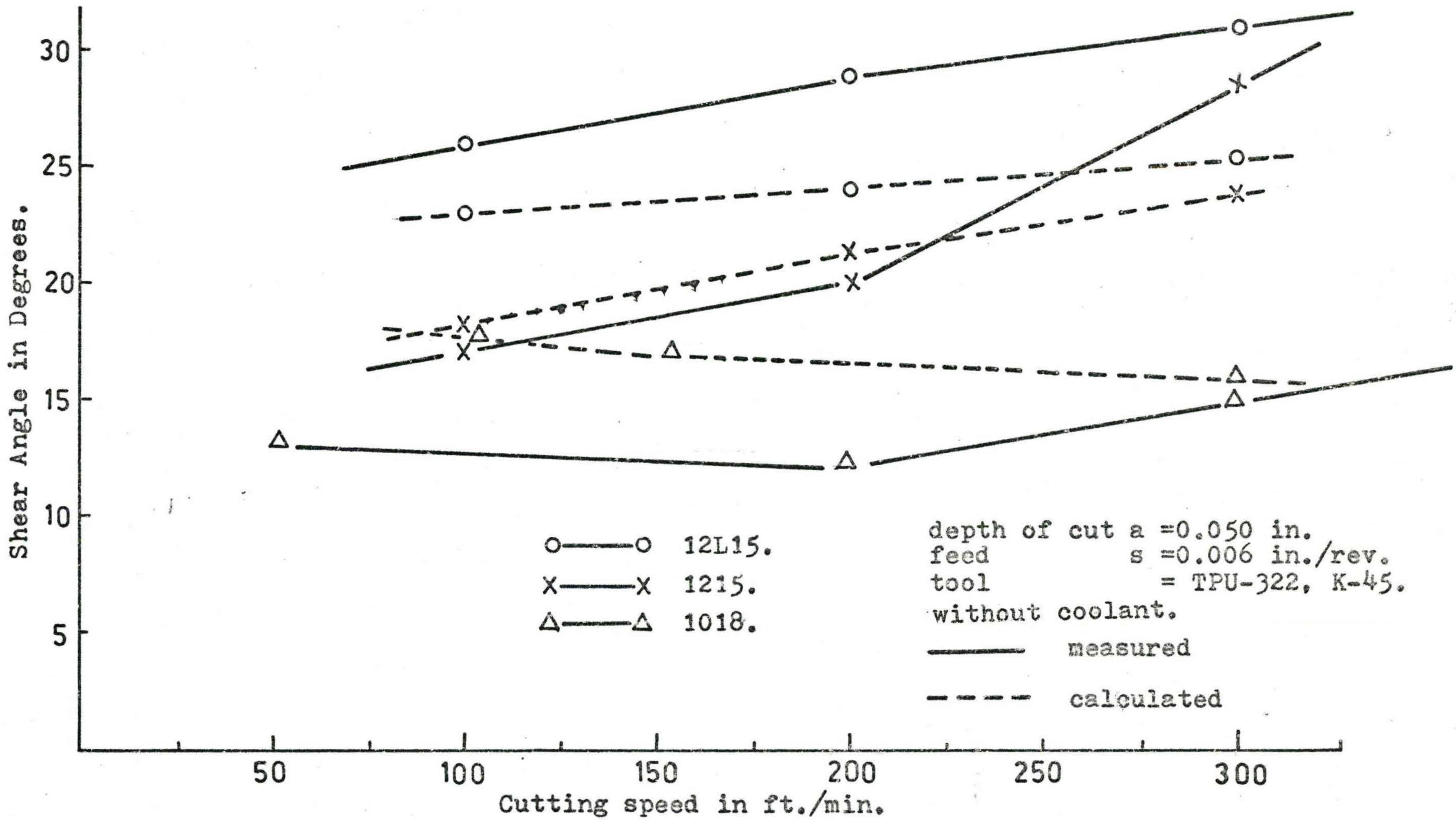

Fig. 3.33 Comparision of Shear Angle Value Versus Cutting Speed.

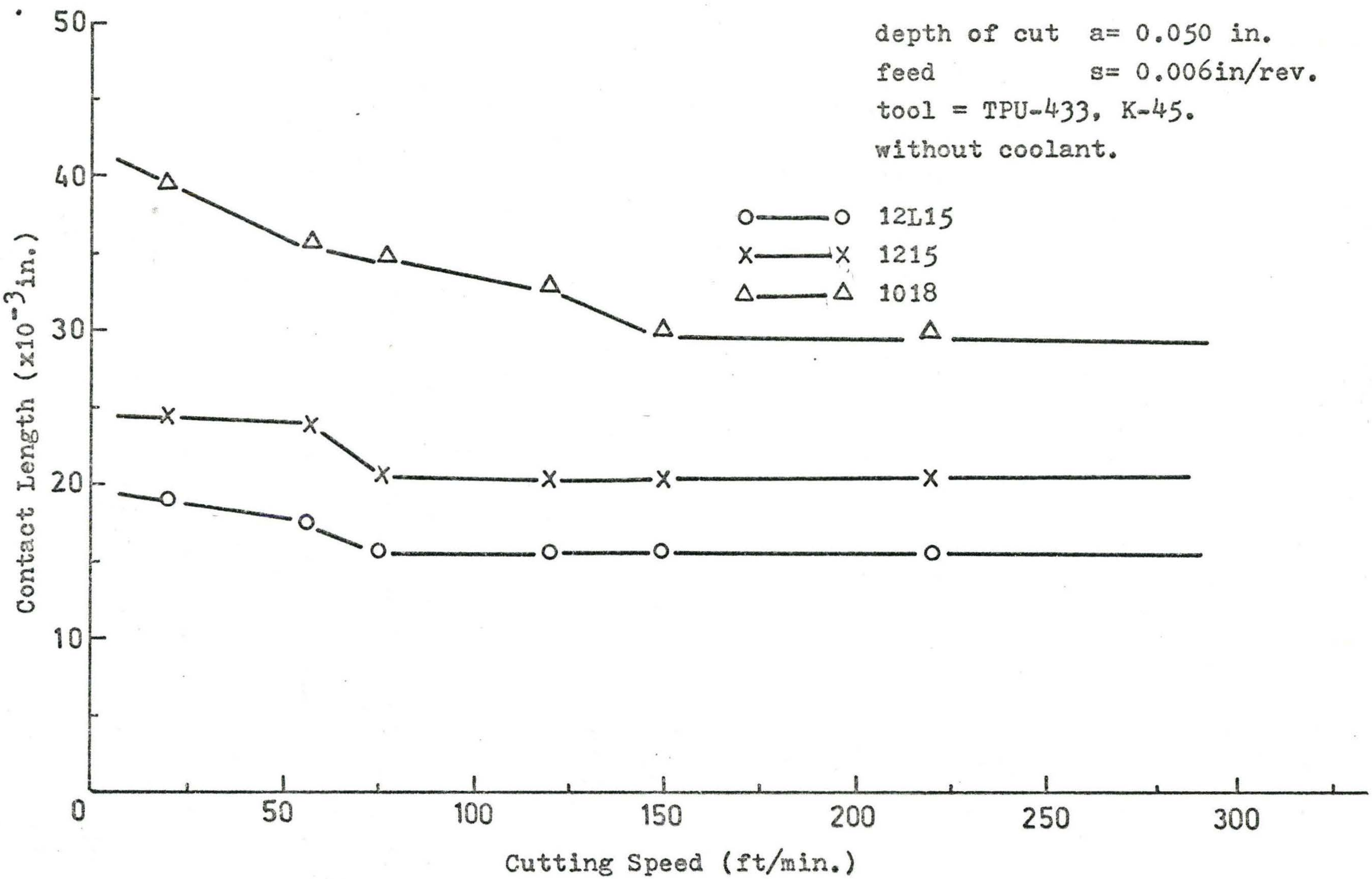

Fig. 3.34. Contact Length Versus Cutting Speed.

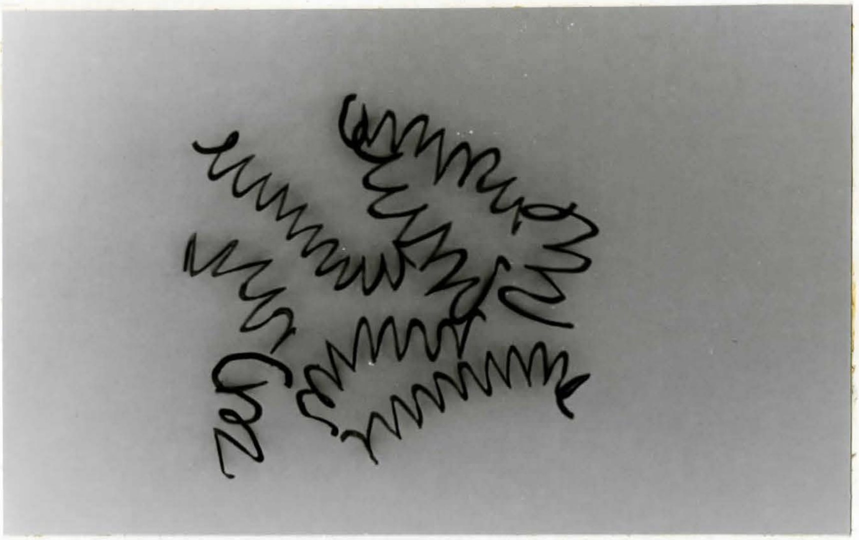

AISI
1018

AISI
1215

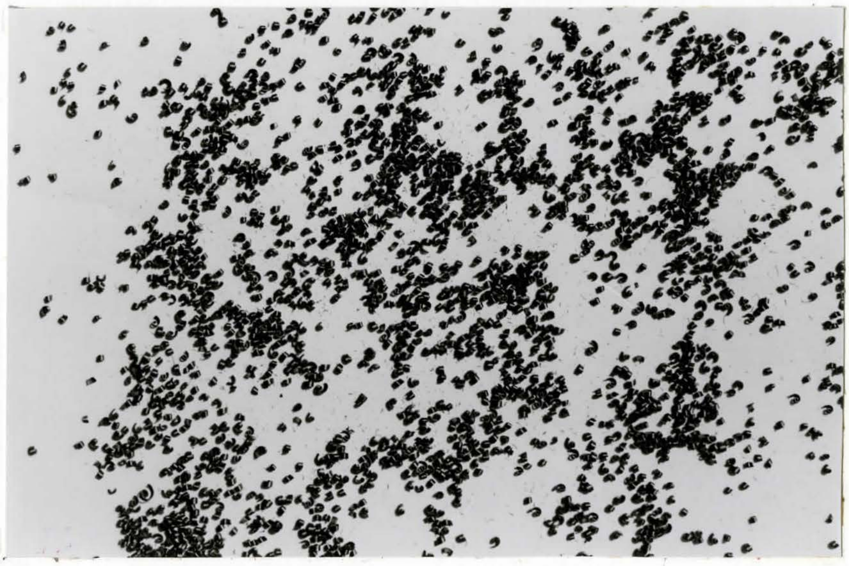

AISI
12L15

Fig. 3.35. Specimen of Chip Produced at the Cutting Speed of 200 ft/min for 3 Steels.

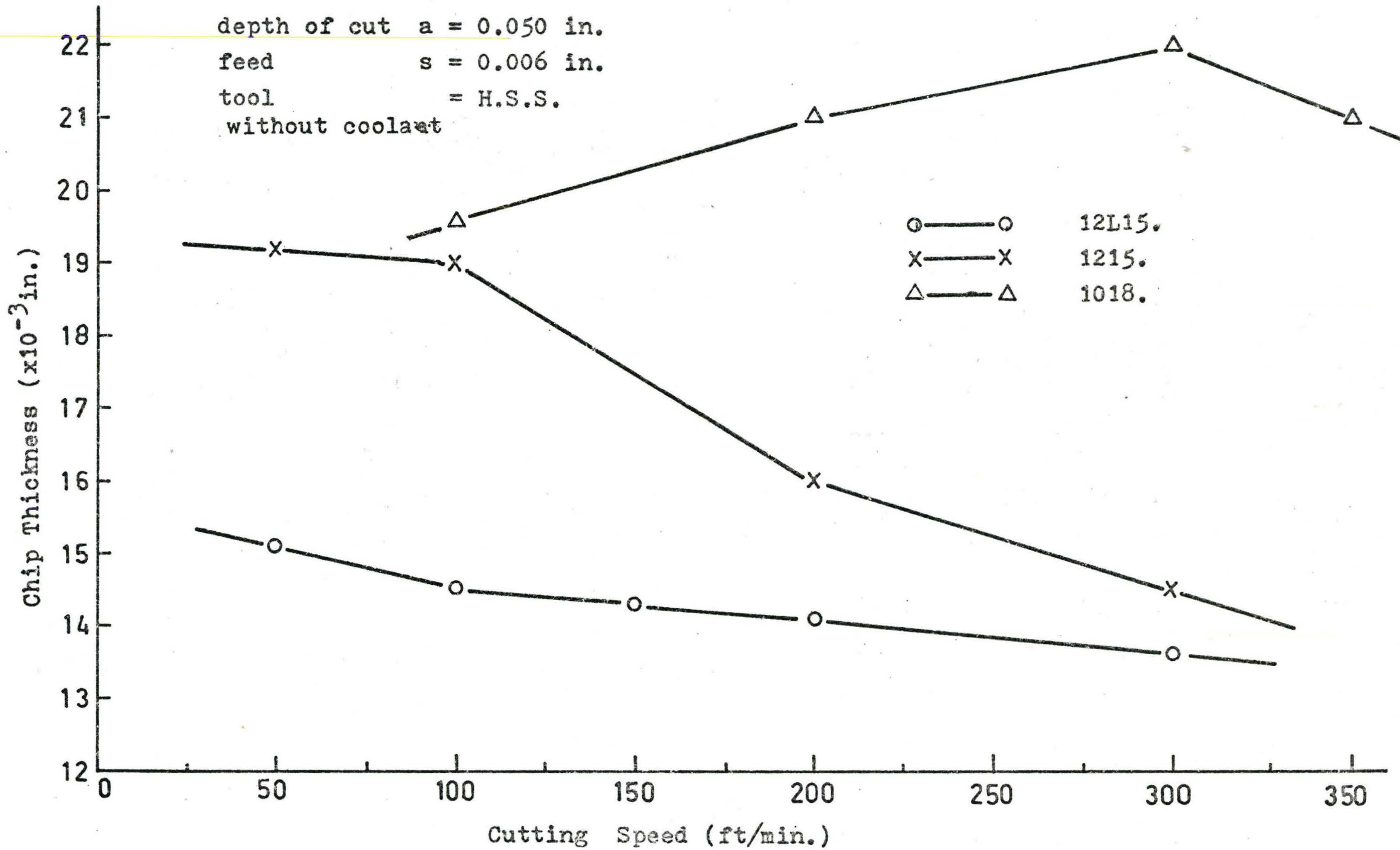

Fig. 4.1: Measured Chip Thickness Versus Cutting Speed.

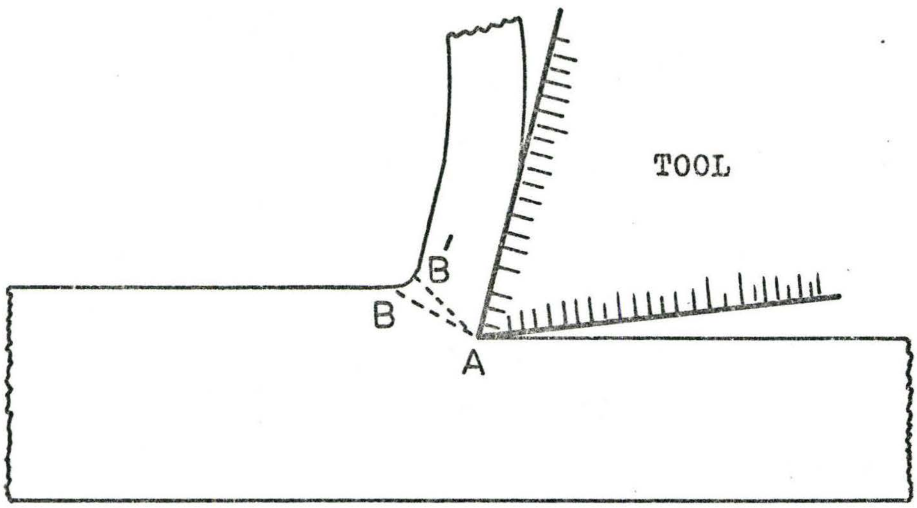

(a) Steel Without Free-Machining Additives

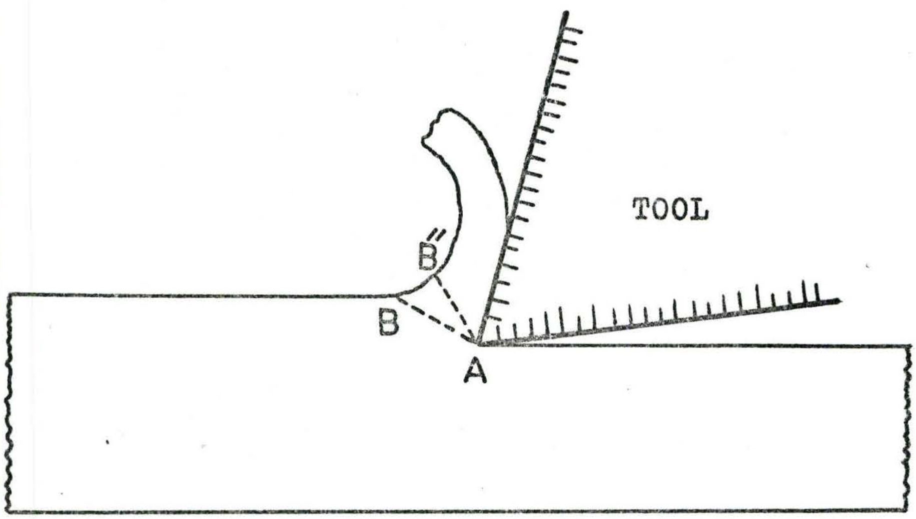

(b) Steel With Free-Machining Additives.

Fig. 4.1a Diagrammatic Sketch Showing the Difference in Shear Volume Associated with Steel.

X150

Fig. 4.2. Chip Photomicrograph of AISI 1018 Steel at the Cutting Speed of 100 ft/min.

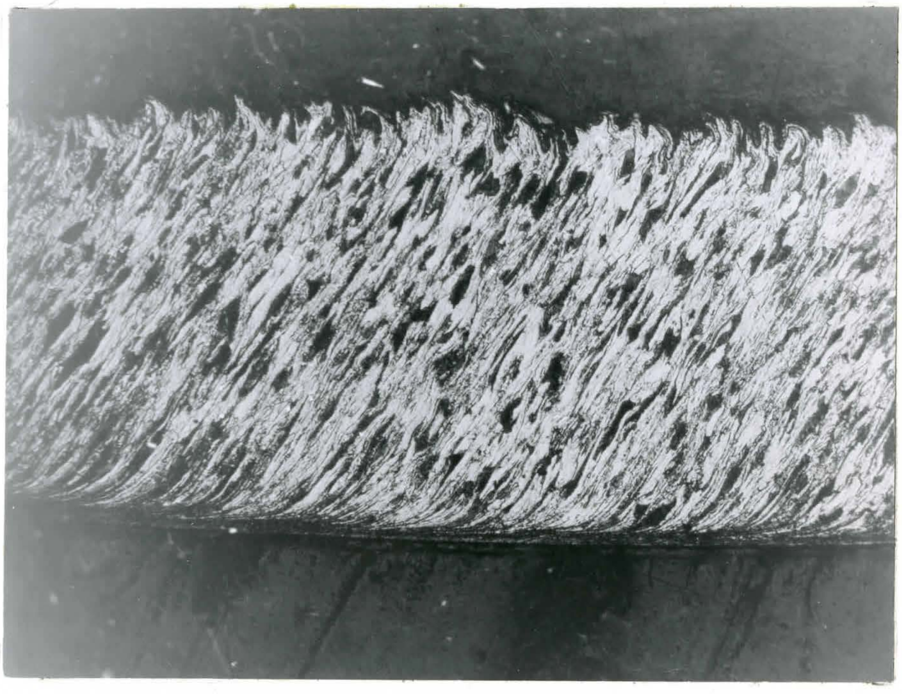

X150

Fig. 4.3. Chip Photomicrograph of AISI 1018 Steel at the Cutting Speed of 200 ft/min.

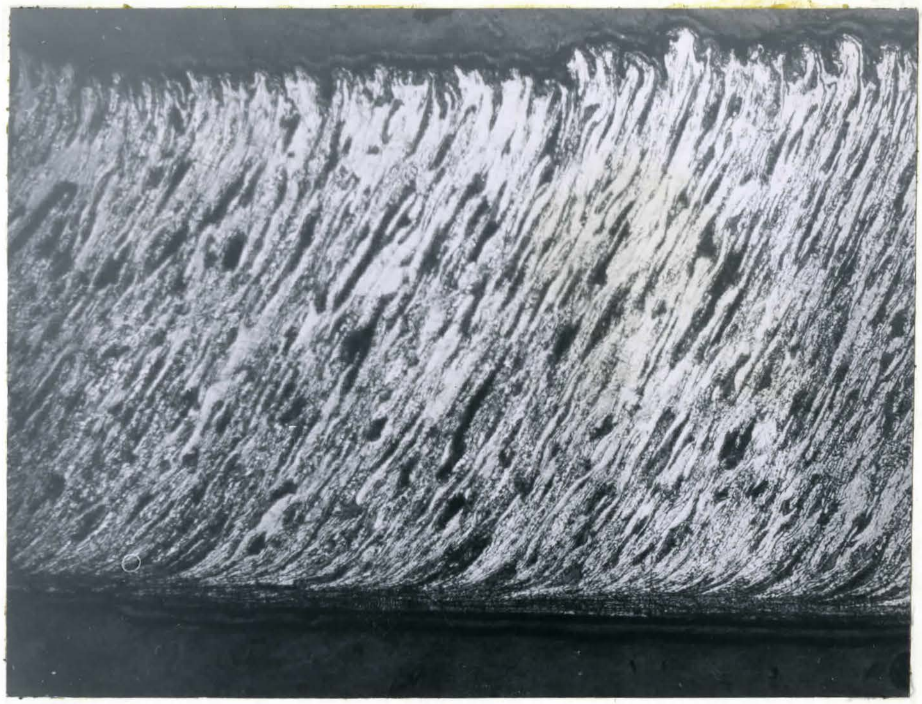

X150

Fig. 4.4. Chip Photomicrograph of AISI 1018 Steel at the Cutting Speed of 300 ft/min.

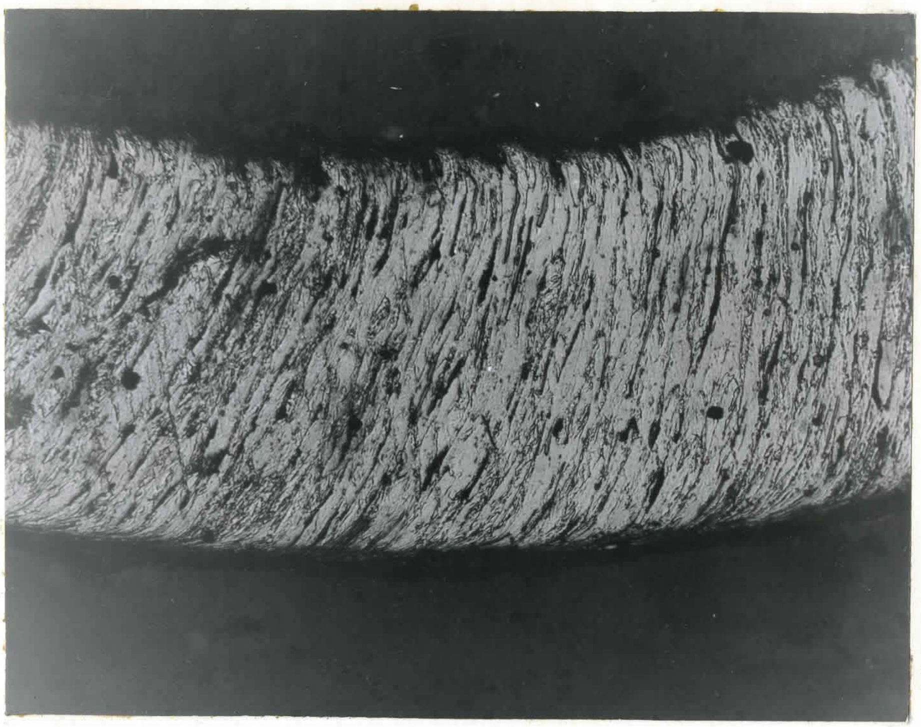

X150

Fig. 4.5. Chip Photomicrograph of AISI 1215 Steel at the Cutting Speed of 100 ft/min.

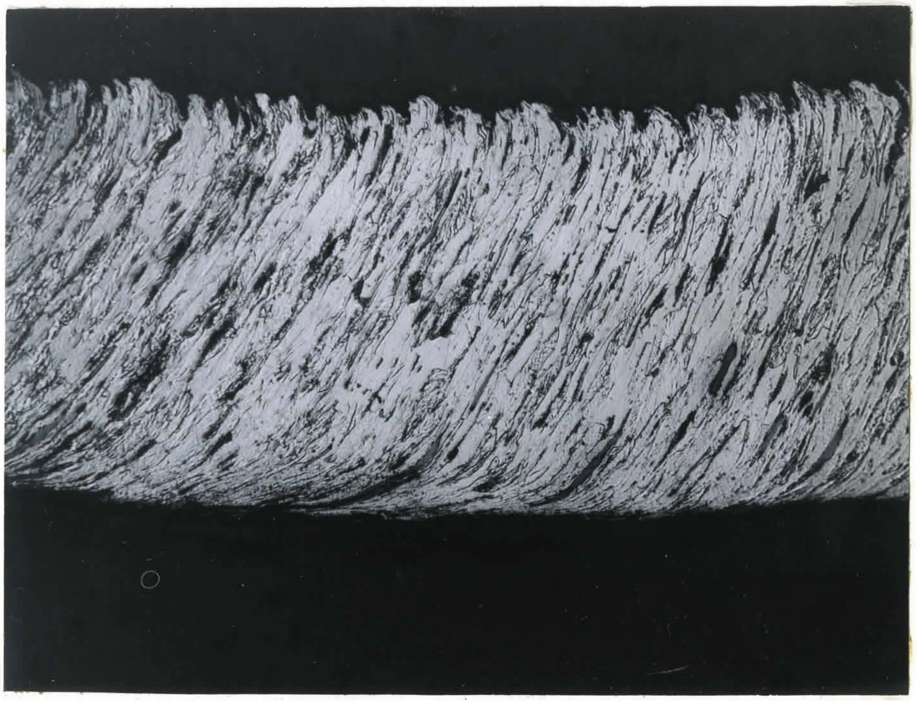

X150

Fig. 4.6. Chip Photomicrograph of AISI 1215 Steel at the Cutting Speed of 200 ft/min.

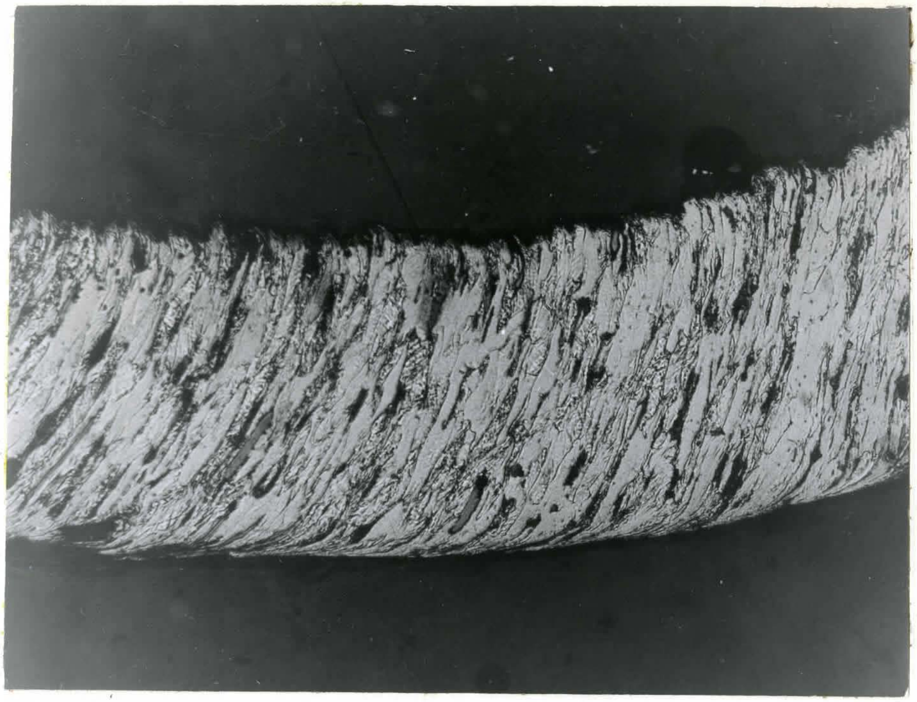

X150

Fig. 4.7. Chip Photomicrograph of AISI 1215 Steel at the Cutting Speed of 300 ft/min.

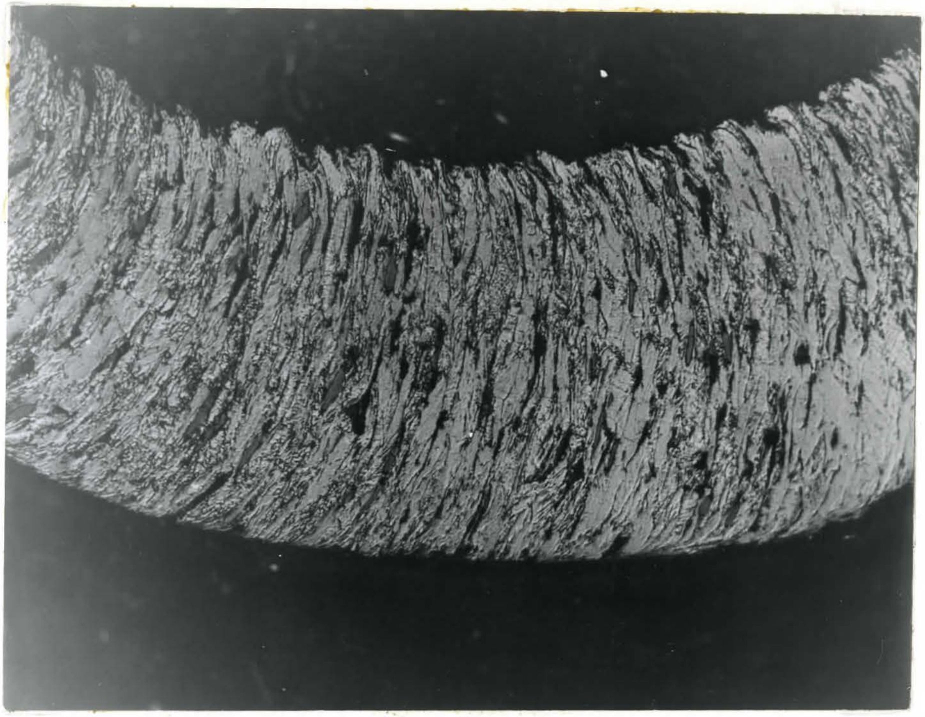

X150

Fig. 4.8. Chip Photomicrograph of AISI 12L15 Steel at the Cutting Speed of 100 ft/min.

X150

Fig. 4.9. Chip Photomicrograph of AISI 12L15 Steel at the Cutting Speed of 200 ft/min.

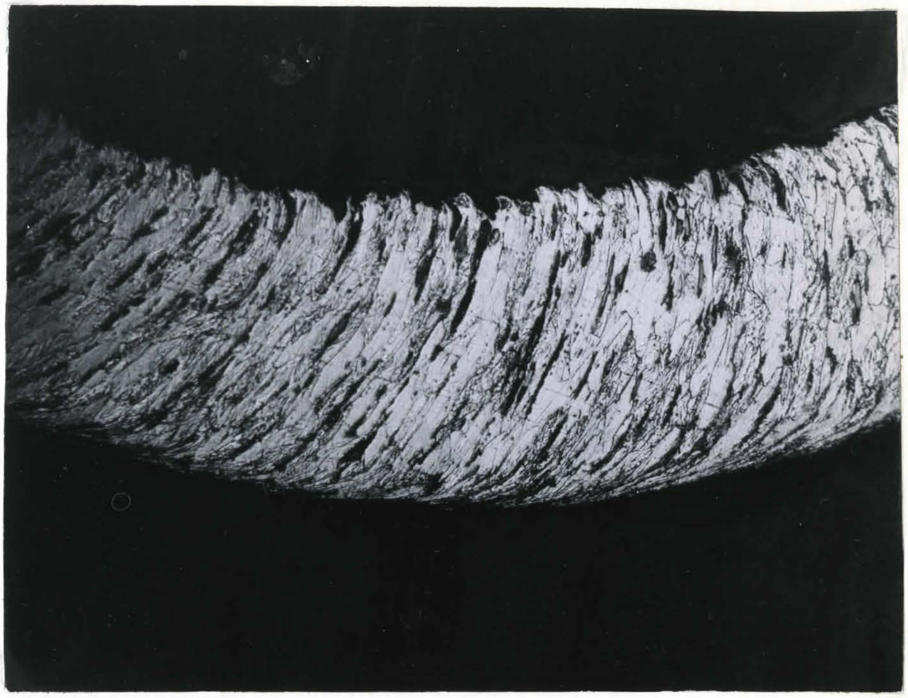

X150

Fig. 4.10. Chip Photomicrograph of AISI 12L15 Steel at the Cutting Speed of 300 ft/min.

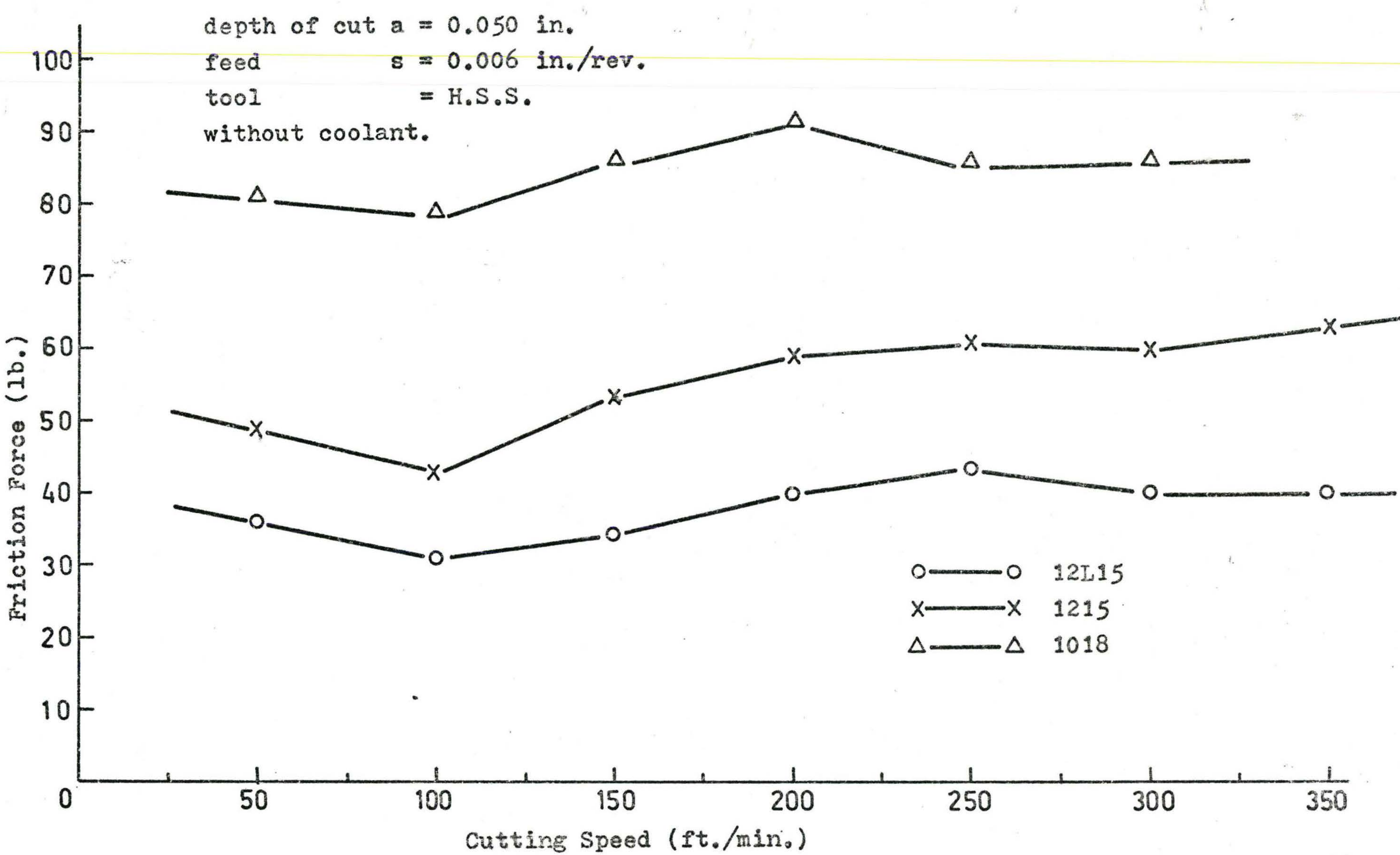

Fig. 4.11. Friction Force Versus Cutting Speed.

LIST OF REFERENCES

1. "The Making, Shaping and Treating of Steel" edited by McGannon, H.E., United States Steel Publication, 9th Edition, 1970.

2. Ramalingam, S., Metallography and Chip Fractography of Free-Machining Steel. Department of Mechanical Engineering, State University of New York at Buffalo, Buffalo, New York.

3. Ramalingam, S., J. Hazra, and D. Caffarrelli, Free-Machining Steels; The Behaviour of Type MnS Inclusions in Machining. ASME Paper No. 73-WA/Prod.-10, 1973.

4. Baker, T.J., and J.A. Charles, Morphology of Manganese Sulphide in Steel, Journal of Iron and Steel Institute, Sept. 1972, Page 702.

5. Moore, C., The Steelmaker's Approach to Machinability. Head of Machinability Studies, The Park Gate Iron and Steel Co. Ltd.

6. Sim, C.E., The Nonmetallic Constituents of Steel. Transactions of the Metallurgical Society of AIME, Volume 215, June 1959, Page 367.

7. Wells, R.G. and W.G. Wilson, Identifying Inclusions in Rare Earth Treated Steels. Metal Progress, Dec. 1973, Page 75.

8. Luyckx, L.,Metallurgical Transactions, Volume I, Dec. 1970.

9. Hazra, J., Ph.D. Thesis 1973. Department of Mechanical Engineering, State University of New York at Buffalo, Buffalo, New York.

10. Baker, T.J. and J.A. Charles. Deformation of MnS Inclusions in Steel, Journal of Iron and Steel Institute, Sept. 1972, Page 680.

11. Paliwoda, E.J., The Role of Oxygen in Free-Machining Steels, AIME Metallurgical Society Conference, Volume 26, 1965, Page 27.

12. Van Vlack, L.H. Correlation of Machinability with Inclusion Characteristics in Resulphurized Bessemer Steels. Transactions of A.S.M., Volume 45, 1953, Page 741.

13. Zlatin, N. and J.V. Gould, The Effect of Lead Additive on the Machinability of Alloy Steels. Journal of Engineering for Industry, ASME. May 1959, Page 131.

14. Chepto, E., What Magazines are Saying About Cold Finished Steel Bars, American Iron and Steel Institute, Purchasor, 1970.

15. Lewis, K.G., Property of Free-Machining Steels. Journal of Iron and Steel Institute, March 1958, Page 133.

16. Shaw, M.C., P.A. Smith and N.H. Cook. Free-Machining Steel - II. Tool Life Characteristics of Leaded Steel. Trans. ASME, May 1961, Page 175.

17. Shaw, M.C., P.A. Smith and E.G. Lowen. Influence of Lead on Metal Cutting Forces and Temperature. Trans. ASME, Volume 45, May 1957, Page 1143.

18. Shaw, M.C., and others. Free-Machining Steel--I, Tool Life Characteristics of Resulphurized Steel. Trans. ASME, May 1961, Page 163.

19. Shaw, M.C. and others. Free-Machining Steel - III Cutting Forces, Surface Finish and Chip Formation, Trans. ASME, May 1961, Page 181.

20. Thompson, R.W. and others. Scanning Electron Microscopy and Auger Electron Spectroscopy Observations on the Role of Lead in the Machining of Steel. Senior Research Engineer, Inland Steel Company, East Chicago, Indiana

21. Lewis, K.G. Property of Free-Machining Steel. Journal of Iron and Steel Institute, March 1958, Page 85.

22. Shaw, M.C. and others. Leaded Steel and Real Area of Contact in Metal Cutting. Trans. ASME, Volume 79, 1957, Page 1165.

23. Weaver, A.P., Impact Properties of Leaded Steel, Trans. ASM, Volume 49, 1957, Page 464.

24. Swinden, T., Journal of Iron and Steel Institute, 1943, Page 441.

25. Barrow, G., Assessment and Application of Machinability, University of Manchester Institute of Technology, 1973.

26. Wong, M., M.Eng. Thesis, 1974, Some Aspects of Tool Wear and Machinability in Turning, McMaster University, Hamilton.

27. Armarego, E.J.A. and R.H. Brown, Machining of Metals, Prentice Hall, 1969.

28. Gautschi, G.H., Cutting Forces in Machining and Routine Measurement, Proc. of 12th International MTDR Conf., University of Manchester, Sept. 1971.

29. Trent, E.M., Proceedings of Conference on Machinability, London, 1967.

30. Enahoro and Welsh, Proceedings of Conference on Machinability, London, 1967.

31. Trigger, K.J. and B.T. Chao, Cutting Temperature and Metal Cutting Phenomena. Trans. ASME, Volume 73, 1951, Page 777.

32. Bagley, F.L. and R. Mennell - Machining Characteristics of Leaded Steel. Trans. ASME, June 1960, Page 347.